

**The physiostat:
Feed-back controlled cultivation of microorganisms
implemented for UVB radiation-influenced
fluorescence kinetics in a photobioreactor for enhanced
production of active agents in *Synechocystis* sp. PCC
6803**

Dissertation
zur Erlangung des Doktorgrades
der Mathematisch-Naturwissenschaftlichen Fakultät
der Christian-Albrechts-Universität
zu Kiel

Vorgelegt von
Kai Marxen

Kiel, Dezember 2006

Referent:
Korreferent:
Tag der mündlichen Prüfung:
Zum Druck genehmigt: Kiel, den

Dekan

Content

Chapter	Page
1. Introduction	1
2. Biological and physical background	3
2.1. Photosynthesis	3
2.2. The electron transport chain	4
2.3. Photosystem II (PSII)	6
2.4. Fluorescence emission originated by PSII and its measurement	8
2.5. Cyanobacterial thylakoids	11
2.6. Phycobilisomes	12
2.7. Carotenoids and xanthophylls	14
2.8. α -Tocopherol	16
3. Materials and methods	17
3.1. Pilot studies of the antioxidative potential	17
3.1.1. Microorganisms and cultivation conditions	17
3.1.2. Preparation of the methanolic extract	17
3.1.3. Spectrophotometric measurements	18
3.1.4. Chemicals	18
3.1.5. Preparation of reference and measuring cuvette	18
3.1.6. Experimental protocol	19
3.1.7. Data analysis	19
3.1.8. Determination of the effective concentration (EC_{50})	20
3.2. Cultivation experiments	20
3.2.1. Cultivation of the microorganisms	20
3.2.2. The photobioreactor and its inline measurement sensors	21
3.2.2.1. Set-up of the classical components of the photobioreactor	21
3.2.2.2. Communication systems	24
3.2.2.3. The complete system	25

Chapter	Page
3.2.2.4. <i>Inline</i> measurements of the optical density	25
3.2.2.5. Fluorescence sensors	26
3.2.2.6. Process strategies and UVB-treatments	27
3.2.3. <i>Offline</i> measurements	28
3.2.3.1. <i>Offline</i> photometric measurements	28
3.2.3.2. Determination of the biological dry mass (BDM)	28
3.2.3.3. Growth rate μ	29
3.2.3.4. Freeze-drying of reactor samples	29
3.2.3.5. Pigment analyses	29
3.2.3.6. Measurements of the phycobilisomes	29
3.2.3.7. Mycosporine-like amino acids (MAAs)	30
3.2.3.8. α -Tocopherol measurements	30
3.2.3.9. Antioxidative potential of reactor samples	31
4. Results of the piloting tests	32
4.1. Testing the method of determining antioxidative potential	32
4.1.1. Wavelength scans	32
4.1.2. Dependence of absorbance from extract concentration	33
4.1.3. Theoretical background	37
4.1.4. Data analyses	39
4.2. Pilot studies for the design of the physiostat	41
4.2.1. Batch process	41
4.2.2. Fluorescence characteristics of the turbidostatic process influenced by stepwise change UVB-radiation	42
4.2.3. Determining the kinetic parameters for the design of the feed-back loop of the Physiostat	46
4.2.4. Testing linearity of the system by sinusoidal modulation of UVB-intensity	46
4.2.5. Sinusoidal modulation of the UVB-intensity for frequency responses	49
4.2.6. Curve fitting of the frequency responses for the determination of the transfer function of the “system to be controlled” microorganisms	51

Chapter	Page
4.2.7. Determination of the frequency response of ϕ_{PSII}	51
4.2.8. Calculation of the transfer function of ϕ_{PSII}	52
4.2.9. Verifying of the transfer function by the ϕ_{PSII} -response induced by stepwise change in UVB-intensity	54
4.2.10. Design of the control loop	55
4.2.10.1. Transfer function of a PI-controller	55
4.2.10.2. Stability of the control loop	56
4.2.10.3. Design of the PI-controller	57
4.2.11. The establishment of a new process strategy named physiostat	60
5. Results of the UVB-influenced cultivation experiments	63
5.1. Biological dry mass (BDM)	63
5.2. Growth rate μ	65
5.3. Fluorescence signals	68
5.3.1. Fluorescence signals from a cultivation not irradiated by UVB	68
5.3.2. Fluorescence signals of cultivation experiments influenced by stepwise changed UVB-intensity in the turbidostat	70
5.3.3. Fluorescence signals of physiostatic cultivation experiments	76
5.4. Pigment analyses	82
5.4.1. Chlorophyll <i>a</i>	84
5.4.2. Myxoxanthophyll	86
5.4.3. Zeaxanthin	88
5.4.4. Echinenone	88
5.4.5. β -Carotene	92
5.4.6. Phycobilisomes	94
5.5. Optimum curves of the carotenoid and xanthophylls	99
5.6. Mycosporine-like amino acids (MAAs; here shinorine)	101
5.7. α -Tocopherol measurements	103
5.8. Antioxidative potential (AOP)	106

Chapter	Page
6. Discussion of the pilot studies	110
6.1. Discussion of the AOP-measuring method	110
6.2. Discussion of the physiostatic pilot studies	112
6.2.1. Performance of the physiostat	113
6.2.2. Biological approach for explaining the time constant τ_2 (17.04 min)	114
7. Discussion of the cultivation experiments	116
7.1. Biological dry mass (BDM) and growth rate (μ)	116
7.2. Fluorescence signals F , F_M' and ϕ_{PSII}	118
7.3. Pigments (chlorophyll a , carotenoids, xanthophylls, and phycobilisomes)	122
7.3.1. Chlorophyll a , carotenoids, and xanthophylls	122
7.3.2. Phycobilisomes	125
7.4. Mycosporine-like amino acids (MAAs; here shinorine)	127
7.5. α -Tocopherol	128
7.6. Antioxidative potential (AOP)	131
7.7. Hypothesis for the explanation of pigment and α -tocopherol synthesis in two different physiostatic processes ($\phi_{PSII,SP} = 0.2$ and $\phi_{PSII,SP} = 0.15$)	133
8. Outlook	136
9. Summary	138
10. Zusammenfassung	141
References	144

Abbreviations

μ :	growth rate
ADP:	adenosine-di-phosphate
AOP:	antioxidative potential
AP:	allophycocyanin
ATP:	adenine-tri-phosphate
BDM:	biological dry mass
DPPH:	2,2-Diphenyl-1-picrylhydrazyl
EC ₅₀ :	effective concentration
F:	actual fluorescence intensity at any time
F _C :	transfer function of the PI-controller.
F _{CS} :	transfer function of the system to be controlled
F _{M'} :	fluorescence intensity with all PS II reaction centres open in the light adapted state
HPLC:	high performance liquid chromatography
k _{DR} :	degradation rate
MAAs:	Mycosporine-like amino acids
MS:	measuring light
NADP:	nicotinamide-adenine-dinucleotide-phosphate
P680:	reaction centre of photosystem II
PAM:	pulse amplitude modulation
PC:	phycocyanin
PE:	phycoerythrin
PSI:	photosystem I
PSII:	photosystem II
r.u.:	relative units
ROS:	reactive oxygen species
SAL:	saturating actinic light
T _N :	integral action coefficient
UVB:	ultraviolet-B radiation
$\phi_{\text{PSII,SP}}$:	set point of the physiostat
ϕ_{PSII} :	photosynthetic efficiency of photosystem II

1. Introduction

Phototrophic growing microorganisms are of increasing interest for research and industry. They are microscopic, phototrophic and ubiquitous single-celled plants or bacteria and grow in different habitats like wetlands, rocks or soils. Most of them prefer fresh or salt water environments, but some of them live in extreme environments. This indicates a high degree of biological adaptation, which has enabled these organisms to thrive and compete effectively in nature. Nutrients, such as ammonia or nitrates, phosphates, certain metals, carbon dioxide and the light regime as photosynthetic energy supply are the major determinants of the growth of phototrophic microorganisms (Geider et al., 1998; Lippemeier et al., 2001; Hammes et al., 2006).

It is well known that a lot of phototrophic microorganisms synthesise substances which are very interesting for cosmetic, pharmacological and food industry (e.g. antioxidants, antibiotics, polyunsaturated fatty acids, vitamins, toxins (Cohen, 1999; Mundt et al., 2003; Richmond, 2004)). Thus, these microorganisms are a potential new source for many products if they can be cultivated adequately.

The cultivation of phototrophic microorganisms seems to be easy, but reality shows a different picture. Difficulties arise from e.g. the need of avoiding contamination, energy supply and cultivation conditions. For example, high light intensities can lead to photoinhibition (Trebst et al., 2002; Barber & Andersson, 1992), but low intensities probably limit the photosynthetic activity and related cellular processes (Keren et al., 1997). Both situations lead to very limited growth, or in the worst case even to the death of the cells. On the other hand, cultivation of phototrophic microorganisms under non-optimal growth conditions (e.g. nutrient or light stress) may be done on purpose. They are employed in order to study cell behaviour and modifications in cellular synthesis steps (Gomez et al., 2003; Lippemeier et al., 2003; Wang et al., 2003) or they may lead to a high yield of commercially important substances (Kobayashi et al., 1997; Eonseon et al., 2003).

Limitation or inhibition often cause dynamic changes in chlorophyll fluorescence (Lippemeier et al., 2001). Thus, monitoring of chlorophyll fluorescence characteristics is an

established tool in microorganisms research providing fast estimation of microorganisms physiological state and photosynthetic rates (Genty et al., 1989; Kolber & Falkowski, 1993).

In order to develop a technique and process strategy for microalgae biotechnology, it is necessary to determine the optimal factors controlling biomass and metabolite production. In consideration of these points, it is very important to operate a process under defined conditions in a closed system in order to estimate the influences of different cultivation parameters on cellular growth and metabolism of phototrophic microorganisms.

In this study, a multiple photobioreactor system is presented as an efficient tool for studying and optimising cultivation parameters and for developing new process features. The new feature is called *physiostat*, i.e., a feed-back loop enabled the manipulation of physiological parameters using chlorophyll fluorescence as a control parameter and UVB-radiation as actuating variable.

This study has three aims:

1. Investigations of *inline* fluorescence measurements of the cyanobacterium *Synechocystis* sp. PCC 6803 influenced by UVB-radiation
2. Testing an *physiostatic* processes as an new approach for microalgae biotechnology
3. Investigations the power of UVB-irradiation for promoting the synthesis of some active agents (pigments and α -tocopherol) in the cyanobacterium *Synechocystis* sp. PCC 6803 under only *turbidostatic* or with additional *physiostatic* control.

2. Biological and physical background

In this chapter, information about the biological and physical background of the intended investigations are given. During the cultivation experiments physiological changes, detected by *inline* fluorescence measurement, are induced. The affected cellular components (e.g. photosystem II, the electron transport chain, phycobilisomes) and the involved mechanisms are described here.

2.1. Photosynthesis

The photosynthesis is a complex process in which absorbed light energy is used for the transformation of water and carbon dioxide into carbohydrate and oxygen. Two reaction types, the light and the dark reaction, are involved in the photosynthesis.

During the light reaction they undergo several transformations. Water is split into oxygen, protons and electrons whereas NADP^+ is reduced to NADPH/H^+ and ADP is transformed into adenine tri-phosphate (ATP).

In the light reaction electrons are transferred from water to NADP.

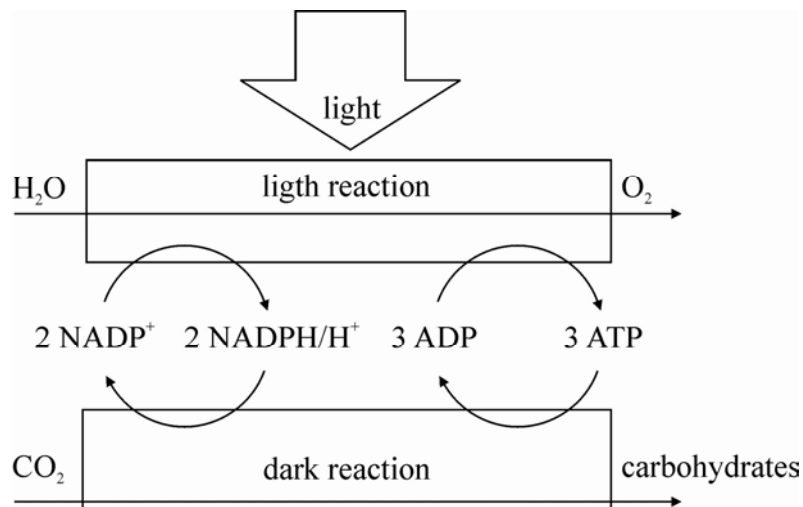
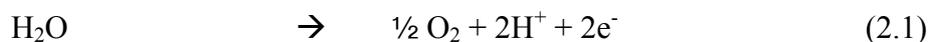


Figure 2.1. Light and dark reactions in the photosynthesis.

An overall chemical basic reaction of the light reaction can be described as follows



Energy-rich carbohydrates are synthesised in the dark reaction. The necessary redox and chemical energies are provided by NADPH/H⁺ and ATP, respectively, generated in the light reaction (Ort & Whitmarsh, 1996; Junge et al., 1997).

Photosynthesis takes place in the thylakoid membranes, a closed membrane system. The aqueous inner volume is called lumen, whereas the outer cytosolic side is called stroma. In cyanobacterial cells as well as in eucaryontical cells the complexes involved in the light reaction are photosystem II (PSII), photosystem I (PSI), and the cytochrome b/f complex. These complexes are connected via a electron transport chain.

2.2. The electron transport chain (ETC)

The light reaction (Falkowki & Raven, 1997; Häder, 1999) is a serial system of redox-reactions in which electrons received from H₂O are transported to NADP⁺ (Fig. 2.2). The electron transfer is driven by the absorption of a photon. This causes the reaction centre of PSII (P680) to change from a ground state into an excited state (P680^{*}) (Dau, 1994a,b). On the luminal side of P680, a manganese cluster splits two water molecules in one oxygen molecule, four protons and four electrons (Dau, 1994b; Haumann et al., 2005).

The excited P680^{*} donates one electron to phaeophytin (Pheo) and a hole to (or takes an electron from) the manganese cluster of the water splitting enzyme (WSE). The reduced phaeophytin is reoxidised by transferring one electron to the primary electron acceptor, the plastoquinone Q_A (Karukstis, 1992; Dau, 1994b). Q_A reduces the plastoquinone Q_B (Dau, 1994b) but unlike the reduction of Q_A two electrons are necessary for complete reduction of Q_B. In its double reduced state, Q_B binds two protons from the cytosolic side and leaves the Q_B-binding site as plastoquinol (PQ). PQH₂ diffuses freely through the membrane. When it meets the binding site of the cytochrome b/f complex (Cyt bf), the two electrons are donated

to Cyt bf and the two protons are released into the lumen. Plastocyanin (PC) transfers the electrons from the cytochrome b/f complex to the reaction centre of PSI (P700) via the luminal phase. If P700 is in an excited state (P700^{*}) it transfers the electron to the mobile electron carrier ferredoxin (Fd) via the primary electron acceptors A₀ and A₁.

The enzyme ferredoxin-NADP-oxidoreductase (FNR) accepts two electrons from two ferredoxins and reduces the final acceptor NADP⁺ to NADPH/H⁺ (Dau, 1994a).

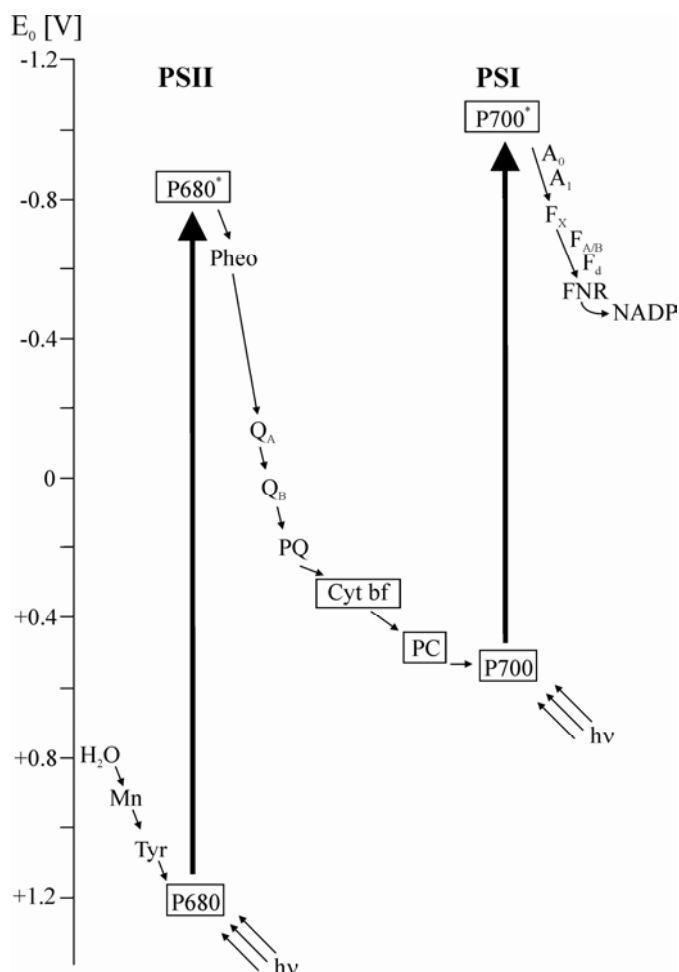


Figure 2.2. Electron transport chain in the thylakoids and the related electrochemical potentials. Mn = manganese cluster; Tyr = tyrosine; P680 = PSII reaction centre chlorophyll (ground state); P680^{*} = PSII reaction centre chlorophyll (excited state); Pheo = phaeophytin; Q_A and Q_B = primary electron acceptor behind P680^{*}; PQ = plastoquinone pool; Cyt bf = cytochrome b/f complex; PC = plastocyanin; P700 = PSI reaction centre chlorophyll (ground state); P700^{*} = PSI reaction centre chlorophyll (excited state); A_0 and A_1 = primary electron acceptors of PSI; F_X and $F_{A/B}$ = iron sulphur centres; F_d = ferredoxin; FNR = ferredoxin-NADP⁺ oxidoreductase; NADP = nicotinamide adenine dinucleotide phosphate.

Several mechanisms are responsible for the generation of the transthylakoid pH gradient. One of them is the generation of protons by the splitting of water on the lumenal side of PSII and the consumption in the reduction of NADP^+ to NADPH/H^+ on the stroma side. A further mechanism is the transfer of two protons with the movement of PQH₂ from the stroma to the lumen (Fig. 2.3). In both mechanisms two protons per two transported electrons are involved (Dau, 1994a).

The resulting pH-gradient provides the driving force for the synthesis of ATP from ADP and phosphate catalysed by the CF_0/CF_1 ATPase (Mitchell, 1977; Witt, 1979; Junge et al., 1997). As mentioned above, NADPH/H^+ and ATP generated in the light reaction provide the redox and chemical energy for the dark reaction (Baldry et al., 1966; Anderson et al., 1978; Buchanan, 1980; Walker, 1981).

However, the stoichiometry of ATP and NADPH/H^+ as provided by the linear electron transfer chain described above is not adequate for driving the Calvin cycle. In order to increase ATP production (pH gradient) without increasing the amount of NADPH/H^+ , additional electron acceptors behind PS I can be employed (Noctor & Foyer 1998; Guo et al. 2003). In the Mehler reaction (also called pseudocyclic electron transport (Hormann et al., 1993)) electrons from PS I are transferred to molecular oxygen (Reising & Schreiber, 1992) whereas in the cyclic electron transport electrons from PSI enter the ETC again via the plastoquinone pool. Another electron acceptor is provided by assimilation of nitrogen in the GOGOT cycle (Noctor & Foyer 1998; Guo et al., 2003). Furthermore, superfluous redox equivalents (NADPH/H^+) can directly be exported from the chloroplasts to the cytosol via shuttles (Krömer, 1995; Noctor & Foyer, 1998; Guo et al., 2003)

Nevertheless, for the investigations here, the branching behind PS I does not play a role. Thus only the linear electron transfer chain has to be taken into account.

2.3 Photosystem II (PSII)

In this study, PSII plays an important role. Therefore, a brief description of the structure of this complex system is given. In Fig. 2.3 a simplified scheme of the architecture of PSII is shown. The two polypeptides CP_{47} and CP_{43} form the inner core complex of PSII (Dau,

1994b). Both polypeptides contain around 20 chlorophyll *a* molecules (Dau, 1994b). Besides their function for light harvesting and transfer absorbed photons to the chlorophyll *a* molecule of P680 they are necessary for forming the structure of PSII.

The two intrinsic polypeptides D1 and D2 form a heterodimer and bind several redox active substances which are involved in the ETC. They contain the chlorophyll *a* molecule P680, four additional chlorophyll *a* molecules, two molecules phaeophytin and the two plastoquinones Q_A (located on D2) and Q_B (located on D1) and Tyrosin Z on the donor side (Dau, 1994b). In addition, two molecules β -carotene are located on these polypeptides.

The function of the extrinsic cytochrome b_{559} is not completely understood but a role in protecting P680 against overexcitation is under discussion (Kruk et al., 2001; Rhee, 2001).

At the lumenal side of PSII the water splitting complex is located. It is surrounded by two 9 kDa- and 33 kDa subunits. 4 manganese ions form the manganese cluster which is involved as a catalytic unit for the splitting of water at the lumen side of PSII (Grabolle et al., 2006).

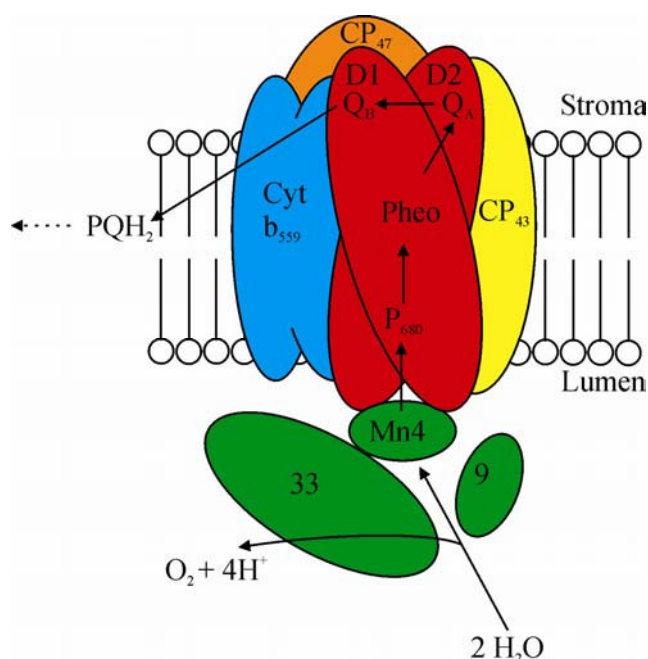


Figure 2.3. Simplified structure of PSII (modified from Campbell et al., 1998).

Both PSII and the redox state of the ETC participate in the modulation of fluorescence. At room temperature it can be assumed that all variable fluorescence originates from PSII (Baker and Webber, 1987; Dau, 1994a).

2.4. Fluorescence emission originated by PSII and its measurement

Chlorophyll molecules when illuminated with a wavelength shorter than 680 nm emit a dark red fluorescence. Only up to 10 % of the absorbed light energy is emitted as fluorescence (Buschmann & Grumbach, 1985; Dau, 1994b). The interpretation of light induced fluorescence kinetics is difficult due to the number of processes involved in consumption of the absorbed light energy (Hansen et al., 1987; Vanselow et al., 1989; Vanselow, 1993). For a qualitative understanding of the interplay of these energy consuming processes a short excursion of the chlorophyll fluorescence origin and measurement of chlorophyll fluorescence is given.

In PSI and PSII, only one chlorophyll molecule per PSII unit is used as a reaction centre and is responsible for charge separation. The major part of chlorophyll (200 to 400 molecules) is in the antennae. Light absorption by these chlorophyll molecules causes a transition of the molecules from the ground state S_0 to higher singlet states S_X (Clausen & Junge, 2004; Haumann et al., 2005). Excitation states higher than S_1 can de-excite radiationless to S_1 (Lavergne & Leci, 1993). From the S_1 state the energy can dissipate via three different pathways:

1. dissipation by fluorescence
2. dissipation via heat emission
3. energy transfer to the reaction centre of PSII or PSI or to a neighbour molecule

The mechanisms involved in de-excitation of the S_1 state of chlorophyll are called quenching mechanisms. The most important distinction is between photochemical and non-photochemical quenching mechanisms. Photochemical quenching mechanisms lower the fluorescence intensity by using the exciton energy for photosynthesis (e.g. Q_A in an open state enables a photochemical quenching mechanism). Non-photochemical mechanisms do not use the absorbed energy for photosynthesis.

The organisation of the antennae of PS II is described by the matrix (or lake) model (free energy transfer between all chlorophyll molecules in one PSII antenna; Dau (1994b)) or the puddle model (no energy transfer between different PS II units; Karukstis (1992)). For

each plant it has to be determined which of the two models applies. Mostly, mixed situation is found, described by the connectivity.

The matrix model is best suited for providing an overview of the mechanisms modulating the intensity of chlorophyll fluorescence (Fig. 2.4). Excitons from the antennae

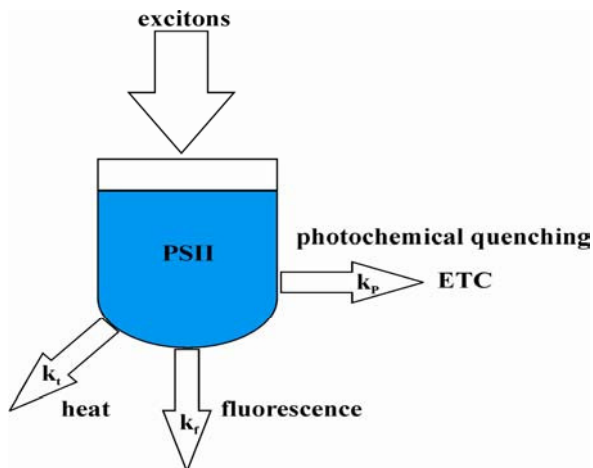


Figure 2.4. Matrix model and energy consumptive processes with: photochemical quenching (k_p), emission of fluorescence (k_f) and thermal dissipation as heat (k_t).

flow into a pool which represents the whole PSII antenna system. The state of excitation is described by the average exciton level E . The excitons can be dissipated by the three pathways mentioned above (with the related rate constants in parentheses):

1. thermal dissipation as heat (k_d)
2. photochemical dissipation (k_p)
3. dissipation as fluorescence emission $k(f)$

For the matrix model, the balance of fluxes into and out of the exciton pool is as follows

$$\frac{d}{dt} E = n \cdot a \cdot I - (k_f + k_t + k_p \cdot [Q]) \cdot E \quad (2.2)$$

with: E = concentration of excitons
 k_f = rate constant of fluorescence
 k_t = rate constant of thermal dissipation

- k_p = rate constant of photochemical use
 a = absorption area of one photosystem II
 n = amount of photosystem II
 I = light intensity
 $[Q]$ = rel. amount of oxidised ('open') reaction centres

Under quasi-stationary conditions Eq. 2.1 can be transformed to

$$(k_f + k_t + k_p \cdot [Q]) \cdot E = n \cdot a \cdot I \quad (2.3).$$

Flourescence F is a direct measure of the exciton level in the antenna system.

$$F = k_f \cdot E \quad (2.4)$$

Fortunately, the rate constant of fluorescence emission is constant (k_f).

Calculating E in Eq. 2.3 leads to the well-known relationship between Fluorescence F and the rate constants of excitation dissipation in PS II

$$F = \frac{k_f}{k_f + k_t + k_p \cdot [Q]} \cdot n \cdot a \cdot I \quad (2.5).$$

The fluorescence yield f is

$$f = \frac{F}{I} \quad (2.6).$$

Measuring of the fluorescence yield requires two light sources: the measuring light I_{ML} providing ΔI in Eq. 2.6 with a very high frequency and the actinic light (consisting of a constant term I_{act} and a variable term ΔI_{act}). Whereas the measuring light must not exert an influence of the (redox) status of the ETC, the issue of the actinic light is the modulation of the state of the ETC (which then is monitored by the measuring light). The high frequency of I_{ML} is a means of preventing an actinic effect of I_{ML} at least with respect to dynamic changes

because I_{ML} can be assumed as a constant parameter as long as the frequency is higher than the investigated time constants of the processes in the ETC.

A problem of the interpretation of chlorophyll fluorescence is the separation between linear (meaningless) effects (F increases linearly with I) and non-linear effects (I_{act} changes the rate constants k_p , k_t and k_f). Taking into considerations that the fluorescence yield consists of a constant term f_s and a variable term Δf and the light of three terms leads to the following form of Eq. 2.5:

$$F = (f_s + \Delta f) \cdot (I_{act} + \Delta I_{act} + I_{ML}) \quad (2.8)$$

$$F = f_s I_{act} + f_s \Delta I_{act} + f_s I_{ML} + \Delta f I_{act} + \Delta f \Delta I_{act} + \Delta f I_{ML} \quad (2.9)$$

In Eq. 2.9 the terms $f_s I_{act}$ and $\Delta f I_{ML}$ contain no information about fluorescence changes induced by the actinic light. A correlator multiplies the fluorescence signal F with I_{ML} and as a consequence thereof all terms without I_{ML} disappear. The remaining terms $f_s I_{ML}$ and $\Delta f I_{ML}$ represent the constant and the variable component, respectively, of the fluorescence signals F and F_M' depending on which lamp is applied (LED or saturation flash).

The above equations have been derived for phototrophic microorganisms (e.g. green plants and algae). However, also cyanobacteria contain PSII in their thylakoid membranes, which are partially similar and partially quite different from that of the "normal" plants.

2.5. Cyanobacterial thylakoids

The photosynthetic apparatus of cyanobacteria is quite different from that one known from green algae or higher plants (Beutler et al., 2004). This holds for the antennae systems and for the organisation of the thylakoid membranes.

Cyanobacteria have three membrane systems: the thylakoid membrane, the cytoplasmic membrane, and the outer membrane (Mohamed et al., 2005). In eukaryotic cells the thylakoid membranes are located in closed cell compartments (named chloroplasts) within

the cells. The thylakoid membrane system of cyanobacteria is free in the cytoplasm and not in chloroplasts.

Unlike eukaryotic cells the thylakoid membranes of cyanobacteria are not continuously connected to the cytoplasmatic membranes and constitute an autonomous membrane system. In contrast to eukaryotic cells, the thylakoids of cyanobacteria are not stacked, an effect caused by the localisation and structure of phycobilisomes (explained in chapter 2.6).

In the cyanobacterial thylakoids the photosystems (PSII and PSI) are serial arranged within the membranes and the peripherally connected phycobilisomes are located on the cytosolic side at the surface of the thylakoids. Besides these two compounds the thylakoids also contains PSI, the cytochrome b/f complex and several other complexes (e.g., ATP-synthase, cytochrome oxidase). The peculiarity of cyanobacteria is the location of the photosynthetic ETC and of the respiratory chain on the same thylakoid membrane thus fulfilling the functions of chloroplasts and of mitochondria. (Campbell et al., 1998; MacColl, 1998).

Unlike higher plants and the most eukaryotic cells, the major light harvesting complexes in cyanobacteria are the phycobilisomes which are located at the surface of the thylakoid membranes.

2.6. Phycobilisomes

Phycobilisomes are part of the outer light harvesting complexes present in prokaryotic cyanobacteria and eucaryotic red algae (MacColl, 1998). In Fig 2.5 the phycobilisomes structure and location of *Synechocystis* sp. PCC 6701 is shown (Campbell et al., 1998).

Unlike eukaryotic microorganisms, no chlorophyll is present in the outer light harvesting complex of cyanobacteria. The chromophores phycocyanobilin and phycoerythrobilin are covalently bound to specific proteins which are organised as α - and β -subunits (Campbell, 1998; MacColl, 1998). Each subunit bounds 1 – 3 chromophores and aggregates as a hexamer $(\alpha\beta)_6$ or trimer $(\alpha\beta)_3$. The hexamers and trimers constitute the structure of the phycobilisomes which is usually hemidiscoidal or ellipsoidal (Campbell et al.,

1998). Allophycocyanin (AP), phycocyanin (PC) and phycoerythrin (PE) build the phycobilisomes structure. Three cylinders of trimers of AP, alongside stacked on the surface of the membranes, constitute the core complex which is directly connected with PSII via a linker protein (L_{CM}). The rod structures consist of PC and PE with PE at the outer position when present. Six cylinders, named rods, converge on the curved surface of the core. These rods comprise of phycobiliprotein hexamers (Campbell et al., 1998).

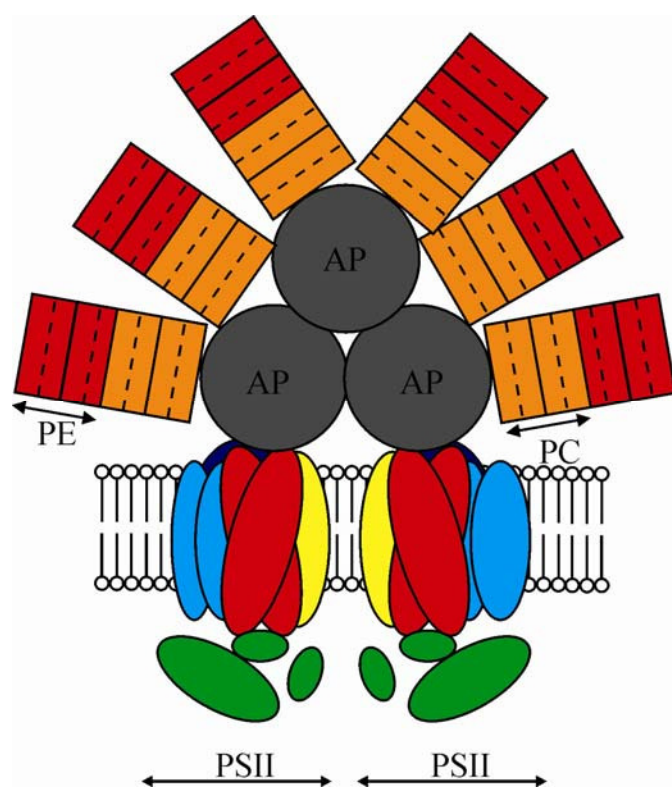


Figure 2.5.

Phycobilisome of *Synechocystis* sp. PCC 6701 (modified from Campbell et al., 1998).

AP = allophycocyanin

PC = phycocyanin

PE = phycoerythrin

PSII = photosystem II

The energy transfer takes place from PE to PC. Subsequently PC transfers the energy to AP which excites P680 by direct energy transfer. It takes about 140 ps to transfer the absorbed light energy through the phycobilisomes to the membrane embedded chlorophyll a of PSII with an efficiency of 95 % or better (Papageorgiou, 1996). Due to their absorptive attributes ($AP_{\lambda_{max}} \approx 650$ nm; $PC_{\lambda_{max}} \approx 620$ nm; $PE_{\lambda_{max}} \approx 550$ nm) phycobilisomes allow cyanobacteria to absorb in a wavelength range in which the absorptive properties of eukaryotic cells are limited.

AP and PC are the dominant pigments in *Synechocystis* sp. PCC 6803 whereas PE is not present (Riethmann et al. 1988; Zolla & Bianchett, 2001). In *Synechocystis* sp. PCC 6803

the blue coloured chromophore phycocyanobilin (PCB) is present in both PC and AP respectively (Ughy & Ajlani, 2004).

Phycobilisomes are known to be influenced not only by changing light conditions but also by nutrient starvation (Duke et al., 1989; Richaud et al., 2001). Cyanobacteria are able to adapt to changing light conditions by varying the ratio of PC to PE (MacColl, 1998). Furthermore phycobilisomes are a major target of UVB-radiation in cyanobacteria (Araoz & Häder, 1997).

Nevertheless cyanobacteria contain also some other biomolecules like carotenoids and xanthophylls which are of importance considering these studies and described below.

2.7. Carotenoids and xanthophylls

Carotenoids and xanthophylls (oxygenated carotenoids) are hydrophobic pigments synthesised by photosynthetic and some non-photosynthetic organisms. They are mainly located in photosynthetic pigment-protein complexes, in the thylakoid membranes and in the cell wall (Jürgens & Mäntele, 1991). Like chlorophylls and phycobilisomes carotenoids are involved in light capture and therefore they play an important role in the photosynthetic apparatus. In addition, carotenoids are able to quench singlet or triplet excited chlorophyll *a* molecules (Peterman et al., 1995; Niyogi et al., 1997) and to protect cells against oxidative damage (Steiger et al., 1999; Mohamed et al., 2005).

Carotenoids (Fig. 2.6) are synthesised via the common precursor isopentenyl diphosphate. Isopentenyl diphosphate is isomerised to dimethylallyl diphosphate by a specific isomerase. Subsequently several condensation reaction steps result in the conversion of dimethylallyl diphosphate into geranylgeranyl pyrophosphate. An enzymatic reaction transforms two geranylgeranyl pyrophosphate molecules into phytoene which undergoes further transformations. Four desaturation steps convert phytoene into lycopene via phytofluene, ζ -carotene, and neurosporene. Via cyclisation reactions lycopene can be converted into γ -carotene which can be used for the synthesis of different carotenoids and xanthophylls (Lagarde et al., 2000).

In *Synechocystis* sp. PCC 6803 the only synthesised carotenoid is β -carotene, but the three xanthophylls zeaxanthin, echinenone and myxoxanthophyll are present (Bramley & Sandmann, 1985).

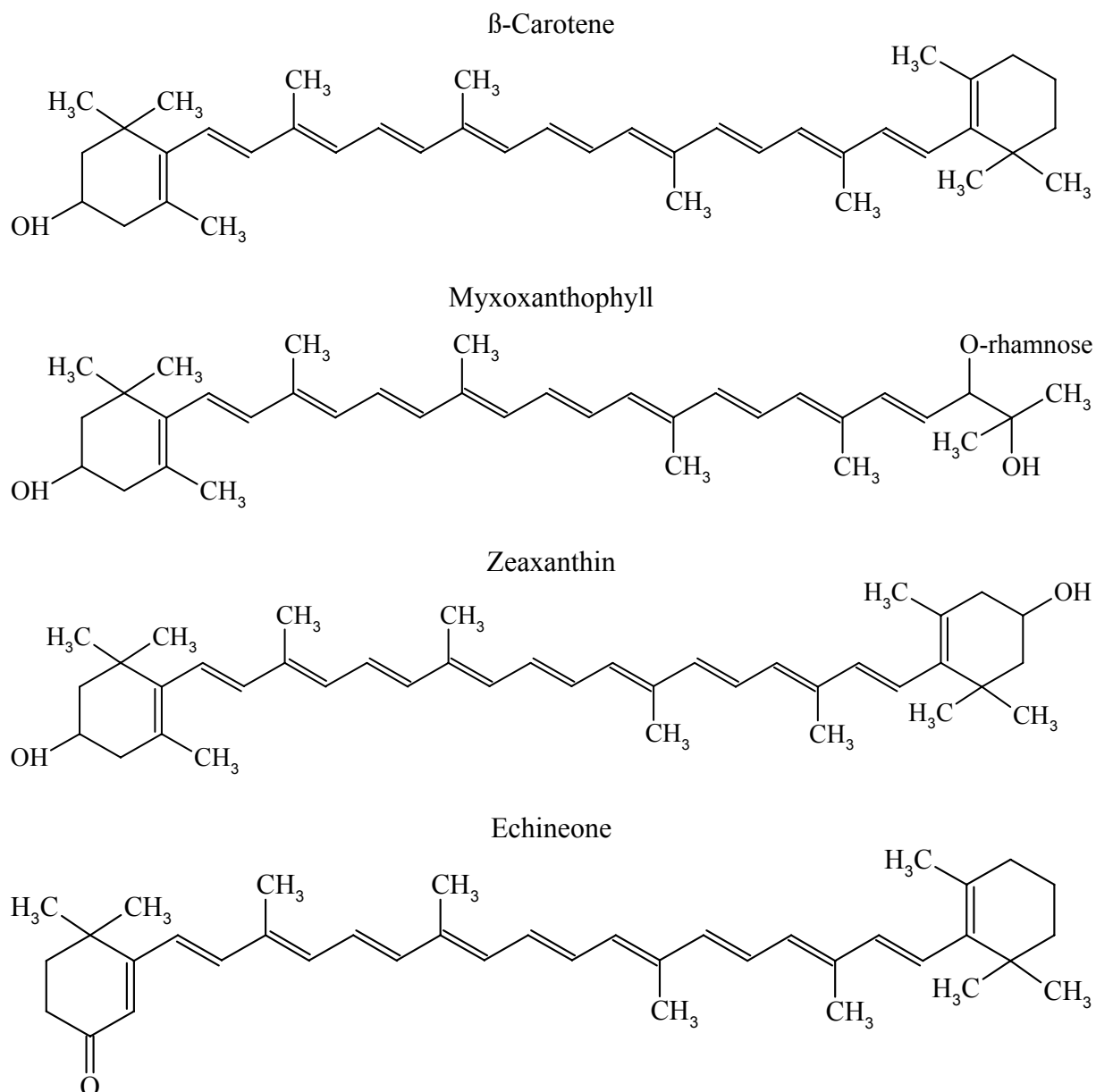


Figure 2.6. Chemical structures of β -carotene, myxoxanthophyll, zeaxanthin and echinenone.

Besides these components α -tocopherol and its function within cyanobacterial cells plays an important role in this study. A brief description of this substance is given below.

2.8. α -Tocopherol

α -Tocopherol belongs to a group of four tocopherols (α -, β -, γ - and δ -tocopherol) which together with a group of four tocotrienols (α -, β -, γ - and δ -tocotrienols) are summarised in one term, Vit E. Both tocopherols and tocotrienols are composed of a polar chromanol head group and a hydrophobic prenyl side chain (Havaux et al., 2005) and are synthesised only by plants and photosynthetic microorganisms (Hofius & Sonnewald, 2003). Embedded in the double lipid layer of membranes the prenyl side chain associate with the lipids and the chromanol head group is exposed to the membrane surface (Havaux et al., 2005). Tocopherols and tocotrienol differ in the degree of saturation of the hydrophobic side chain. Nevertheless both groups possess antioxidative potential and are therefore important for protecting cells against oxidative stress (Rippert et al., 2004). In these groups of lipid soluble substances α -tocopherol (Fig. 2.7) is the most abundant form in nature and the most potent in terms of antioxidative potential (Shintani, 2001).

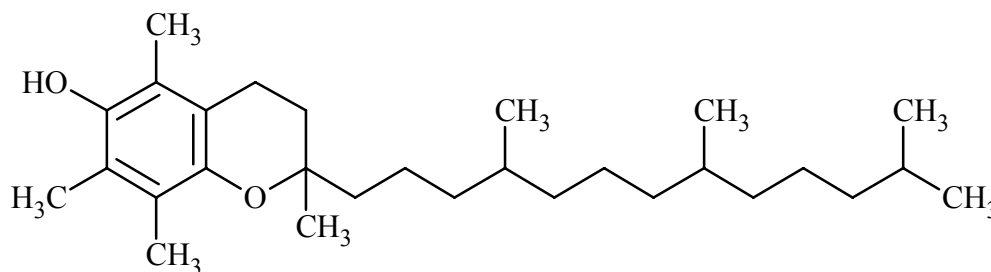


Figure 2.7. Chemical structure of α -tocopherol.

The tocopherol biosynthetic pathway has been fully elucidated in *Synechocystis* sp. PCC 6803 (Cheng et al., 2003; Sattler et al., 2003). Derived from the shikimate pathway homogentisate and the phytyl pyrophosphate derived from the non-mevalonate pathway were condensate through the action of homogentisate prenyltransferase. The resulting 2-methyl-6-phytylplastoquinone is the first tocopherol intermediate and precursor of all tocopherols. Subsequently a ring cyclisation and methylation reactions result in the synthesis of the four tocopherols.

α -Tocopherol is located in all cyanobacterial membranes and functions mainly as a protecting substance against oxidative stress (Trebst et al., 2002; 2003).

3. Materials and methods

3.1. Pilot studies of the antioxidative potential

3.1.1. Microorganisms and cultivation conditions

Two species of cyanophyceae (*Synechocystis* sp. PCC6803, *Anabaena* sp.), one of rodophyceae (*Porphyridium purpureum*) and haptophyceae (*Isochrysis galbana*) and bacillariophyceae (*Phaeodactylum tricorutum*) were tested. *Isochrysis galbana*, *Porphyridium purpureum*, *Phaeodactylum tricorutum* were grown in artificial seawater (Tropic Marin, TAGIS, Germany) enriched with F/2 medium nutrients (Guillard & Ryther, 1962) at 24°C with a constant pH-value of the cultures at 8.3. *Anabaena* sp. and *Synechocystis* sp. PCC 6803 were grown at 26°C in BG-11 medium (Rippka et al., 1979) with a constant pH-value of 8.0. Each culture was grown at a constant light regime of 120 $\mu\text{mol photons m}^{-2} \text{s}^{-1}$. The pH-values were kept constant by automatic addition of pure CO₂. At the end of the cultivation, the cultures were centrifuged, freeze-dried and stored at -20 °C.

3.1.2. Preparation of the methanolic extract

The protocol of Bandoniene et al. (2002) with minor modifications was used for the preparation of the methanolic extracts.

Samples of the freeze-dried microorganisms were portioned in aliquots of 0.025 - 1 g. Each of these aliquots was homogenized in 5 mL of 100 % methanol (instead of 80 % methanol) for 30 s on ice with an ULTRA-TURRAX T25 (IKA-Labortechnik, Staufen, Germany). Afterwards, the homogenates were injected through 0.2 μm PTFE-filter (A-Z Analytik-Zubehoer, Langen, Germany) (instead of paper filter) into test tubes.

The extracts with different biomass concentrations were used for the determination of the antioxidant properties.

3.1.3. Spectrophotometric measurements

Wavelength scans from 400 to 750 nm and the decrease in absorbance at 550 nm were measured with a dual-beam UV-VIS spectrophotometer (Uvikon XL, Bio-Tek Instruments, Bad Friedrichshall, Germany). A_{550} as used in Eq. 3.1. below was obtained by switching the spectrophotometer modus from a wavelength scan to a fixed wavelength modus.

3.1.4. Chemicals

DPPH radical. DPPH was obtained from Fluka (Buchs, Switzerland). 2.5 mg DPPH were solved in 5 mL methanol ($\approx 1.27 \text{ mmol L}^{-1}$). This stock solution was daily prepared, used for the spectrophotometric measurements, and kept in the dark at ambient temperature when not used. Using this stock solution enables the measurement of a calibration curve at 550 nm for calculating the DPPH concentration as follows

$$c_{\text{DPPH}} [\mu\text{mol L}^{-1}] = 143.06 A_{550} \quad (3.1)$$

with a correlation coefficient (R^2) of 0.999.

α -Tocopherol. α -Tocopherol was obtained from Fluka (Buchs, Switzerland). α -Tocopherol is an effective antioxidant (Vaya & Aviram, 2001). 25 mg α -tocopherol were solved in 100 mL methanol ($\approx 0.58 \text{ mmol L}^{-1}$). The solution was used for a calibration curve of DPPH reduction and as a chemical reference in comparison to the antioxidant capacities of the microorganisms extracts (described below).

3.1.5. Preparation of reference and measuring cuvette

2.25 mL methanol, 0.1 mL extract and 0.15 mL DPPH stock solution (resulting in a DPPH concentration of $76 \mu\text{mol L}^{-1}$) were mixed in one measuring cuvette.

Furthermore, the extracts were measured with a second measuring cuvette containing 2.325 mL methanol, 0.1 mL extract and 0.075 mL DPPH stock solution (resulting in a DPPH concentration of $38 \mu\text{mol L}^{-1}$) for verification of the data obtained with the higher DPPH

concentration. Additionally, a reference cuvette filled with 2.4 mL methanol and 0.1 mL extract was used.

3.1.6. Experimental protocol

For a proper measurement of the antioxidative potential of the tested microorganisms using the DPPH radical, the following procedure was successfully executed. For choosing the suitable wavelength, wavelength scans from 440 to 750 nm were done for both measuring and reference cuvette. The scans were run against pure methanol. Measurements in the measuring cuvette were performed 30 min after addition of DPPH in order to give enough time for the reaction of the cellular antioxidants with DPPH. During this 30 min, reference and measuring cuvette were kept in the dark at ambient temperature. Additionally, the reference cuvette was measured before and after the reaction in the measuring cuvette had taken place for verification that no changes of the absorptive properties of the microorganisms extract had occurred in the absence of DPPH.

After wavelength scans were done (3 min) 0.3 mL of the α -tocopherol solution was added to both measuring and reference cuvette in order to achieve full reduction of the DPPH radicals. Then, the wavelength scans were repeated. This served to select an adequate wavelength which is influenced only by the DPPH radical (here 550 nm).

The absorbance decrease was then measured by using measuring and reference cuvette prepared and treated in the same way described above. But here the absorbance of the measuring cuvette was measured at 550 nm against the reference cuvette for elimination of the absorptive properties of the microorganisms extract.

All measurements were performed in triplicate. Averages and standard deviations are presented.

3.1.7. Data analysis

The linear range of the absorbance decrease (see Fig. 4.2A and Fig. 4.3A, see below) was evaluated by means of a simple linear regression by using microsoft-excel (Microsoft, Redmond, USA)

$$c_{\text{DPPH}} = c_{\text{DPPH},0} + a_1 c_E \quad (3.2).$$

with c_{DPPH} obtained from Eq. 1, $c_{\text{DPPH},0}$ is the concentration added to the cuvette, c_E the concentration of the microorganisms extract. The slope a_1 is determined by linear regression of graphs like those in Fig. 4.2, below. The slope is used as a parameter for estimating the antioxidative potential of the investigated microorganisms.

3.1.8. Determination of the effective concentration (EC_{50})

The EC_{50} value expresses the amount of microorganisms extract necessary to decrease the absorbance of DPPH by 50 % (Antolovich *et al.*, 2002). The value can be determined graphically by plotting the absorbance against the applied extract concentration or calculated by using the slope of the linear regression (Eq. 3.2).

3.2. Cultivation experiments

3.2.1. Cultivation of the microorganisms

The cyanobacterium *Synechocystis sp.* PCC6803 is a non-nitrogen fixing organism. This requires the use of a qualified medium. Here nitrogen containing BG11 medium (Rippka *et al.*, 1979) was used (Tab. 3.1). The microorganisms were cultivated in a photobioreactor system with a constant pH-value of 10, a photosynthetically active radiation (PAR) of 200 $\mu\text{mol photons m}^{-2} \text{s}^{-1}$ and a constant temperature of 26 °C. The basic process strategy for all conducted experiments were turbidostatic processes (see below).

Table 3.1. BG11 medium for cyanobacteria (Rippka et al., 1979).

	Stock solution	Nutrient solution
	[g / 100 mL]	[ml]
NaNO ₃	15.00	10
K ₂ HPO ₄ • 3H ₂ O	0.4	10
MgSO ₄ • 7H ₂ O	0.75	10
CaCl ₂ • 2H ₂ O	0.36	10
citric acid	0.06	10
ferric ammonium citrate	0.06	10
EDTA (dinatrium-salt)	0.01	10
Na ₂ CO ₃	0.2	10
micronutrient solution*	0.2	1
distilled water		919

* micronutrient solution

Add to 1000 mL of distilled water

	[mg]
H ₃ BO ₃	61
MnSO ₄ • 1H ₂ O	169
ZnSO ₄ • 7H ₂ O	287
CuSO ₄ • 5H ₂ O	2.5
(NH ₄) ₆ O ₂₄ • 4H ₂ O	12.5

3.2.2. The photobioreactorsystem and its inline measurement sensors

3.2.2.1. Set-up of the classical components of the photobioreactor

The set-up shown in Figure 3.1. allows the cultivation of microorganisms under well defined conditions in both, fresh and salt water medium. An important feature is the airlift-loop-system with a volume of 6 liters. Two glass tubes (SIMAX-glass, Kavalier, Sazava, Czech Republik, length 1.5 m, diameter 50 mm) are connected by the top space and at the bottom

space made from non-toxic PVC. Aeration at the bottom of the left-hand tube with a CO₂-enriched air supplies the energy for upwards stream of the algal suspension. The flow velocity ranging from 0 to 16 l h⁻¹ is adjustable by a mass flow controller (DK800N, Krohne, Duisburg, Germany).

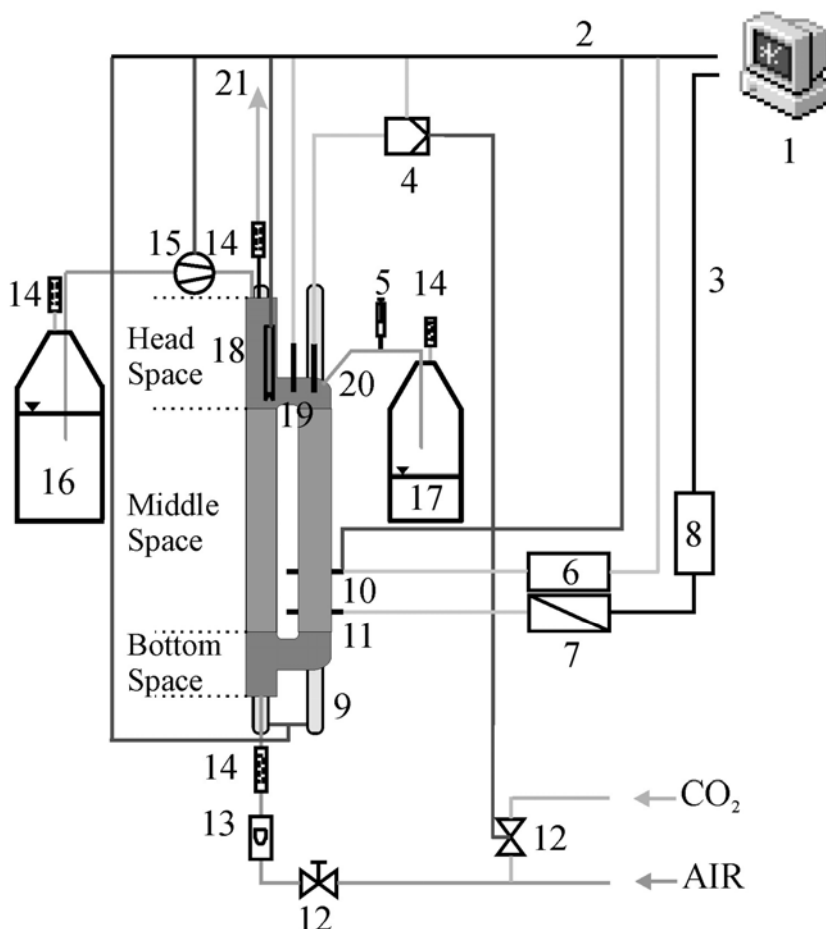


Figure 3.1. Technical design of one single photobioreactor. 1 = PC; 2 = CAN-BUS; 3 = RS232; 4 = pH-Controller; 5 = Syringe for sampling; 6 = PAM-101; 7 = AD-Converter; 8 = RS232-Converter; 9 = Fluorescence tubes for PAR and UV; 10 = Fluorescence probe; 11 = Probe for optical density; 12 = CO₂-valve; 13 = Mass flow controller; 14 = Sterile filter; 15 = Pump; 16 = Reservoir with fresh medium; 17 = Waste; 18 = Immersion heater; 19 = Probe for temperature; 20 = Probe for pH; 21 = Exhaust air.

Monitoring of chlorophyll-fluorescence and optical density is done in the bubble-free downward stream at the lower part of the right-hand column (see Fig. 3.1). The fluorescence tubes in the middle space shown in Fig. 3.1 enable illumination of the microorganisms with a wavelength range of 280 up to 750 nm. The photosynthetically active radiation (PAR) is adjustable over a range from 0 up to $350 \mu\text{mol photon m}^{-2} \text{s}^{-1}$ at the surface of the glass tubes. The light protocol for the supply of PAR is generated by two fluorescence tubes (TL58W/25, Osram, Muenchen, Germany). One fluorescence tube (TL40W/12 RS, Philips, Eindhoven, Netherlands) provides UV-radiation (280 – 380 nm, peak 315 nm, $0 - 1.82 \mu\text{mol photon m}^{-2} \text{s}^{-1}$ UVB, $0 - 69 \mu\text{mol photon m}^{-2} \text{s}^{-1}$ UVA, measured with UVAB Sensor E 1.1 Thies, Goettingen, Germany) which is also adjustable. Due to the large impact of UVB-radiation on cyanobacteria (Lao & Glazer, 1996; MacDonald et al., 2003; Sinha & Häder, 2002) only the UVB-part of the UV-radiation as the main active component is presented although the UVA-radiation is still part of the UV-spectrum.

Sensors for temperature (PT-100, Prosensor, Amanvillers, France), pH-value (2GEP-2-GV-U-O, Jumo, Fulda, Germany) and an immersion heater (Sicce, 50W, Pozzoleone, Italy) are installed in the top space. There are also three more ports. The first one enables for the exhaust of air, the second one can be used for the supply of fresh medium to the reactor vessel by a pump (WM101, WatsonMarlow, Cornwall, UK), and the third one controls the upper filling level of the reactor by passive overflow of culture suspension. In addition, this port is connected to syringes enabling taking of samples. The reactor inlets for aeration, medium, outlets for the exhaust air and for the volume control by overflow are equipped with sterile filters ($0.22 \mu\text{m}$ Millipore filter, Sartorius, Goettingen, Germany).

An autonomous pH-controller (dTrans pH01, Jumo, Fulda, Germany) regulates the pH-value in the suspension by controlling a CO_2 -valve to modulate the CO_2 -concentration in the aeration stream (see Fig. 3.2). For instance, the autonomous pH-controller opens the CO_2 valve when the pH has reached a critical deviation from the set-value.

The temperature is kept constant by means of a **p**roportional-**i**ntegral-**d**erivative (PID)-controller installed in the process control system providing a signal for pulse duration modulation of the immersion heater. The ambient temperature determines the lower limit whereas the upper limit is given by the immersion heater.

3.2.2.2. Communication systems

The system makes use of two communication systems, the CAN-Bus and the RS232-port (Figure 3.2).

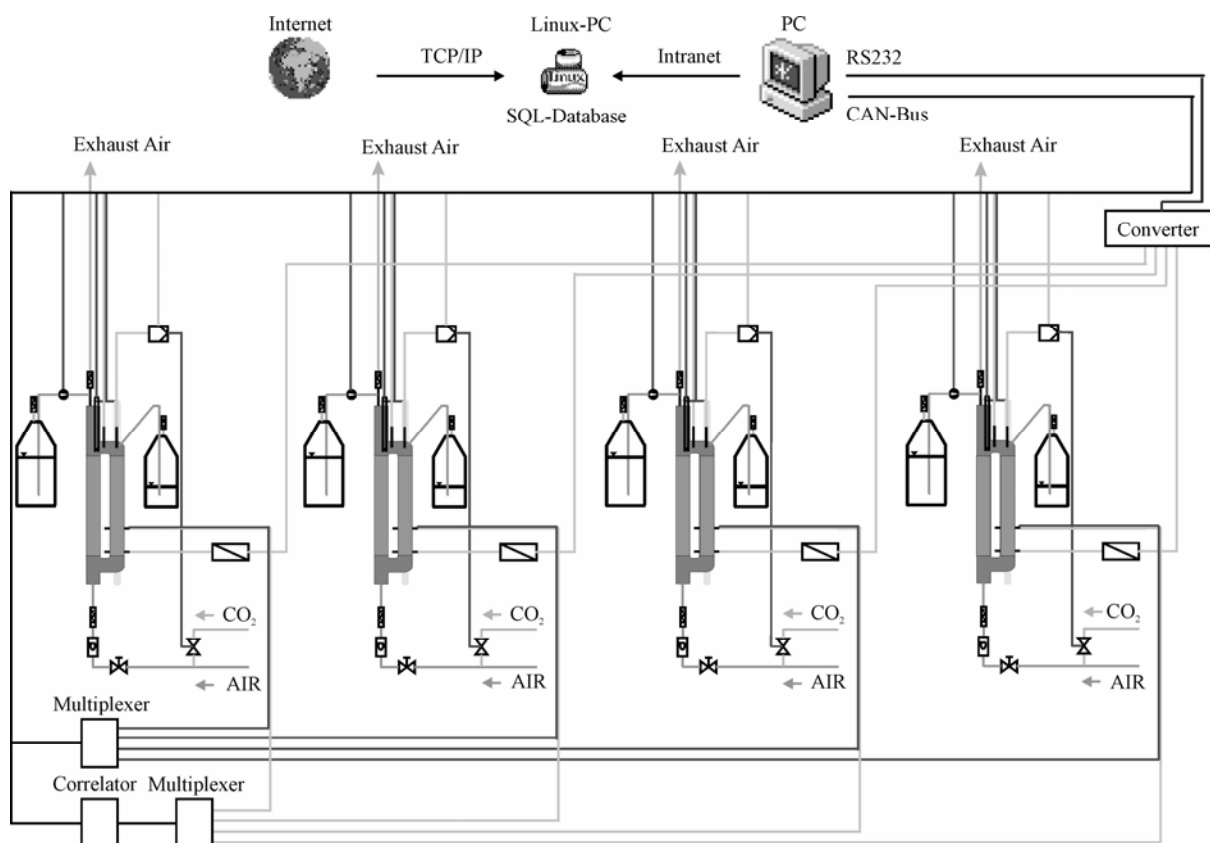


Figure 3.2. Communication systems (CAN-Bus and RS232) and internet connection of the parallel photobioreactor system.

Both systems are connected to a PC which runs a lab made process control system. The CAN-Bus working with the CANopen-protocol transmits the signals from the temperature- and pH-sensors to a PC with a PentiumII- or higher processor equipped with a CAN-Bus-Mastercard (CIF50-COM, Hilscher, Hattersheim, Germany) including an OPC-server which provides the signals for the process control system. Digital inputs/outputs, analogue/digital converter and digital/analogue converter (EA515-8I/O-1A, EA515-4A/D, EA515-4D/A, MKT Systemtechnik, Buende, Germany) enable the data exchange between the CAN-Bus and the actors and sensors. The RS232-port is used for the acquisition of the optical density

measurement. The computer transmits all data to a SQL-database at a preset time (fastest possible sampling rate 0.5 min^{-1}), defined by the experimenter. Via TCP/IP-protocol it is possible to recall the data from the database.

3.2.2.3. The complete system

The complete system consists of four autonomous bioreactors connected to one PC as shown in Figure 3.2. All four reactors are identical in design and technical equipment (described above). The devices for the chlorophyll fluorescence measurements are connected to the central PC via multiplexers under the control of the process control system. It decides which of the installed four fluorescence measurement probes is active. One multiplexer serves to allocate the signals for the measuring and actinic light. The second multiplexer transmits the output signal of the selected photodetector of the PAM-chlorophyll fluorometer.

pH-controller, CO₂-valve, the pump for the medium and temperature sensor of each individual reactor are permanently connected to the PC via the CAN-Bus. This is necessary because the communication of basic environmental parameters must not be disabled by the selection of an individual reactor.

The process control system enables the adjustment of the irradiance intensity and irradiance quality (PAR with/without UV) and allows the manual or automatic switching of the reservoir pump. Also the converters for the optical density measurement are permanently connected via the RS232-communication protocol to the PC. The integration of up to 254 additional devices for the measurement of the optical density is possible.

3.2.2.4. *Inline* optical measurements

The sensor for the *inline* measurement of the optical density consists of a light emitting diode (870 nm, HSDL-4230 17°, Hewlett Packard, Palo Alto, USA) and a photodiode with daylight filter (SFH 205 F, Siemens, Muenchen, Germany). The light emitting diode is used as a modulated light source and the synchronous detection of the transmitted light signal allows the separation of the signal from the ambient irradiance. Using a wavelength of 870 nm yields the optical density just hardly influenced by the absorption of the pigment matrix of the algae.

3.2.2.5. Fluorescence sensor

Chlorophyll fluorescence of light-adapted cells, due to the illumination during the cultivation process, was measured by means of the PAM technique as described by Schreiber et al. (1995a). The technical generation and interpretation of the single chlorophyll fluorescence signals are illustrated in Figure 3.3.

The PAM method requires two light sources, the measuring light and the actinic light, respectively. The measuring light (LED, 630 nm, TLRH180P, Toshiba, Neuss, Germany) is filtered (DTCyan, Schott, Mainz, Germany) and is switched on for 1 s to receive the chlorophyll *a* fluorescence signal (F) (for nomenclature see v. Kooten and Snel, 1990).

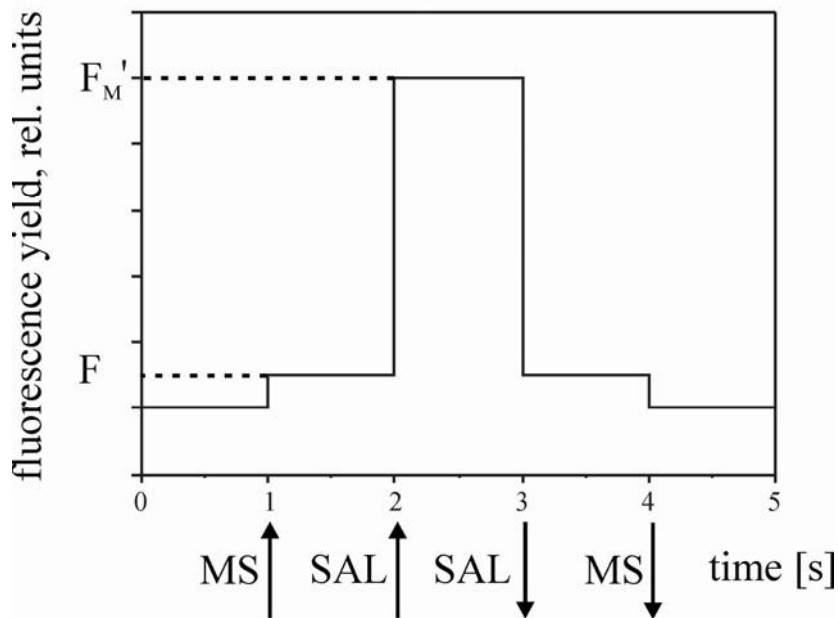


Figure 3.3. Light protocol and idealised responses of the fluorescence signals. No details of the fluorescence kinetics are shown. Due to the circular flow of the microorganisms the F_M' -signal remains nearly constant during the saturating light impulse. F_M' = fluorescence intensity with all PS II reaction centres closed in the light adapted state; F = actual fluorescence intensity at any time; MS = measuring light; SAL = saturating actinic light.

After this second the saturating actinic light (halogen lamp, 64255, Osram, Muenchen, Germany) is activated for 1 s in order to generate the maximum fluorescence signal (F_M'). The photodiode (S3590-01, Hamamatsu, Hamamatsu City, Japan), equipped with a filter (RG9, Schott, Mainz, Germany), detects the emitted fluorescence light (> 720 nm) of the

microorganisms and sends an analogue signal to a commercially available chlorophyll fluorometer (PAM-101, Walz, Effeltrich, Germany). The analogue output signal of the PAM-101 is transmitted via the CAN-Bus (see below) to the PC. A special software analyzes the signal and calculates the photosynthetic efficiency of PSII (ϕ_{PSII} , Eq. 3.3, Schreiber et al., 1995b) for estimating the physiological state of the cultivated microorganisms with the following equation:

$$\phi_{\text{PSII}} = (F_{\text{M}'} - F) / F_{\text{M}'} \quad (3.3)$$

3.2.2.6. Process strategies and UVB-treatments

Different process strategies are executable in the multiple photobioreactor system. They differ mainly in the influence on the medium inside the reactor by the experimenter.

Generally, the starting situation for all conducted experiments were turbidostatic processes. The used process strategy is shortly described as follows.

Turbidostatic process: In the turbidostatic process, the biomass in the reactor is kept constant. Growth is compensated by diluting the microorganisms suspension in the reactor under the control of a feed-back loop (which is described below). The volume of microorganisms suspension (with constant biomass) leaving the reactor via the overflow outlet is equal to the added volume of fresh nutrient solution. This should ensure the receiving of steady state conditions in the photobioreactors. These steady state conditions should avoid nutrient or light limitations.

The turbidostatic process is realised by using one port of the top space of the reactor. A controller installed in the process control system activates the pump (Fig. 3.1) for supply of fresh medium to the reactor vessel when the optical density exceeds the set-value and deactivates the pump when the optical density is equal or below the set-value. This process strategy is used for most of the experiments. The optical density of the suspension was kept constant at a value of 0.8 by adding fresh BG11 medium from a medium reservoir.

The turbidostatic processes were radiated with additional UVB-radiation by two different ways:

1. Cultivation cultures were influenced by stepwise changing of UVB-radiation using intensities of 0.57, 0.83; 1.25 or 1.61 $\mu\text{mol photons m}^{-2} \text{ s}^{-1}$ in four independent cultivation experiments.
2. By using the results of the piloting studies (see below) cultivations were influenced by modulated UVB-intensities for keeping ϕ_{PSII} in a defined state. Three set points were tested ($\phi_{\text{PSII,SP}} = 0.25; 0.2; 0.15$).

Furthermore one cultivation experiment was conducted without UVB-radiation using the results as reference for “unstressed” growing.

3.2.3. Offline measurements

Before the start of the UVB-treatments offline samples from the reactors were taken. These samples were used for the determination of the initial values which were not UVB-influenced.

For further *offline* measurements samples from the reactors were taken every 12 – 14 h during the cultivation experiments.

3.2.3.1. Offline photometric measurements

The optical density was measured at 750 nm in a spectrophotometer (U-1100, HITACHI, Tokyo, Japan) by using 2 mL samples. If the density was above a value of 0.8, the samples were diluted with BG11 medium. Then, the optical density was calculated by using the dilution volume.

3.2.3.2. Determination of the biological dry mass (BDM)

For the measurement of the dry mass, a 2 mL sample was taken. The sample was filtered through a combusted and weighed glass microfibre filter (\varnothing 25 mm, Whatman, Brentfort, UK). The filter was heated (104 °C) for 24 h and weighed again. The difference between the weights was used for the calculation of the biological dry mass. All samples were measured in triplicate and average and standard deviation were calculated.

3.2.3.3. Growth rate μ

During turbidostatic processes the growth rate μ of the cultivated microorganisms can be calculated by the following expression:

$$\mu = \frac{\Delta V_R}{V_L \cdot \Delta t} \quad (3.4)$$

where μ is the growth rate, V_L is the liquid reactor volume, ΔV_R is difference of the added volume of fresh medium and Δt is the considered time slice. The growth rates were calculated every 24 h and normalised to the growth rate before the UVB-radiation started.

3.2.3.4. Freeze-drying of reactor samples

Reactor samples were stored at $-80\text{ }^\circ\text{C}$ for at least 24 h. Subsequently the samples were dried under vacuum at $-90\text{ }^\circ\text{C}$ using a freeze-dryer (FREEZE-DRYTM MP, FTS[®] Systems, Inc, New York, USA) for 24 h.

3.2.3.5. Pigment analyses

Pigment composition of the microorganisms were measured according to the High Performance Liquid Chromatography (HPLC)-method described by Mantoura et al. (1983). 1 mL samples of the reactor suspension were centrifuged, frozen at $-80\text{ }^\circ\text{C}$ and subsequently freeze-dried. In this state, the samples were mixed for extraction with 2 mL ethanol and stored in a cooled ($4\text{ }^\circ\text{C}$) ultrasonic bath for 90 min. The extracts were injected through $0.2\text{ }\mu\text{m}$ PTFE-filter (A-Z Analytik-Zubehoer, Langen, Germany) into glass tubes for the HPLC-analysis. All samples were measured in triplicate. Average and standard deviation were calculated. The measurements were normalised to the first measurement.

3.2.3.6. Measurements of the phycobilisomes

The phycobilisomes content was measured according to Götzt et al. (1999). 1 mL of freeze-dried reactor samples were homogenised with 2 mL 0.2 M Tris-HCl-buffer (pH 7.5) and 1 mg lysozyme. Afterwards the prepared samples were continuously shook for 24 h at $30\text{ }^\circ\text{C}$. Subsequently after centrifugation (3500 rpm ; $4\text{ }^\circ\text{C}$; 10 min) the supernatant was measured spectrophotometrically (Uvikon XL, Bio-Tek Instruments, Bad Friedrichshall, Germany)

against a cuvette filled with Tris-HCl-buffer and 1 mg lysozyme. For a relative comparison of the samples the area between 640 and 550 nm was calculated (A_{Phyco}). Samples were measured in triplicate. Average and standard deviation were calculated and the samples were normalised to the first measurement.

Phycobilisome degradation rates were evaluated on the basis of the normalised phycobilisome values by using a simple exponential function

$$A_{\text{Phyco}} = A_{\text{Phyco},0} \exp\left(-\frac{t}{T_{\text{DR}}}\right) + A_{\text{OFF}} = A_{\text{Phyco},0} \exp(-k_{\text{DR}} t) + A_{\text{OFF}} \quad (3.5)$$

with A_{Phyco} is the calculated area, $A_{\text{Phyco},0}$ is the amplitude of the exponential function, A_{OFF} is an offset, and t is the process time. T_{DR} is used as a parameter for calculating the degradation rate (k_{DR}) of the investigated microorganisms.

3.2.3.7. Mycosporine-like amino acids (MAAs)

A modified protocol described by Korbee et al. (2004) was implemented for the determination of mycosporine-like amino acids.

10 mL of freeze-dried reactor samples were mixed with 2 mL methanol (20 %; pH 7) and stored at 45 °C for 2.5 h. After centrifugation for 30 min at 4 °C and 3500 rpm the supernatant were injected through 0.2 µm PTFE-filter (A-Z Analytik-Zubehoer, Langen, Germany) into HPLC compatible test tubes.

The HPLC solvents were 100 % methanol and 0.005 M oxalic acid dehydrate ($\text{C}_2\text{H}_2\text{O}_4 \cdot 2\text{H}_2\text{O}$) solution. The methanol flow rate was adjusted at 0.21 mL min⁻¹. The flow rate of the oxalic acid solution was 0.09 mL min⁻¹. The HPLC-column was a Phenomenex (250x3 mm). During the measurements a pressure of 95 – 100 bar occurred.

3.2.3.8. α-Tocopherol measurements

The α-tocopherol concentration of the cells was measured by using 10 mL samples from the reactor suspension. The samples were freeze-dried. For the extraction of α-tocopherol the samples were mixed with 3 mL of 100 % methanol. Subsequently the samples were homogenised 30 s on ice with an ULTRA-TURRAX T25 (IKA-Labortechnik, Staufen, Germany). Afterwards, the homogenates were injected through 0.2 µm PTFE-filter (A-Z

Analytik-Zubehoer, Langen, Germany) into HPLC compatible test tubes. The HPLC solvent was 100 % methanol with a beginning flow rate of 1 mL min⁻¹. After 2 min the flow rate was linearly increased up to 3 mL min⁻¹ within 3 min and kept constant for the next 10 min. Afterwards the flow rate was linearly decreased within 2 min from 3 mL min⁻¹ to 1 mL min⁻¹. The HPLC-column was a Nucleosil 100-5 C18 (250x4 mm). α -Tocopherol was measured at a wavelength of 340 nm and an excitation wavelength of 296 nm. As reference and for a calibration curve a α -tocopherol standard (Fluka, Buchs, Switzerland) was run under the same conditions. Samples were measured in duplicate. Average and standard deviation were calculated and the measurements were normalised to the first measurement.

3.2.3.9. Antioxidative potential of reactor samples

The antioxidative potential was determined by using the 2,2-diphenyl-1-picrylhydrazyl (DPPH) radical (Fluka, Buchs, Switzerland). 10 mL samples were freeze-dried and solved in 3 mL methanol (100%). The samples were homogenised 30 s on ice with an ULTRA-TURRAX T25 (IKA-Labortechnik, Staufen, Germany) and the homogenates were injected through 0.2 μ m PTFE-filter (A-Z Analytik-Zubehoer, Langen, Germany) into test tubes for further analyses.

1.85 mL methanol, 0.5 mL extract and 0.15 mL DPPH stock solution (resulting in a DPPH concentration of 76 μ mol L⁻¹) were mixed in the measuring cuvette. Additionally a reference cuvette filled with 2 mL methanol and 0.5 mL extract was prepared. Both cuvettes were kept in the dark at ambient temperature. After 30 min the absorbance at 550 nm was detected by measuring the measuring cuvette against the reference cuvette. The absorbance was compared with the absorbance of a cuvette filled with 2.35 mL methanol and 0.15 mL DPPH stock solution (also kept in the dark at ambient temperature).

Samples were measured in duplicate. Average and standard deviation were calculated. The measurements were normalised to the first measurement before the UV-illumination started.

4. Results of the piloting tests

The approaches in this chapter are designed to test both the method of measuring antioxidative potential and the performance of the photobioreactor system and its technical equipment. Furthermore, the development of a new cultivation process is presented which is used for further experiments.

4.1. Testing the method of determining antioxidative potential

4.1.1. Wavelength scans

Wavelength scans served to find the optimum wavelength for the measurement of antioxidant potential. They were obtained from single extracts of the microorganisms. In Fig. 4.1, wavelength scans of reference and measuring cuvette of methanolic extracts of *Synechocystis* sp. PCC6803 are shown.

Whereas the signal from the reference cuvette remained constant in the time between the two measurements at 0 and 30 min (coincident curves in Fig. 4.1) the measuring cuvette showed an absorbance decrease below 530 nm after 30 min of DPPH addition. After adding α -tocopherol to this cuvette, the decrease continued. But the absorbance decrease below 530 nm in the measuring cuvette in the presence of α -tocopherol was not representative for all extracts.

In contrast to results below 530 nm, the absorbance measured at 550 nm obtained the same value in the measuring cuvette after adding α -tocopherol (Fig. 4.1) as the absorbance measured in the reference cuvette.

Nevertheless, for all tested extracts a minimum occurred near 550 nm, and same values were obtained in the measuring and in the reference cuvette at 550 nm after adding α -

tocopherol. Therefore, 550 nm was selected as the most adequate wavelength for testing all microorganisms extracts.

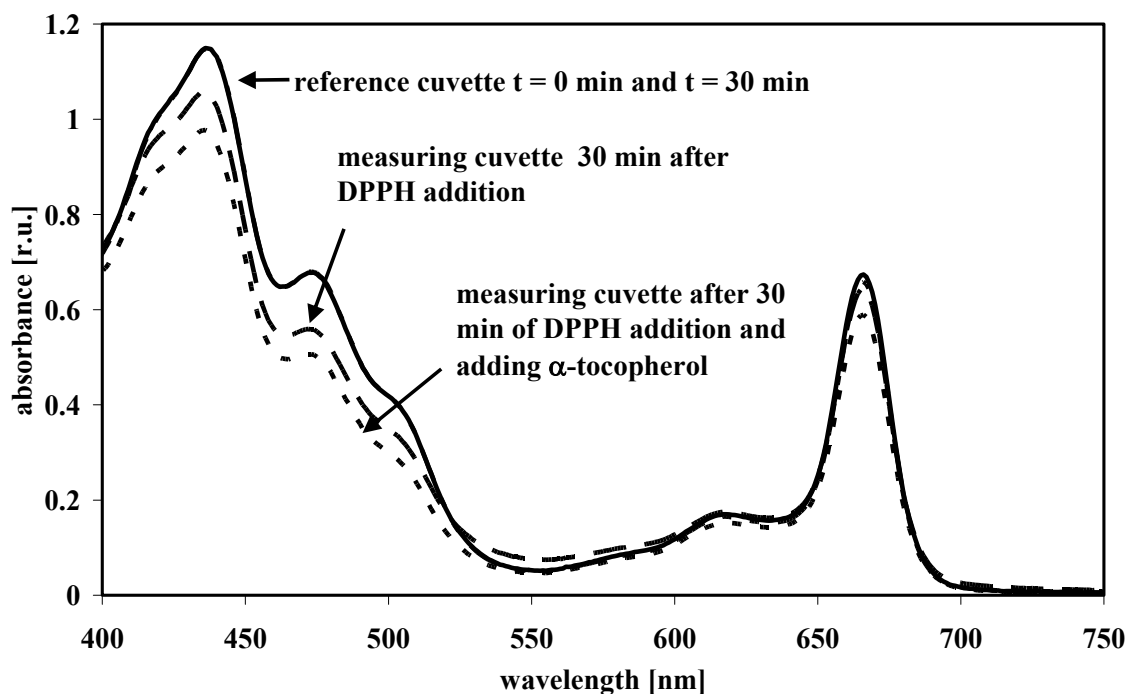


Figure 4.1. Wavelength scans of *Synechocystis* sp. PCC 6803. Both measuring and reference cuvette are measured against pure methanol.

4.1.2. Dependence of absorbance from extract concentration

The absorbance measurements were done by the same protocol for all five species of microorganisms. In Fig. 4.2 below, representative records for two species of microorganisms are shown. The good signal-noise ratio for all measurements enables a straight-forward interpretation of the data.

Absorbance measurements were done for two concentrations of DHHP. After adding oxidised DPPH (as a radical) to the cuvette, the absorbance increases according to the wavelengths scans in Fig. 4.1 at 550 nm. This increase is not shown in the following graphs. In the graphs, the first data point at extract concentration zero is that one obtained after this initial jump. From this point, the signal decreased when DPPH is reduced with increasing extract concentration. The value "0" at the y-axis is that of the extract without DPPH.

Absorbance measurements were done for two concentrations of DHHP. In Fig. 4.2A, both curves obtained from *Synechocystis* sp. PCC 6803 start with linear, parallel decreases at

low extract concentration and end up in horizontal lines. The lower curve approaches values close to zero at approximately 3 g L^{-1} extract concentration. The upper curve saturates at $20 \text{ }\mu\text{mol L}^{-1}$ DPPH concentration.

Figure 4.2B displays the effect of α -tocopherol on the absorbance measurements at 550 nm for *Synechocystis* sp. PCC 6803. The response to adding α -tocopherol after the DPPH treatment indicates that the remaining DPPH radicals are responsible for the remaining absorbance in Fig. 4.2A. The addition of α -tocopherol causes a nearly complete decrease of the absorbance to values close to zero. Since this occurs for all extract concentrations it becomes evident that the remaining signal in the absorbance decrease in Fig. 4.2A is due to DPPH radicals not reduced by the extract concentrations of *Synechocystis* sp. PCC 6803.

Figure 4.3A and Fig. 4.3B present results obtained from *Isochrysis galbana*. Similar to the measurements of *Synechocystis* sp. PCC 6803, the measurements at low and high DPPH concentrations in Fig. 4.3A show also a linear, parallel decrease at low extract concentrations.

Again, the curves obtained at both DPPH concentrations saturate at higher extract concentrations. However, in contrast to the upper curve in Fig. 4.2A, the upper curve in Fig. 4.3A reaches values near zero. Again, adding α -tocopherol shows that the remaining absorbance in Fig. 4.3A is due to unreduced DPPH radicals, as it decreases the absorbance to values close to zero (Fig. 4.3B).

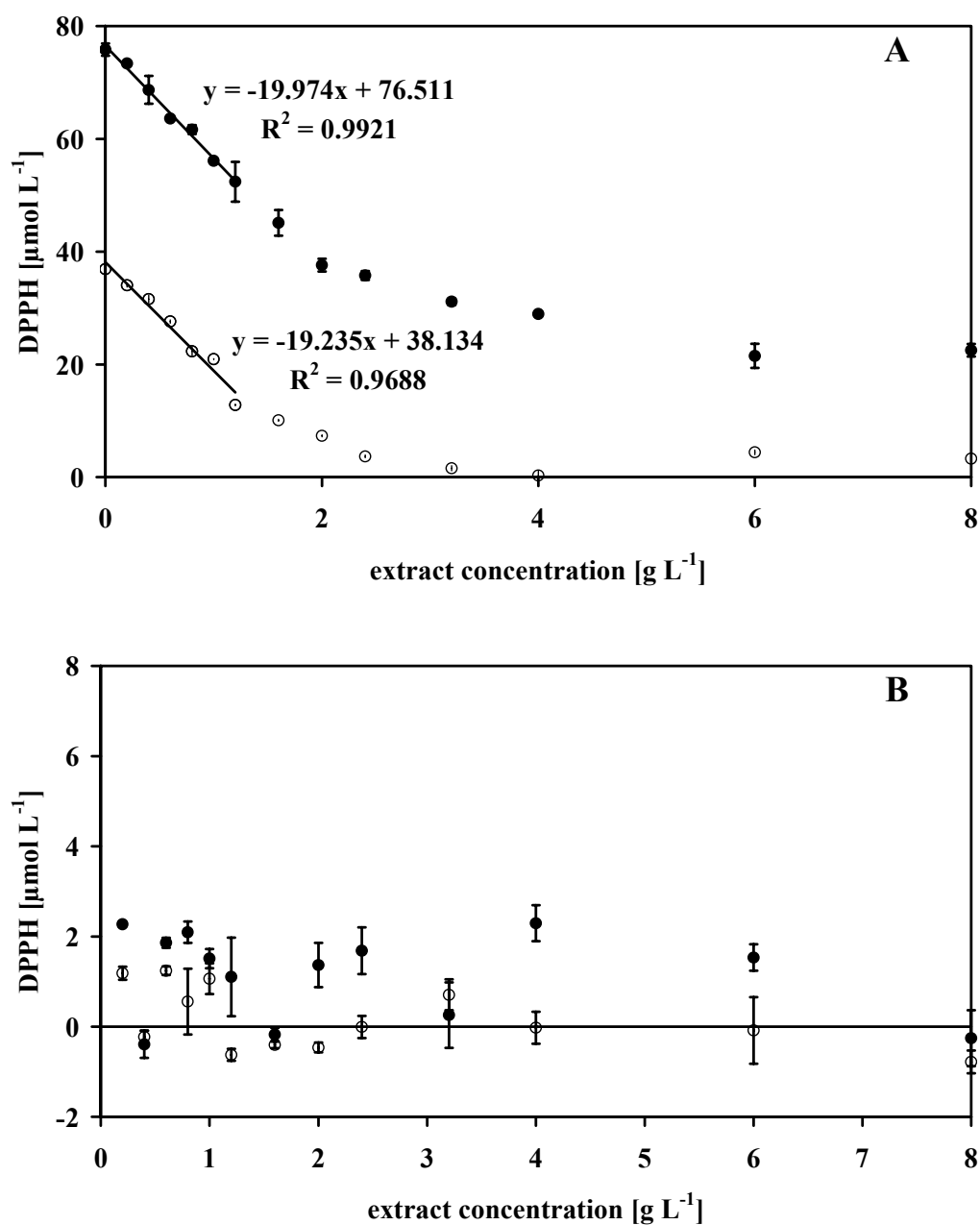


Figure 4.2. Concentration of DPPH radicals measured at 550 nm for *Synechocystis* sp. PCC 6803. The concentration was calculated by inserting the absorption value at 550 nm in Eq. 3.1. Open circles represent the data for using the low DPPH concentration ($38 \mu\text{mol L}^{-1}$). Closed circles represent the data for using the high DPPH concentration ($76 \mu\text{mol L}^{-1}$). (A) without α -tocopherol (B) after adding α -tocopherol.

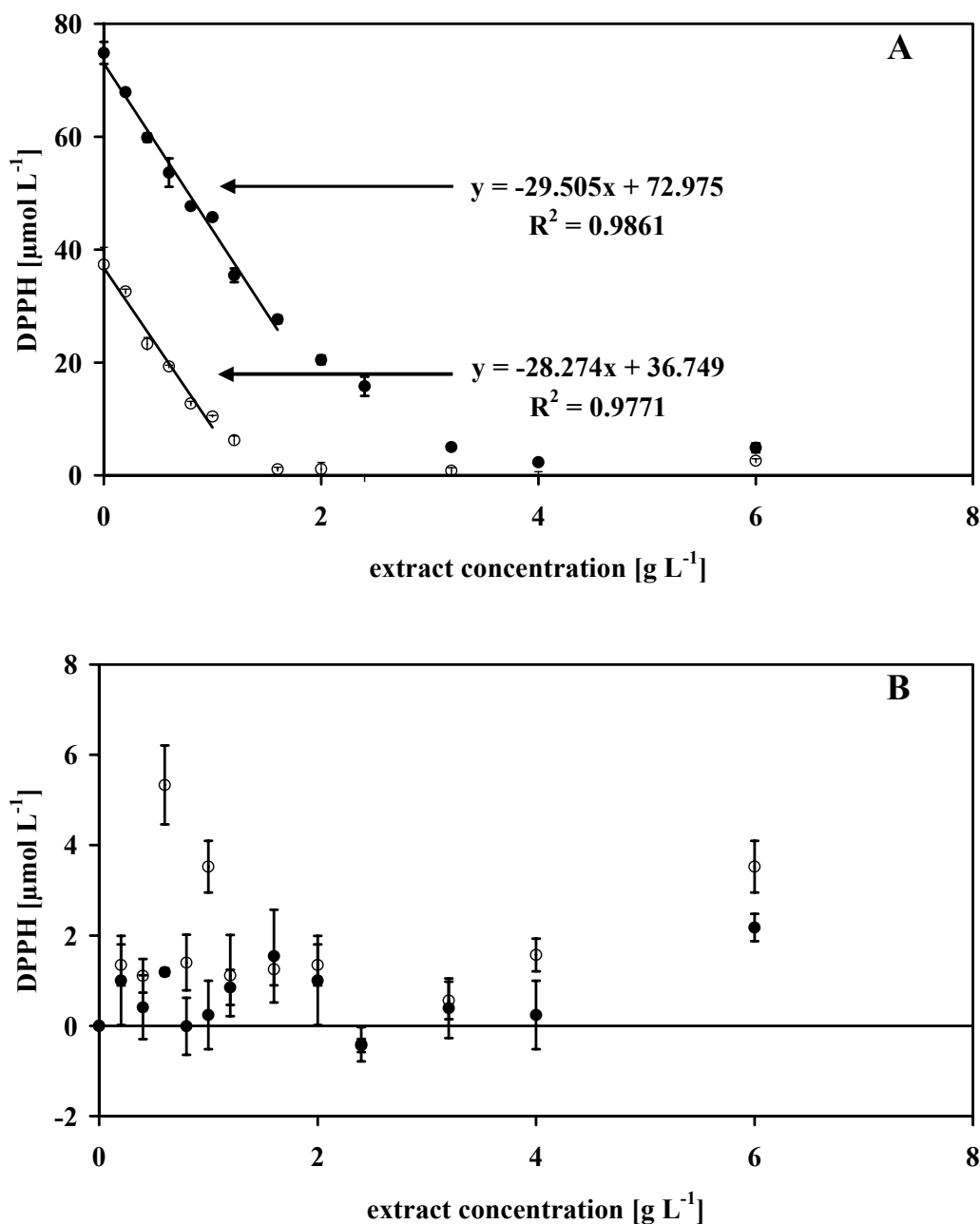


Figure 4.3. Concentration of DPPH radicals measured at 550 nm for *Isochrysis galbana*. The concentration was calculated by inserting the absorption value at 550 nm in Eq. 3.1. Open circles represent the data for using the low DPPH concentration ($38 \mu\text{mol L}^{-1}$). Closed circles represent the data for using the high DPPH concentration ($76 \mu\text{mol L}^{-1}$). (A) without α -tocopherol (B) after adding α -tocopherol.

4.1.3. Theoretical background

DPPH is added to the extract in its oxidized form and is reduced by the antioxidants in the extract. Describing the reaction of DPPH with the antioxidant as a bimolecular reaction leads to



with $[\text{DPPH}]_{\text{OX}}$ being the amount of added DPPH radicals, A_{OX} is the amount of antioxidants oxidized by DPPH, $[\text{A}]_{\text{RED}}$ is the remaining amount of reduced antioxidants in the extracts, DPPH_{RED} is the amount of reduced DPPH radicals, and k_1 and k_{-1} are rate constants. With

$$A_{\text{RED}} + A_{\text{OX}} = A_{\text{SOL}} \quad \text{and} \quad \text{DPPH}_{\text{RED}} + \text{DPPH}_{\text{OX}} = \text{DPPH}_{\text{T}} \quad (4.2 \text{ a,b})$$

where A_{SOL} is the amount of antioxidants initially extracted from the algae and DPPH_{T} is the total amount of added DPPH radicals, the following steady state concentrations can be calculated.

$$\frac{[\text{DPPH}]_{\text{RED}}}{[\text{DPPH}]_{\text{T}} - [\text{DPPH}]_{\text{RED}}} = \frac{k_1 ([A]_{\text{SOL}} - [A]_{\text{OX}})}{k_{-1} [A]_{\text{OX}}} \quad (4.3)$$

For high values of $[\text{DPPH}]_{\text{T}}$, the following simple equivalences are obtained

$$\lim_{[\text{DPPH}]_{\text{T}} \rightarrow \infty} [A]_{\text{OX}} = [A]_{\text{SOL}} \propto [\text{DPPH}]_{\text{RED}} \quad (4.4).$$

In Fig. 4.2A, where $[\text{DPPH}]_{\text{OX}}$ comes close to zero, this can only hold if k_1/k_{-1} is very high, i.e., if DPPH reduction is quite irreversible. Under this condition, the maximum decrease in the absorbance signal is independent of the amount of added $[\text{DPPH}]_{\text{T}}$. The amount of reduced DPPH radicals is proportional to the amount of oxidized antioxidants. These implications of Eq. 4.4 verify the results of Figs 4.2A and 4.3A.

Saturation as observed in Figs 4.2A and 4.3A is related to the methanolic extraction of antioxidants from the microorganisms samples. This can be described as follows



$$A_{US} \cdot S_F^n = \frac{k_2}{k_1} A_{SOL} \quad (4.6)$$

with A_{US} being the amount of undissolved antioxidant [mol]. A_{SOL} is the amount of antioxidants initially extracted from the microorganisms [mol], S_F is the amount of free solvent [mol], n is the number of mols of solvent necessary for binding one mol antioxidants, and k_1 and k_2 are rate constants. As the system is not open, the mass of law conservation holds:

$$A_T = A_{US} + A_{SOL} \quad \text{and} \quad S_T = S_F + n \cdot A_{SOL} \quad (4.7 \text{ a,b})$$

with A_T being the total amount of antioxidant [mol] and S_T being the total amount of solvent [mol]. Inserting Eq. 4.7 into Eq. 4.6 and using

$$K = \frac{k_2}{k_1} \quad (4.8)$$

leads to

$$(A_T - A_{SOL}) \cdot (S_T - n \cdot A_{SOL})^n = K \cdot A_{SOL} \quad (4.9).$$

Rearranging Eq. 4.9 results in

$$(S_T - n \cdot A_{SOL})^n - \frac{K \cdot A_{SOL}}{A_T - A_{SOL}} = 0 \quad (4.10).$$

With A_T being very high, Eq. 4.10 obtains a simpler form

$$(S_T - n \cdot A_{SOL})^n = 0 \quad (4.11).$$

Equation 4.11 is correct only when

$$\lim_{A_T \rightarrow \infty} A_{SOL} = \frac{S_T}{n} \quad (4.12).$$

Equation 4.12 still holds when $A_T \gg (K \cdot A_{SOL})$. This result explains the saturation effect of the solvent with increasing A_T in Figs 4.2A and 4.3A. The dissolved amount of antioxidants is limited by the capacity of the solvent.

4.1.4. Data analyses

The analysis of the absorbance measurements was done by means of Eq. 3.2 for each extract (listed in Tab. 4.1). The determination of the slope was restricted to the range of low concentrations. It revealed different slopes for different microorganisms. The values for both high and low DPPH concentrations are presented in Table 4.1.

The highest slope is determined for *Anabaena* sp. ($34.45 \mu\text{mol DPPH [g extract]}^{-1}$ for a measurement starting with the high DPPH concentration and $31.74 \mu\text{mol DPPH [g extract]}^{-1}$ for a measurement starting with the low DPPH concentration) followed by *Isochrysis galbana* ($29.51 \mu\text{mol DPPH [g extract]}^{-1}$ and $28.27 \mu\text{mol DPPH [g extract]}^{-1}$). The difference of the slopes between *Synechocystis* sp. PCC6803 ($19.97 \mu\text{mol DPPH [g extract]}^{-1}$ and $19.24 \mu\text{mol DPPH [g extract]}^{-1}$) and *Phaeodactylum tricornutum* ($20.58 \mu\text{mol DPPH [g extract]}^{-1}$ and $18.71 \mu\text{mol DPPH [g extract]}^{-1}$) is low. A minimum slope is obtained from *Porphyridium purpureum* ($7.26 \mu\text{mol DPPH [g extract]}^{-1}$ and $5.97 \mu\text{mol DPPH [g extract]}^{-1}$).

The calculated effective concentrations (EC_{50}) of the different extracts obtained from experiments like those in Figs 4.2 and 4.3 are shown in Table 4.1. EC_{50} of *Anabaena* sp. is 1.103 g extract in the absorbance measurement starting with the high DPPH concentration and 0.599 g extract in the measurement starting with the low DPPH concentration. *Isochrysis galbana* reaches values of 1.285 g extract and 0.672 g extract, respectively. The EC_{50} values of *Synechocystis* sp. PCC6803 (1.902 g extract and 0.985 g extract) and *Phaeodactylum*

tricornutum (1.847 g extract and 1.016 g extract) are in the same range. *Porphyridium purpureum* (5.235 g extract and 3.182 g extract) reaches the highest EC₅₀ values.

Table 4.1. Comparison of the slopes of the absorbance measurements, correlation coefficients and calculated EC₅₀ values of the different microorganisms samples and α -tocopherol. The EC₅₀ value expresses the amount of microorganisms extract necessary to decrease the absorbance of DPPH by 50 % (Antolovich *et al.*, 2002).

High DPPH concentration (76 μM)			
Microorganisms	Slope [μ mol DPPH g ⁻¹ extract]	R²	EC₅₀ [g extract]
<i>Anabaena</i> sp.	34.45	0.994	1.103
<i>Isochrysis galbana</i>	29.51	0.986	1.288
<i>Synechocystis</i> sp. PCC6803	19.97	0.992	1.902
<i>Phaeodactylum tricornutum</i>	20.58	0.968	1.847
<i>Porphyridium purpureum</i>	7.26	0.978	5.234
α -Tocopherol	3300.3	0.999	0.0115

Low DPPH concentration (38 μM)			
Microorganisms	Slope [μ mol DPPH g ⁻¹ extract]	R²	EC₅₀ [g extract]
<i>Anabaena</i> sp.	31.74	0.998	0.599
<i>Isochrysis galbana</i>	28.27	0.977	0.672
<i>Synechocystis</i> sp. PCC6803	19.24	0.969	0.988
<i>Phaeodactylum tricornutum</i>	18.71	0.996	1.016
<i>Porphyridium purpureum</i>	5.97	0.992	3.182

4.2. Pilot studies for the design of the physiostat

4.2.1. Batch process

A batch process is a process without any care. The cells are added to the nutrient solution and grow until the nutrients become limiting. This process is used here because BDM and OD change with time and provide a wide range of data for enable the test of sensor for the OD measurements. This is done by checking whether the OD_{inline} data have a unambiguous relationship to $OD_{offline}$ (measured in a cuvette) and to BDM. The results in Fig. 4.4. show that the relationship between OD_{inline} and BDM and $OD_{offline}$ can be fitted by an exponential growth as expected from theoretical considerations. Thus, both graphs in Fig. 4.4 were fitted with the following functions.

$$A: \quad BDM_{fit} = 0.120 \cdot \exp(OD_{inline}/0.921) \quad (4.13)$$

$$B: \quad OD_{fit} = 0.142 \cdot \exp(OD_{inline}/0.643) \quad (4.14)$$

The regression coefficients (BDM_{fit} , $R^2 = 0.968$, OD_{fit} , $R^2 = 0.990$) show the high reliability of the relationship between the *inline* measured optical density and the *offline* measurements.

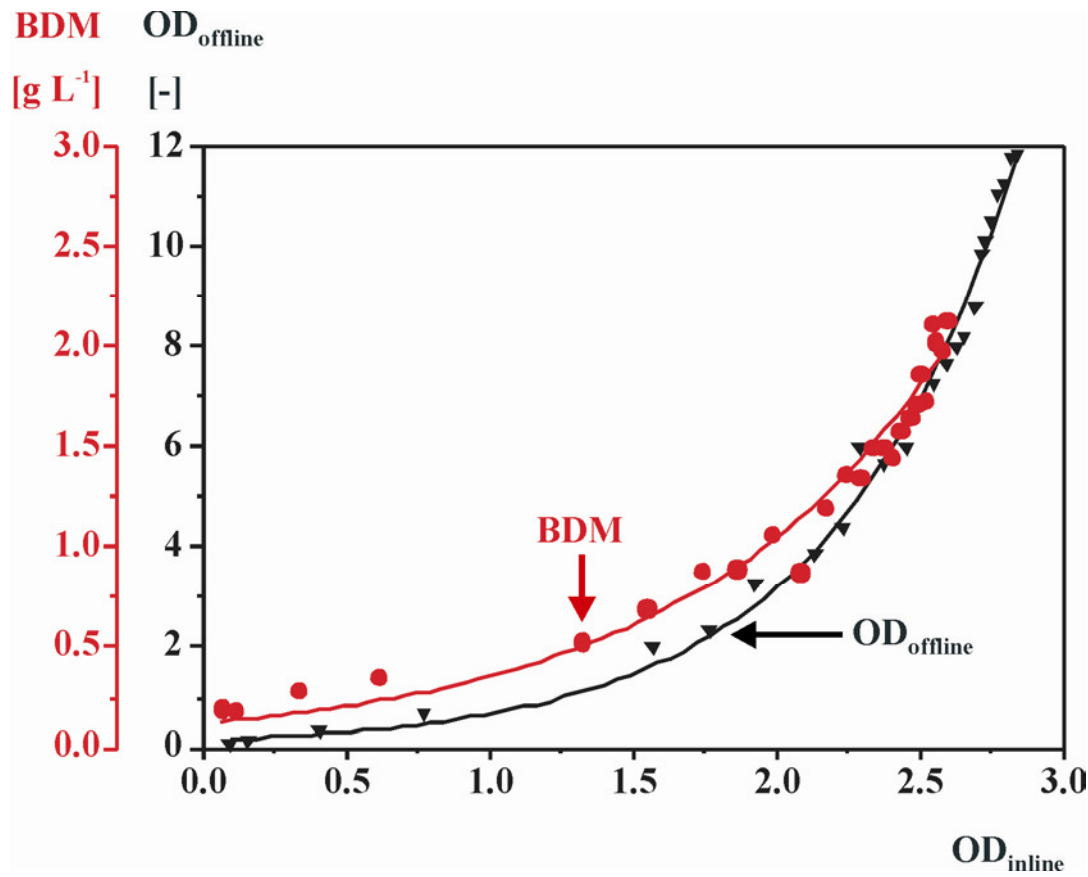


Figure 4.4. Comparison of the biological dry mass (BDM) and *offline* measured optical density (OD_{offline}) with the *inline* measured optical density (OD_{inline}) of *Synechocystis* sp. PCC 6803. The data were fitted by means of Eq. 4.13 and 4.14.

4.2.2. Fluorescence characteristics of the turbidostatic process influenced by UVB-radiation

In the adaptation phase, the cells in all four photobioreactors grew in batch-like processes solely under PAR irradiation. At $t_1 = 78$ h (Fig. 4.5), the turbidostatic process started. The suspension density was maintained at an optical density OD of 1.35 with fresh medium from the reservoir. The addition of fresh medium avoided possible nutrient limitations. The fluorescence signals F and F_M' (Fig. 3.3) and the calculated photosynthetic efficiency ϕ_{PSII} of PSII still increase but at much lower rates than during the non OD-controlled phase (Fig. 4.5). These small increases justified the assumption that the cell number remained constant (due to the turbidostatic process), and that no changes of the light conditions in the reactor occurred.

Additional UVB irradiation ($1.53 \mu\text{mol photons m}^{-2} \text{s}^{-1}$) started at ($t_2 = 186 \text{ h}$) in three of the four photobioreactors. The fourth photobioreactor was used as a control without additional UVB-radiation. Figure 4.5 shows the induced changes of the actual photosynthetic efficiency ϕ_{PSII} (Eq. 3.3) of UVB-radiated cultures of *Synechocystis* sp. PCC 6803.

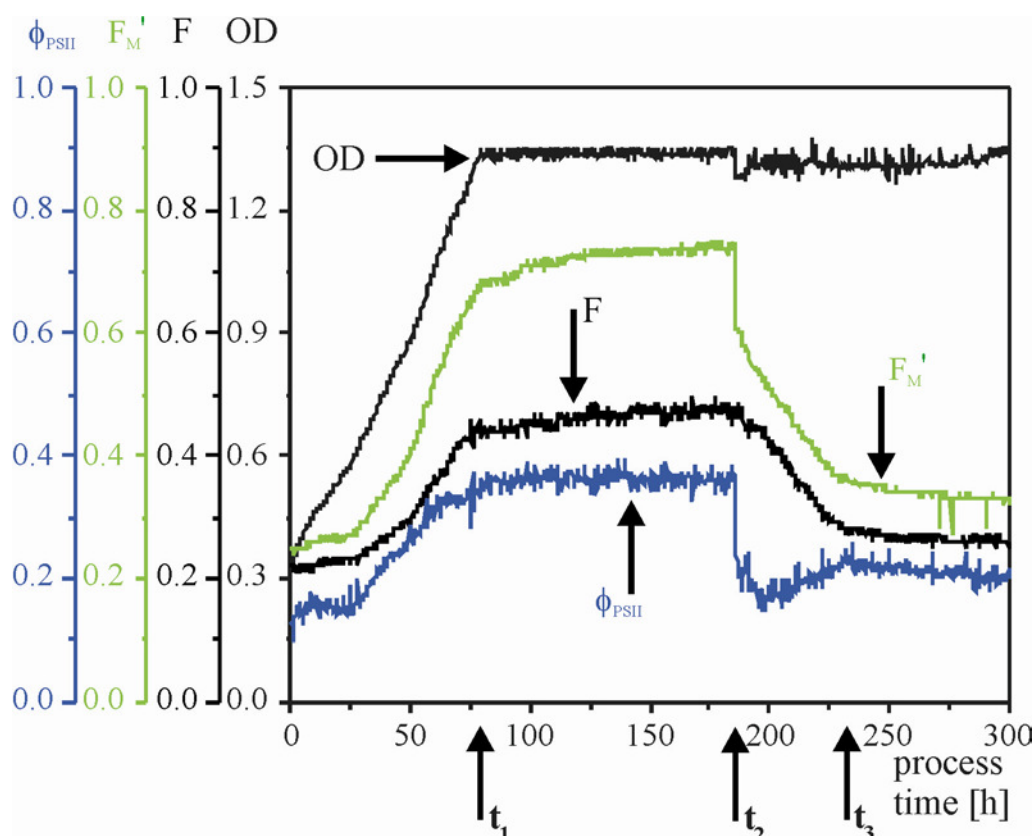


Figure 4.5. Turbidostatic process of *Synechocystis* sp. PCC 6803. t_1 = start of the turbidostatic process; t_2 = start of the UV-radiation; t_3 = the F-signal remains nearly constant whereas the F_M' -signal still decrease.

The F_M' -signal decreased approximately exponentially after $t_2 = 186 \text{ h}$ whereas the F-signal showed a linear decrease from $t_2 = 186 \text{ h}$. Then, a remarkable point was observed. At $t_3 = 230 \text{ h}$ (Fig. 4.5), the decays nearly stopped without any external stimulus. After t_3 (Fig. 4.5), the F-signal remains nearly constant whereas the F_M' -signal still decreases but at a lower rate than at the beginning of the UVB-radiation which is discussed below (Chapter 7).

The quantum yield ϕ_{PSII} (calculated by means of Eq 3.3) decreased rapidly during the first 12 h of UVB-radiation resulting from the rapid decrease in F_M' -decrease and the weak decrease in F . In the remaining 32 h before t_3 , ϕ_{PSII} increased again resulting from a stronger decrease of the F -signal (Eq. 3.3). During the next 32 h following t_3 both F - and F_M' -signals fell at nearly similar rates. Afterwards ϕ_{PSII} decreases again due to the constant value of the F -signal and the decreasing F_M' -signal.

Figure 4.6 shows the same data (photosynthetic efficiency ϕ_{PSII} and fluorescence signals) of the control reactor which is not UVB-radiated. The cultivation parameters were identical to the described process above. After $t_4 = 112$ h (Fig. 4.6) the turbidostatic process (the optical density is kept constant) started. The two fluorescence signals F and F_M' remained nearly constant during the OD-controlled phase until the end of the experiment.

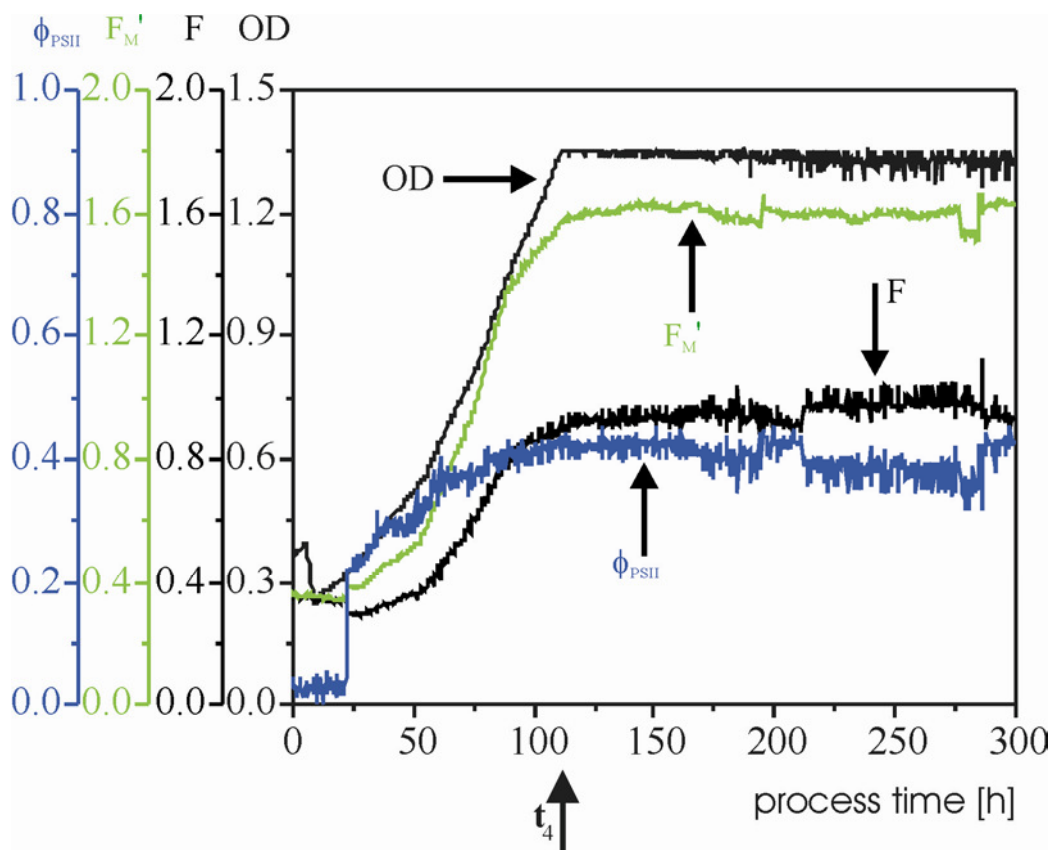


Figure 4.6. Turbidostatic process of *Synechocystis* sp. PCC 6803 in the reactor not radiated by UV. t_4 = start of the turbidostatic process.

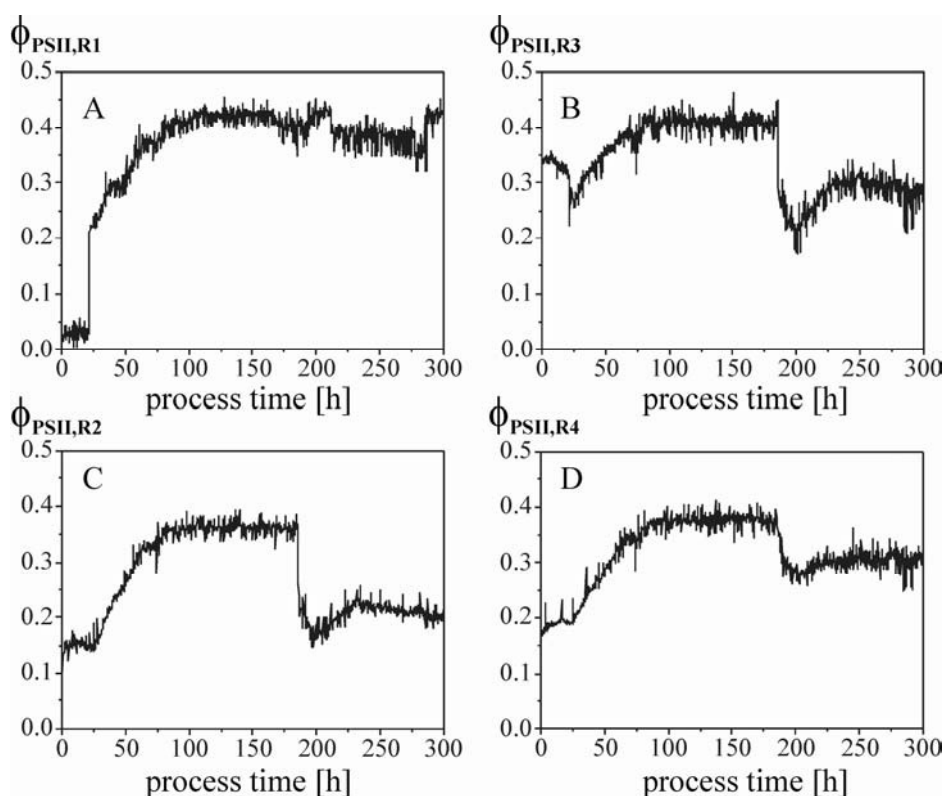


Figure 4.7. Comparison of all four reactors in turbidostatic processes of *Synechocystis* sp. PCC 6803. (A) $\phi_{\text{PSII,R1}}$ obtained from irradiation only with PAR. (B), (C), (D): $\phi_{\text{PSII,R2}}$, $\phi_{\text{PSII,R3}}$, $\phi_{\text{PSII,R4}}$ obtained under equal conditions, i.e., PAR with additional UV-radiation after $t_2 = 186$ h; $\phi_{\text{PSII,R1}}$ is part of Fig. 4.6.; $\phi_{\text{PSII,R2}}$ is part of Fig. 4.5.

In Fig. 4.7, the calculated actual photochemical efficiencies ϕ_{PSII} (Eq. 3.3) of all four photobioreactors are shown. The physiological signals of the three UVB-irradiated reactors in Fig. 4.7 B,C,D indicate the high reproducibility under UVB-radiation.

4.2.3. Determining the kinetic parameters for the design of the feed-back loop of the physiostat

The new facility of the reactor described here is the computer-controlled operation as physiostat. This mode enables the control of a physiological parameter as monitored by chlorophyll fluorescence. The crucial problem of feedback loop design is stability (Bode, 1964). In order to find a solution for a stable system the kinetic (temporal) behaviour of the system has to be investigated. For this issue, an input signal (like UVB-light) is required which exerts a measurable effect on the biological system and which facilitates a continuous modulation over a wide range of frequencies.

Characterisation of the system "microorganism" which is to be controlled can be achieved by the measurement of the kinetic (temporal) properties. The principal reproducibility of the ϕ_{PSII} -changes induced by UVB-radiation (Fig. 4.7) was the encouragement for the following experiments.

Here, the kinetic analysis is done by two different approaches: measuring frequency responses with sinusoidal input signals and measuring step responses by stepwise changes in the input signal.

4.2.4. Testing linearity of the system by sinusoidal modulation of UVB-intensity

For feed-back loop design, linearity of the system is an important advantage (Vanselow et al., 1988; Hansen et al., 1991). Thus, the linearity of the modulator of the UVB light source and of photosynthetic efficiency of PSII (ϕ_{PSII}) is checked first. The amplitude of the variable UVB-intensity was modulated with a constant frequency of 1.32 h^{-1} . The sine wave was superimposed to a constant offset of $0.65 \mu\text{mol photons m}^{-2} \text{ s}^{-1}$. The modulation started with an amplitude of $0.078 \mu\text{mol photons m}^{-2} \text{ s}^{-1}$. After a gap of at least 12 h in which the fluorescence signals (F , F_M') induced by visible light (chapter 3.2.1) could return to their initial values, amplitude and offset were increased gradually by steps of $0.08 \mu\text{mol photons m}^{-2} \text{ s}^{-1}$ until the upper limit of the linear range of UVB-intensity ($0.52 - 1.56 \mu\text{mol photons m}^{-2} \text{ s}^{-1}$) was achieved (for details see Table 4.2).

In the case of sinusoidally modulated UVB radiation, first the linear component has to be extracted from the time course of the response of ϕ_{PSII} . This can be done by fitting it as follows:

$$\phi_{\text{PSII,fit}} = A_1 \cdot \exp(-t/\tau_{\text{exp}}) + A_2 \cdot \sin(\omega \cdot t + \varphi) + A_3 \cdot t + A_4 \quad (4.15)$$

where A_1 , A_2 , A_3 , are the amplitudes of the related functions, A_4 is a constant offset, t is the process time, τ_{exp} is the time constant of the exponential function, ω is the angular frequency of the input signal ($\omega = 2 \pi f$, f being the frequency), and φ is the phase shift of the output signal. The theory of linear analysis predicts that A_1 , A_3 , A_4 , and τ_{exp} should be the same in Eq. 4.15 and 4.16 (see below). A_2 and φ are the parameters used for the test of linearity.

Table 4.2: UVB-amplitudes and offsets used in the test of linearity (Fig. 4.9). The frequency was 1.32 h^{-1} .

Amplitude ($\mu\text{mol photons m}^{-2} \text{ s}^{-1}$)	Offset ($\mu\text{mol photons m}^{-2} \text{ s}^{-1}$)
0.08	0.65
0.16	0.73
0.23	0.81
0.31	0.88
0.39	0.96
0.47	1.04

A typical response induced by the input signal employed in the linearity test is presented in Fig 4.8. Both the measured values of ϕ_{PSII} and the fitted data (Eq 4.15.) are shown. All experiments with modulated UVB-amplitudes were conducted threefold. Mean values and standard deviations of the fitted data were calculated. The amplitudes (X_a) obtained from fitting the ϕ_{PSII} -data plotted versus the different amplitudes (X_e) of the input

signal (UVB-intensity) lead to the “amplification” characteristic of the “system” microorganisms (Fig. 4.9). Figure 4.9 shows the linearity of the amplitude A_2 of the output signal ϕ_{PSII} and the constancy of the phase shift φ up to a maximum amplitude of the input signal of $0.39 \mu\text{mol photons m}^{-2} \text{s}^{-1}$. At higher amplitudes of UVB-intensity, a bending of the phase shift of ϕ_{PSII} indicates the end of the linear range.

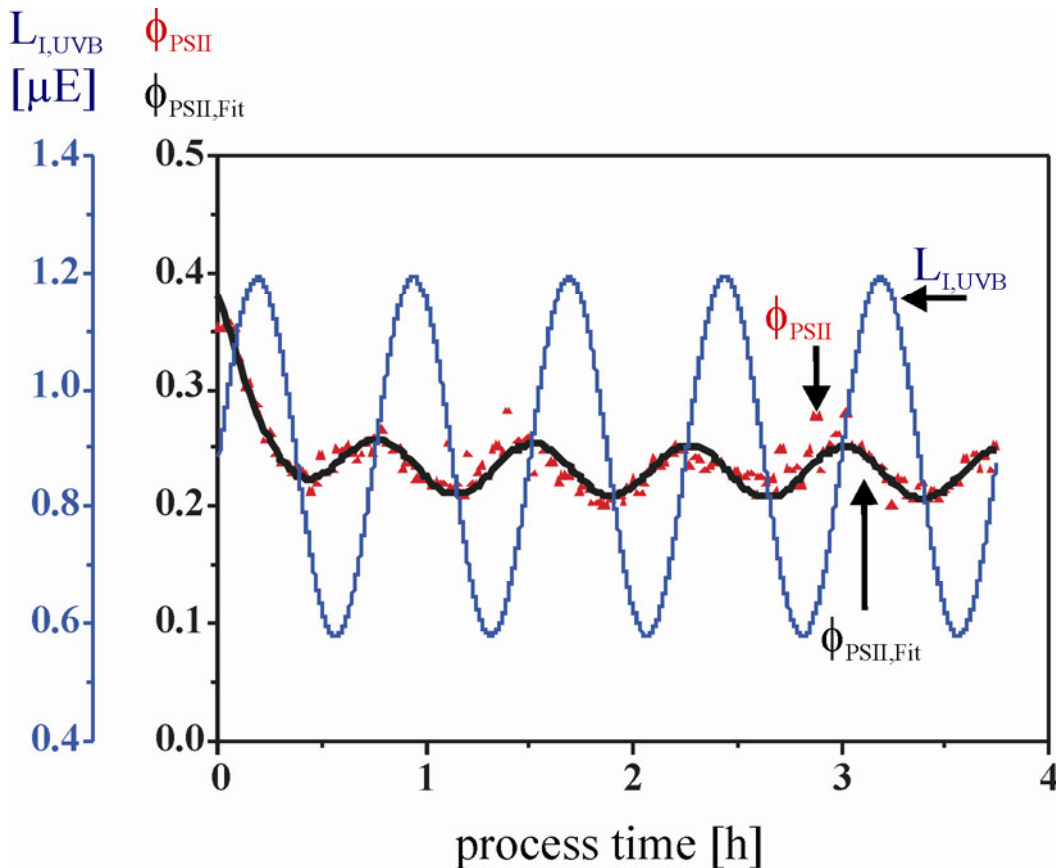


Figure 4.8. Typical chlorophyll fluorescence response induced by visible light to sinusoidally modulated UVB-intensity at a frequency of 1.32 h^{-1} . ϕ_{PSII} = measured actual photosynthetic efficiency of PSII; $\phi_{\text{PSII,Fit}}$ = fitted photosynthetic efficiency of PSII; $L_{\text{I,UVB}}$ = intensity of the UVB-radiation. $\mu\text{E} = \mu\text{mol photons m}^{-2} \text{s}^{-1}$.

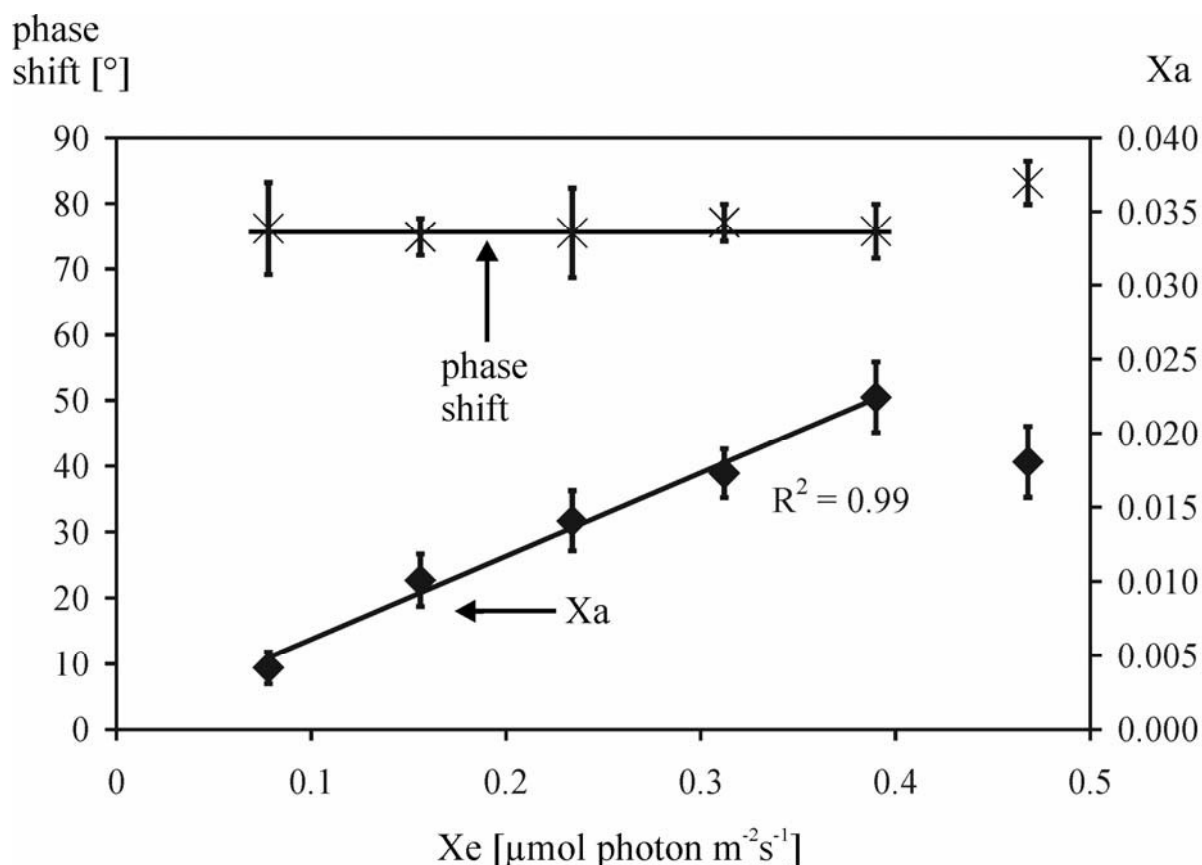


Figure 4.9. Linearity of the amplification factor of the “system” microorganisms. Changes in chlorophyll fluorescence were induced by sinusoidally modulated UV irradiation with different amplitudes (as given on the abscissa) at constant frequency. The linear component of the responses amplitude was obtained by fitting the responses of chlorophyll fluorescence by means of Eq. 4.15. X_e = amplitude of the input signal; $X_a = A_2$ = amplitude of the output signal; phase shift = φ = phase shift of the output signal.

4.2.5. Sinusoidal modulation of the UVB-intensity for frequency responses

A frequency response describes the dependence of the output signal (amplitude and phase shift) on the frequency of the sinusoidal input signal. For its measurement, the intensity of the UVB-radiation was modulated sequentially with sine waves of 8 different frequencies (0.09 h^{-1} , 0.175 h^{-1} , 0.4 h^{-1} , 0.99 h^{-1} , 1.32 h^{-1} , 1.85 h^{-1} , 3.93 h^{-1} , 8.84 h^{-1}). The amplitude of the input signal was constant (0.31 $\mu\text{mol photons m}^{-2}\text{s}^{-1}$) and superimposed to an constant offset of 0.83 $\mu\text{mol photons m}^{-2}\text{s}^{-1}$. Five periods of the high UVB-frequencies (0.4 h^{-1} - 8.84 h^{-1}) and three

periods of the low frequencies (0.09 h^{-1} , 0.175 h^{-1}) were applied and the responses evaluated by means of Eq. 4.15. The UVB-radiation was switched off after each frequency measurement. After a gap of at least 12 h, the measurement of the frequency response was repeated. The length of the gap was sufficient to let the chlorophyll fluorescence signals (F) measured before the start of the modulated UVB-radiation. The employed amplitude and offset and the used frequencies of the input signal are listed in Table 4.3.

Table 4.3: UVB-Amplitudes, offset and used frequencies used for the measurement of frequency response.

Amplitude ($\mu\text{mol photons m}^{-2} \text{ s}^{-1}$)	Offset ($\mu\text{mol photons m}^{-2} \text{ s}^{-1}$)	Frequency (h^{-1})
0.31	0.83	0.09
		0.175
		0.4
		0.99
		1.32
		1.85
		3.93
		8.84

In contrast to the previous experiment, here the density was lowered to a constant optical density of 0.8. Because of the averaging effect of mixing the cells in the circular stream, all cells received the same (averaged) amount of irradiation. Thus, a decrease of the optical density causes an increase of the average UVB-intensity per cell. The other cultivation parameters were identical to those in the previous experiments described above. All experiments were conducted threefold. Mean values and standard deviations were calculated (see Fig. 4.10 below).

4.2.6. Curve fitting of the frequency response for the determination of the transfer function of the “system to be controlled” microorganisms

Equation 4.15 can directly be used for the evaluation of the important parameters A_1 , A_3 , A_4 , and τ_{exp} . In the case of the sinusoidal modulation, the frequency responses $A(\omega)$ and $\varphi(\omega)$ have to be generated from the values A_2 and φ delivered by Eq. 4.15. These two frequency responses are jointly fitted by a so-called transfer function

$$A_2(\omega) \exp(j\varphi) = \sum_{i=1}^n \frac{K_i}{1 + j\omega \cdot \tau_i} \quad (4.16)$$

with n = number of processes, K_i = amplitude factor, τ_i = time constant and $j = \sqrt{-1}$.

Curve-fitting was done with a custom-made program using a simplex algorithm for the non-linear parameters (τ_i) and gaussian linear regression for the coefficients K_i (Lübke, 1991). The usage of complex numbers is avoided by splitting the terms in Eq. 4.16 in real and imaginary component before they are fitted.

4.2.7. Determination of the frequency responses of ϕ_{PSII}

Choosing an amplitude of $0.31 \mu\text{mol photons m}^{-2} \text{s}^{-1}$ in the linear range of UVB-intensity and ϕ_{PSII} (Figure 4.9) and an offset of $0.83 \mu\text{mol photons m}^{-2} \text{s}^{-1}$ (for working in the linear range of UVB-intensity and ϕ_{PSII}) enables the identification of the frequency response. The results of the phase shift φ and the ratios A_2/X_e of the amplitudes of the output to the input signal in relation to different frequencies are shown in Fig. 4.10.

The fit program (using Eq. 4.16 with $n = 2$) determined two time constants (τ_1 , τ_2) and two amplitude factors (K_1 , K_2) from the frequency response in Figure 4.10. The values of these parameters are given in Table 3.

4.2.8. Calculation of the transfer function of ϕ_{PSII}

The transfer function of the system to be controlled (Eq. 4.17) can be calculated from the parameters of Table 4.4 and converted to a quotient of polynomials in $j\omega = j2\pi f$

$$\begin{aligned}
 y(s) &= A_0 \frac{1 - j\omega Z_1}{(1 + j\omega\tau_1)(1 + j\omega\tau_2)} = \frac{K_p + 0.068}{1 + j\omega T_1 + (j\omega)^2 T_2} \\
 &= \frac{-0.033 + 0.068}{1 + j\omega 17.94 + (j\omega)^2 15.34}
 \end{aligned}
 \tag{4.17}$$

A_0 = Amplification factor coefficient of the system to be controlled

Z_1 = inverse zero (= +0.068 / 0.033)

τ_1 = time constant

τ_2 = time constant

K_p = transfer coefficient of the system to be controlled (= -0.033)

T_1 = compensation time of the system to be controlled (= $\tau_1 + \tau_2 = 17.94$ min)

T_2 = effective dead time of the system to be controlled (= $\tau_1 \cdot \tau_2 = 15.34$ min)

In Eq. 4.17, a serious problem becomes obvious. There is a positive zero of the transfer function ($Z_1 = +0.068 / 0.033$) which causes the strong phase shift visible in Fig. 4.10. This zero prevents that the characteristics of the system can be compensated by an additional network in order to speed up response time. Thus, the loop amplifications greater than 1 have to be restricted to very slow frequencies less than $0.68 / (0.033 \cdot 2\pi) \text{ h}^{-1}$. In addition, the loop amplifications greater one have to be implemented by an additional controller (see Fig. 4.12). This is done by the algorithm related to the Hurwitz criterion in section 4.2.10.2.

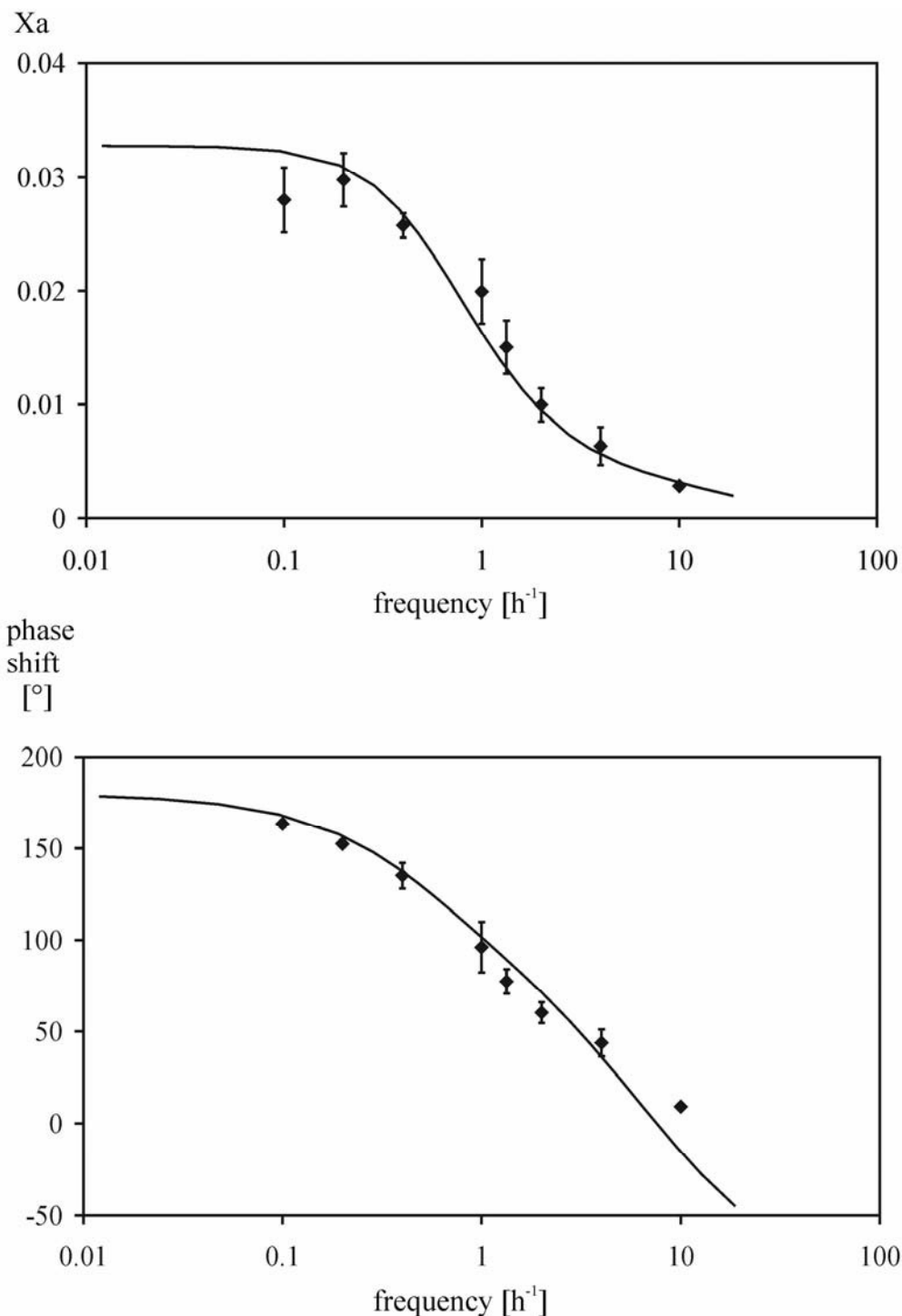


Figure 4.10. Frequency response of the “system” microorganisms. Results of the fitted chlorophyll fluorescence data in relation to the UVB-amplitudes of the input signal provoked by constant amplitude and varying frequencies. $X_a = A_2$ in Eq. 4.15 = amplitude of the output signal; phase shift = φ in Eq. 4.15 = phase shift of the output signal. The solid lines present the fitted data, i.e. amplitude and phase shift calculated from Eq. 4.16 with the parameters in Table 4.4 as determined by the fit program.

Table 4.4. Time constants and amplitude factors (Eq. 4.16) determined by the fit-program. The values results from three independent frequency responses with standard deviation.

i	τ	K
1	0.90 min \pm 0.26	0.00605 \pm 0.00055
2	17.04 min \pm 1.37	-0.0388 \pm 0.0052

4.2.9. Verifying of the transfer function by the ϕ_{PSII} -response induced by stepwise change in UVB-intensity

As an alternative to sinusoidal modulation, also a stepwise change in the input signal can be used for a kinetic analysis and may be employed as a test for the validity of the evaluated kinetic data. The cultivation parameters were identical to those in the previous experiment using sine waves. UVB-intensity was switched from 0 to 0.83 $\mu\text{mol photons m}^{-2} \text{s}^{-1}$ during a turbidostatic process and both chlorophyll fluorescence signals (F , F_M') were measured and ϕ_{PSII} was calculated by means of Eq. 4.18.

The ϕ_{PSII} -response to a stepwise change in UVB-intensity can fitted with the following equation:

$$\phi_{\text{PSII,fit}} = A_1 \cdot \exp(-t/\tau_{\text{exp}}) + A_3 \cdot t + A_4 \quad (4.18).$$

The first term presents an exponential decay with the time constant τ_{exp} . The second term corresponding to an integrator describes the light-induced adaptation of the microorganisms.

Figure 4.11 shows the chlorophyll fluorescence signals F and F_M' and the calculated ϕ_{PSII} induced by stepwise changed UVB-radiation (0.83 $\mu\text{mol photons m}^{-2} \text{s}^{-1}$). The sampling rate was 0.5 min^{-1} . It is obvious that first F_M' is influenced by the radiation. Thus, ϕ_{PSII} decreased due to the decline of the F_M' -signal. After switching on the UVB-radiation, the F_M'

decrease starts after 12 – 16 min. The fitting-analysis with Equation 4.18 delivers a time constant for the exponential decline of F_M' of 17.7 min. This time constant is close to the determined compensation time of the system to be controlled ($T_1 = 17.94$ min, Eq. 4.17) and verifies the transfer function of the system.

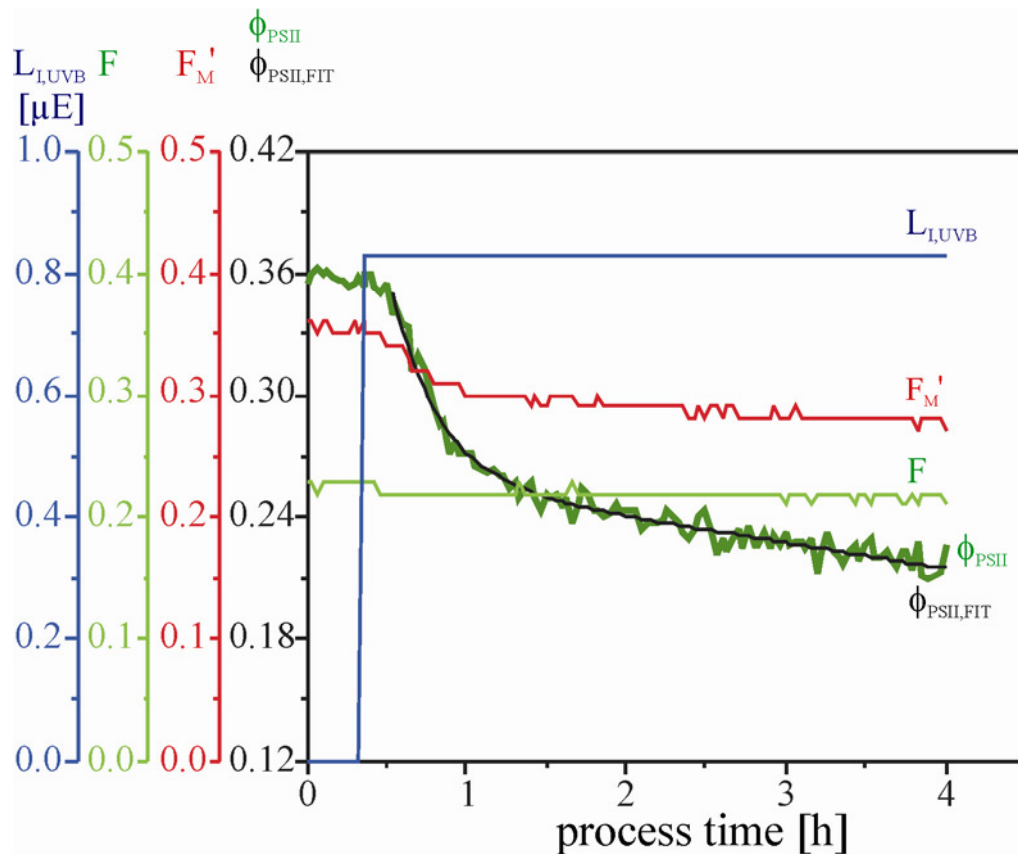


Figure 4.11. Changes of F , F_M' and ϕ_{PSII} induced by stepwise changes in UVB-radiation. ϕ_{PSII} is the photosynthetic efficiency of PSII (Eq. 3.3.), and the smooth line presents the fit by means of Eq. 4.18. $\mu E = \mu\text{mol photons m}^{-2} \text{ s}^{-1}$.

4.2.10. Design of the control loop

4.2.10.1. Transfer function of a PI-controller

For the control of UVB-fluorescence tube, a PI-controller is employed (Fig. 4.13; part of F_C) with the following transfer function

$$y(s) = K_P \cdot \left(1 + \frac{1}{sT_N} \right) \quad (4.19)$$

The function contains two characteristic parameters: the proportional gain K_P and the integral action coefficient T_N .

4.2.10.2. Stability of the control loop

The stability of control loops is the crucial requirement for a reliable control system. According to the law of Bode (1964), both loop amplification and the overall phase of the control loop have to keep certain conditions. The loop amplification has to decay with a 1/f slope and the phase shift has to remain within 0° - 180° . A further typical test of the stability of control loops is the *Hurwitz-criterion* which follows from work of Bode. This method for determining whether or not a system is stable is based on the evaluation of the coefficients in the system's characteristic equation which is defined as:

$$0 = 1 + F_{CS}(s) \cdot F_C(s) \quad (4.20)$$

where $F_{CS}(s)$ is the transfer function of the system to be controlled and $F_C(s)$ is the transfer function of the controller. Arranging the equation in ascending power of the s-terms leads to the individual coefficients (Eq. 4.21 to 4.24). They are used for the determination of the *Hurwitz-determinant* (Beretta et al., 1990).

For the stability of control loops the following conditions must be strictly adhered to:

1. The individual Hurwitz-coefficients have to be positive
2. The Hurwitz-determinant has to be positive

With this commensurate conditions it is possible to adjust the selected controller parameter (Eq. 4.19). A suitable adjustment should lead to a stabilisation of the control loop and enables a correct realisation of physiostatic processes.

4.2.10.3. Design of the PI-controller

Installing a PI-controller and solving the Hurwitz-criterion leads to the following Hurwitz-coefficients:

$$a_0 = K_P \cdot A_1 \quad (4.21)$$

$$a_1 = K_P \cdot (T_N \cdot A_1 + A_2) + T_N \quad (4.22)$$

$$a_2 = T_N \cdot (K_P \cdot A_2 + T_1) \quad (4.23)$$

$$a_3 = T_N \cdot T_2 \quad (4.24)$$

with $A_1 = -0.033$, $A_2 = 0.068$, $T_1 = 17.94$ min and $T_2 = 15.34$ min and K_P and $T_N =$ chosen value. The Hurwitz-coefficients a_0 , a_1 , a_2 , and a_3 are used for the calculation of the Hurwitz-determinant (Eq. 4.25).

The first Hurwitz-coefficient a_0 determines the controller mode. To fulfil the Hurwitz-criterion the proportional gain K_P has to be negative for a stable control loop. This negative proportional gain causes an inverse controller mode which means that an increase of ϕ_{PSII} induces an increase of the controller output. In addition, the Hurwitz-determinant, defined as

$$D = a_1 \cdot a_2 - a_3 \cdot a_0 \quad (4.25)$$

and with the condition that

$$0 \leq D \quad (4.26)$$

must be strictly adhered, enables the calculation of the critical integral action coefficient T_N at the limit where the control loop will be stable. The following equation for T_N is defined as:

$$T_N = \frac{K_P (A_1 T_2 - K_P A_2^2 - A_2 T_1)}{K_P (K_P A_1 A_2 + A_1 T_1 + A_2) + T_1} \quad (4.27)$$

The proportional gain was set to -1 ($K_P = -1$). The integral action coefficient was set to 0.3 min ($T_N = 0.3$ min) which is close to the critical value of T_N (0.09 min). This choice of the

integral gain should avoid the rapid increase of ϕ_{PSII} observed during the second experiment (see above, Figs. 4.5 and 4.7). Both K_P and T_N are adjustable (Eq. 4.19) via the process control system in which the PI-controller is installed. Figure 4.12 shows the frequency responses of the amplification factor Ampl and the phase shift of the controller, system to be controlled and the control loop. The controller conveys (for a loop amplification greater than 1) the phase shift of the system to be controlled into the stable range of $0^\circ - 180^\circ$.

The determination of the transfer function of the system to be controlled “microorganisms” enables the design of the control loop shown in Fig. 4.13. It is mainly characterised by two transfer functions both the system to be controlled (F_{CS}) and the controller transfer function (F_C). The following tasks depicted in Fig. 4.13 are converted by the process control system. ϕ_{PSII} is determined by using the chlorophyll fluorescence parameters F and F_M' (Eq. 3.3).

Afterwards the difference (e) between set point ($\phi_{\text{PSII,SP}}$) and actual value (ϕ_{PSII}) are calculated. This difference and the adjusted specific controller parameter (K_P and T_N) are used for the calculation of the controller output signal (y_C). This output signal (y_C) is converted into the gating signal of the UV-fluorescence tube for generating the UVB-intensity ($L_{\text{I,UVB}}$). Due to the defined cultivation condition no disturbance (z) is assumed. Disturbances like e.g. changes of the PAR intensities, changes of the temperature, provoke changes in ϕ_{PSII} and may lead in the worst case to a destabilisation of the control loop.

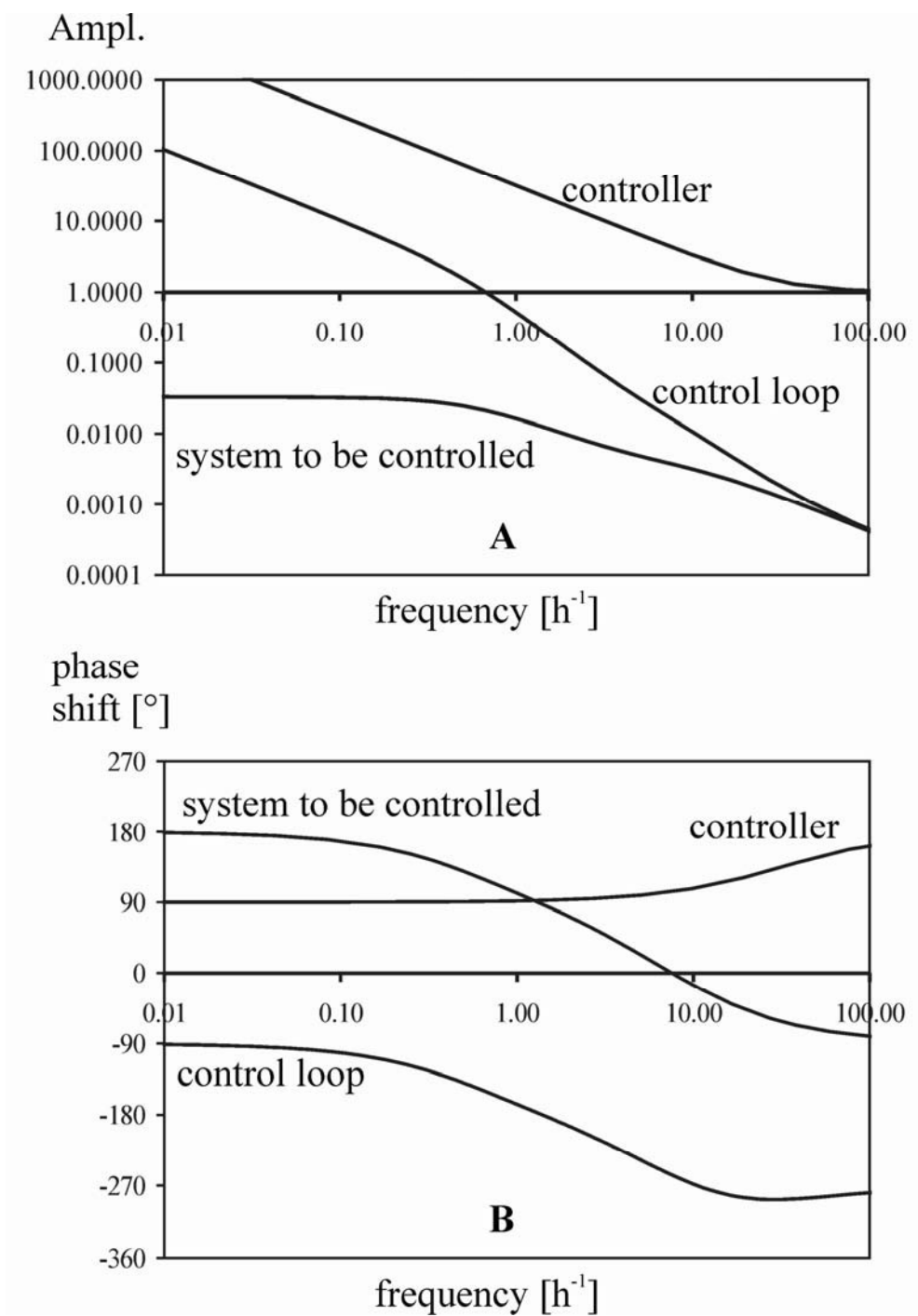


Figure 4.12. Frequency responses of system to be controlled, controller and control loop. Ampl = amplification factor of the transfer functions.

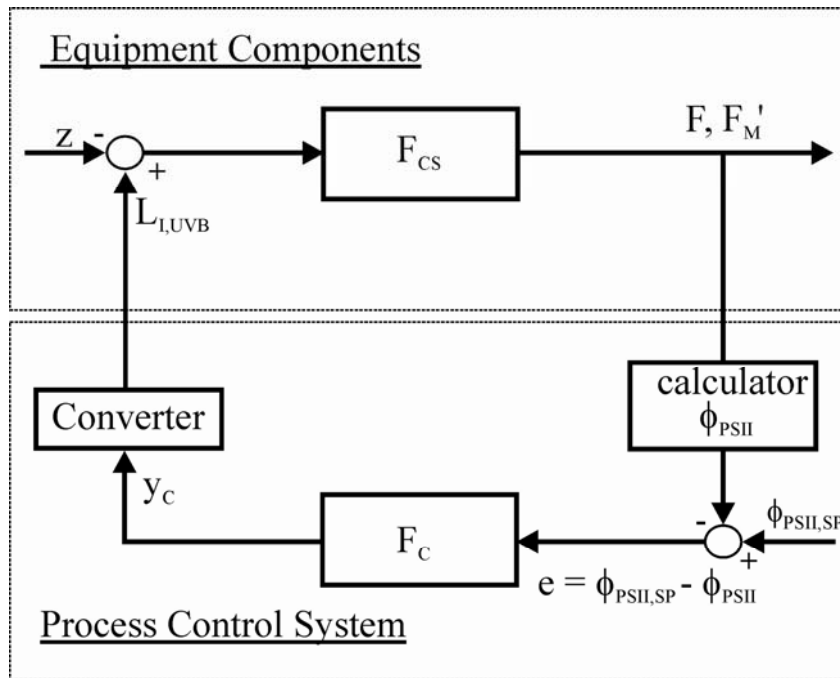


Figure 4.13. Design of the closed control loop. F_{CS} = transfer function of the system to be controlled; F_C = transfer function of the PI-controller.

4.2.11. The establishment of a new process strategy named physiostat

The data presented in Fig. 4.14A and 4.14B are representative for a physiologically controlled reactor system for microorganisms by UVB-radiation during a turbidostatic process. After a free run of 2 hours (t_5) without UVB radiation, the control loop was activated with the set point ($\phi_{PSII,SP}$) set to 0.2.

Figure 4.14A shows the rapid increase of the UVB-intensity at t_5 and as a consequence thereof the decrease of ϕ_{PSII} measured by visible light. Within 2 hours the controller lowers ϕ_{PSII} from 0.37 down to the set point of 0.2. The intensity of the UVB-radiation increases rapidly during these two hours, thus shifting ϕ_{PSII} from 0.37 to the designed set point of 0.2. This response time of 2 h of the closed loop seems to be slow with respect to the slowest time constant of 17 min of the open loop. However, it has to be considered that it is the all-pass behaviour in Fig. 4.12B which imposes such a severe limitation on the velocity of the response.

The behaviour of the feed-back loop after having reached the set-point is shown in Fig. 4.14B. Of course, ϕ_{PSII} remains constant for the next 76 hours, until the feed-back loop is opened again by switching of the UVB radiation. After ϕ_{PSII} has reached the set-point, there is a small decrease of the UVB radiation and reaches a shallow plateau after 12 h of the process time. This phase is followed by linear increase of UVB radiation up to a maximum of $1.56 \mu\text{mol photons m}^{-2} \text{s}^{-1}$ within 53 hours. The intensity remains constant for the next 5 hours and decreases again by the end of the experiment. Due to the decrease of the chlorophyll fluorescence signals F and F_M' the noise of the calculated ϕ_{PSII} (Eq. 3.3) signal increases as obvious from the noisy trace in Fig. 4.14B.

The feed-back controlled phase ends after 78 hours. The controller output was set to zero, and the UVB-intensity was switched off.

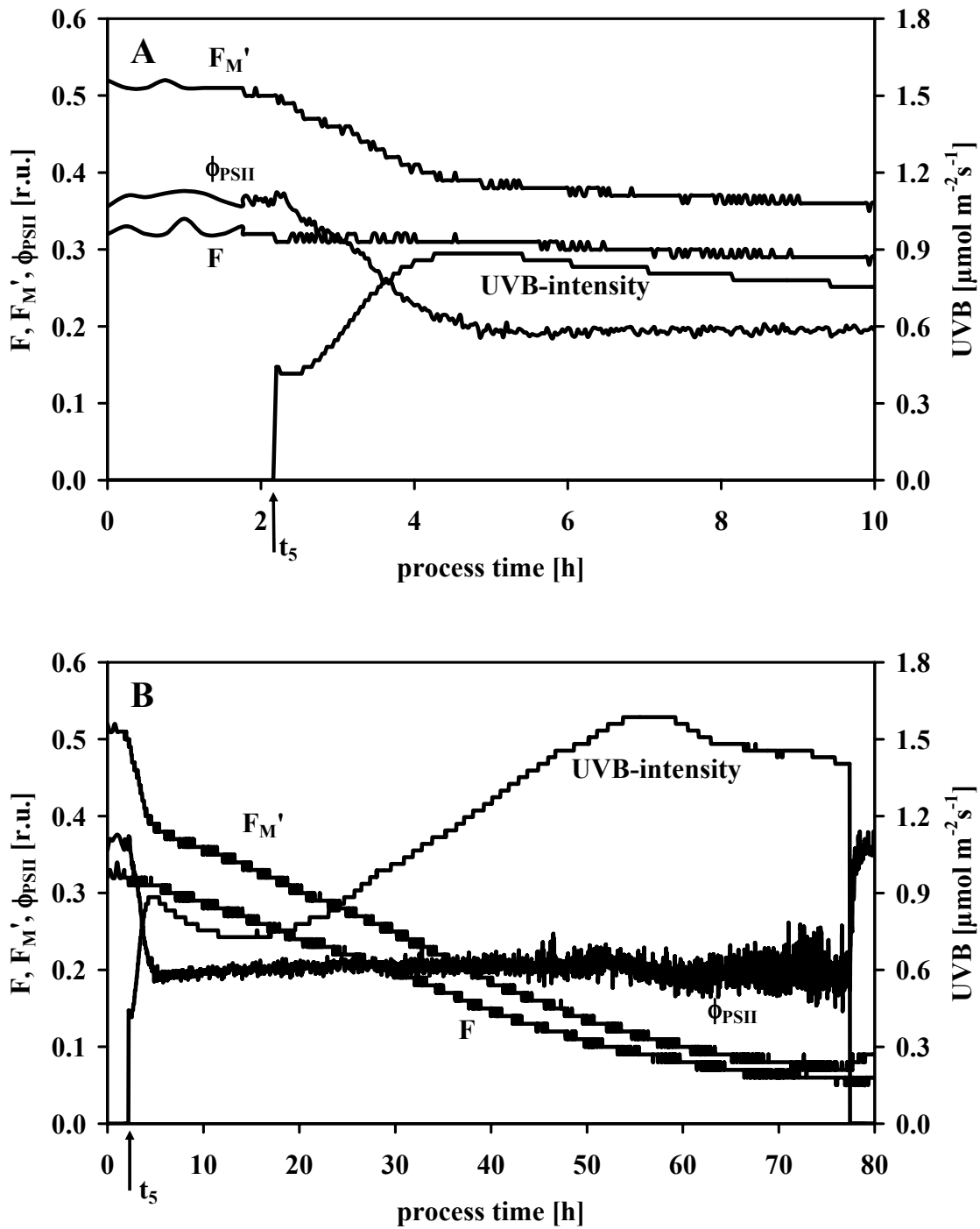


Figure 4.14. Time courses of the parameters of the growing culture obtained under the condition that ϕ_{PSII} , the actual photosynthetic efficiency of PSII is kept constant. UVB-intensity = intensity of the UVB-radiation; F , F_M' = fluorescence signals; t_5 = start of the physiological controlling system. $\mu\text{E} = \mu\text{mol photons m}^{-2} \text{s}^{-1}$.

5. Results of the UVB-influenced cultivation experiments

All documented initial values were determined *offline* before the start of the UVB-treatments (in turbidostatic or physiostatic processes) and listed in the tables. Values measured during the processes were related to these initial values in order to receive relative changes.

All listed results (except the fluorescence signals which were measured *inline*) were determined by means of *offline* measurement methods (chapter 3.2.3). Samples from the reactors for *offline* measurements were taken every 12 – 14 h during the cultivation experiments.

5.1. Biological dry mass (BDM)

The biological dry mass (BDM) was measured *offline* according to the protocol described in chapter 3.2.3. All *offline* measured concentrations (e.g. pigments, phycobilisomes, α -tocopherol) were normalised by the BDM-values.

Figure 5.1 displays BDM-measurements of three experiments. UVB-light was applied at $t = 0$. Before $t = 0$ an initial value was taken. It is displayed in Table 5.1. These three experiments are representative for the different process types, a not UVB-radiated process ($\text{UVB} = 0 \mu\text{mol photons m}^{-2} \text{s}^{-1}$), a process with a stepwise changed UVB-intensity ($\text{UVB} = 0.83 \mu\text{mol photons m}^{-2} \text{s}^{-1}$), and a physiostatic process ($\phi_{\text{PSII, SP}} = 0.25$).

The curves in Fig. 5.1 and in Table 5.1 seem to indicate an increase of BDM of about 10% as caused by UVB-irradiation. However, these changes are of stochastic origin. The initial values taken before the irradiation were at the same level. Furthermore there is no temporal development in the curves of Fig. 5.1.

Thus, it can be stated that in the reactor vessels no significant changes of the BDM-values are caused by UVB-radiation. Of course, changes are not expected because the processes were conducted as turbidostatic process, i.e. the optical density of the reactor

suspension was kept constant. These results are representative for all experiments in which no influence of the UVB-radiation on the BDM could be found.

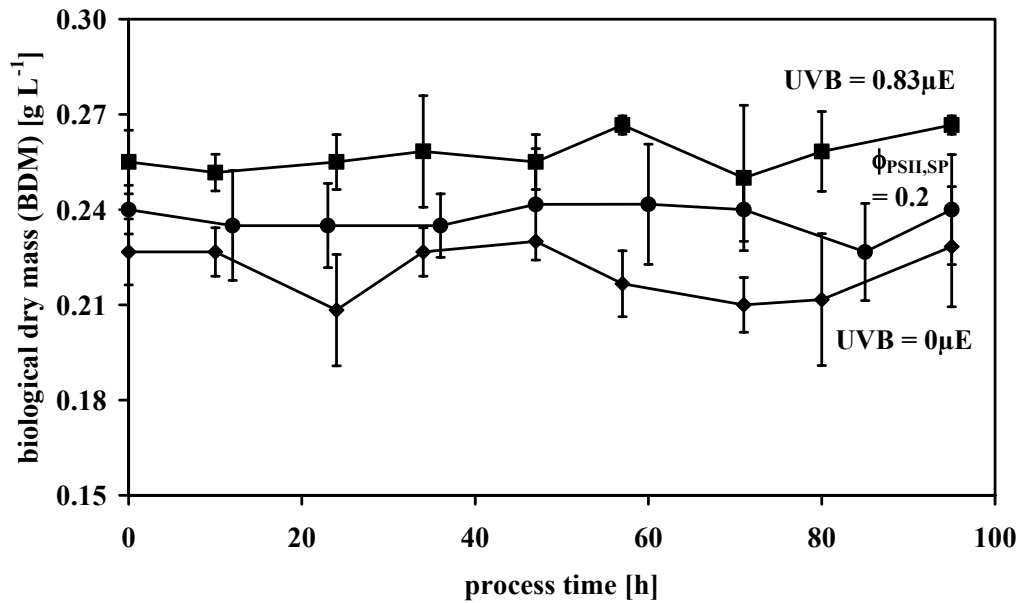


Figure 5.1. Biological dry mass (BDM) of three cultivation experiments. Without UVB-radiation (UVB = 0 $\mu\text{mol photons m}^{-2} \text{s}^{-1}$ (\blacklozenge)), a physiostatic process $\phi_{\text{PSII,SP}} = 0.2$ (\bullet); with stepwise changed UVB-intensity and (UVB = 0.83 $\mu\text{mol photons m}^{-2} \text{s}^{-1}$ (\blacksquare)). UVB was switched on at $t = 0$. Initial values at $t = 0$ are listed in Table 5.1. Initial values were measured before UVB-radiation was applied. $\mu\text{E} = \mu\text{mol photons m}^{-2} \text{s}^{-1}$.

In Table 5.1. averages of the BDM-values of all experiments are listed. The deviations of the BDM-values for all experiments were below 5 %. An overall deviation of the BDM-values of 7.9 % between maximum (0.27 g L^{-1}) and minimum (0.22 g L^{-1}) was calculated for an overall average of the 0.24 g L^{-1} .

Table 5.1. Averages and standard deviations of the biological dry masses (BDM) determined for all cultivation experiments before UVB-treatments started. Each initial value is the average of three samples. $\phi_{\text{PSII,SP}}$ = set point of the physiostatic control.

Turbidostat with stepwise changed UVB-intensity [$\mu\text{mol photons m}^{-2}\text{s}^{-1}$]	BDM [g L⁻¹]	Turbidostat with additional physiostatic control ($\phi_{\text{PSII,SP}}$)	BDM [g L⁻¹]
0.00	0.22 ± 0.01	0.25	0.24 ± 0.01
0.57	0.23 ± 0.01	0.20	0.24 ± 0.00
0.83	0.26 ± 0.01	0.15	0.22 ± 0.01
1.25	0.27 ± 0.01		
1.61	0.26 ± 0.01		
Overall average	0.24		
Deviation [%]	7.9		

5.2. Growth rate μ

As mentioned above, BDM is kept constant under turbidostatic control (which holds also for the physiostat). However, the growth rate is not zero, and can be measured by the amount of substance extruded from the reactor vessel. Experiments were done in the turbidostat (no feed-back control of physiological parameters) and under feed-back control (physiostat). The stepwise changed parameter was UVB-irradiation or $\phi_{\text{PSII,SP}}$, respectively.

By means of Eq. 3.4, the growth rates were calculated from the outflow of the reactor vessel every 24 h and normalised to the initial growth rates (obtained before the UVB-experiments started).

In Fig. 5.2A the initial values of growth rates in the turbidostat for the experiments without UVB-radiation and stepwise changed UVB-radiation are shown. In Fig. 5.2B, the changes of the normalised growth rates in the physiostat are shown.

Without UVB-radiation and at the lowest UVB-intensity of $0.57 \mu\text{mol photons m}^{-2} \text{s}^{-1}$ no significant changes are detectable. At an UVB-intensity of $0.83 \mu\text{mol photons m}^{-2} \text{s}^{-1}$, the growth rate decreases within 24 h to 60 % of the initial value and remains constant until the end of the experiment after 96 h. An UVB-intensity of $1.25 \mu\text{mol photons m}^{-2} \text{s}^{-1}$ causes a decrease to 52 % within 24 h and a final decrease to 40 % at the end of the experiment.

Radiating the microorganisms with $1.61 \mu\text{mol photons m}^{-2} \text{s}^{-1}$ lead to a decrease to 40 % in the first 24 h. This decrease continues and reaches a minimum of 10 % of the initial value at the end.

In the physiostat, a set point of 0.25 or 0.20 ($\phi_{\text{PSII, SP}} = 0.25$; $\phi_{\text{PSII, SP}} = 0.20$) shows similar results on the growth rates (Fig. 5.2B). Both decrease to 82 % after 24 h and reach constant values (61 % and 50 %) after 72 h and remain constant thereafter. Adjusting the set point to 0.15 ($\phi_{\text{PSII, SP}} = 0.15$) leads to a different behaviour. The growth rate decreases to 50 % after 24 h. This decrease continues in a linear manner to a minimum of 5 % of the initial value after 96 h. In Table 5.2, the growth rates at $t = 0$ before UVB-irradiation are listed. The values varied from 0.44 d^{-1} to 0.71 d^{-1} .

These results demonstrate the great influence of UVB-radiation on the growth rate of *Synechocystis* sp. PCC 6803. But contrary to the decrease of the growth rate other cellular components were enhanced synthesised when *Synechocystis* sp. PCC 6803 is influenced by UVB-radiation (described below).

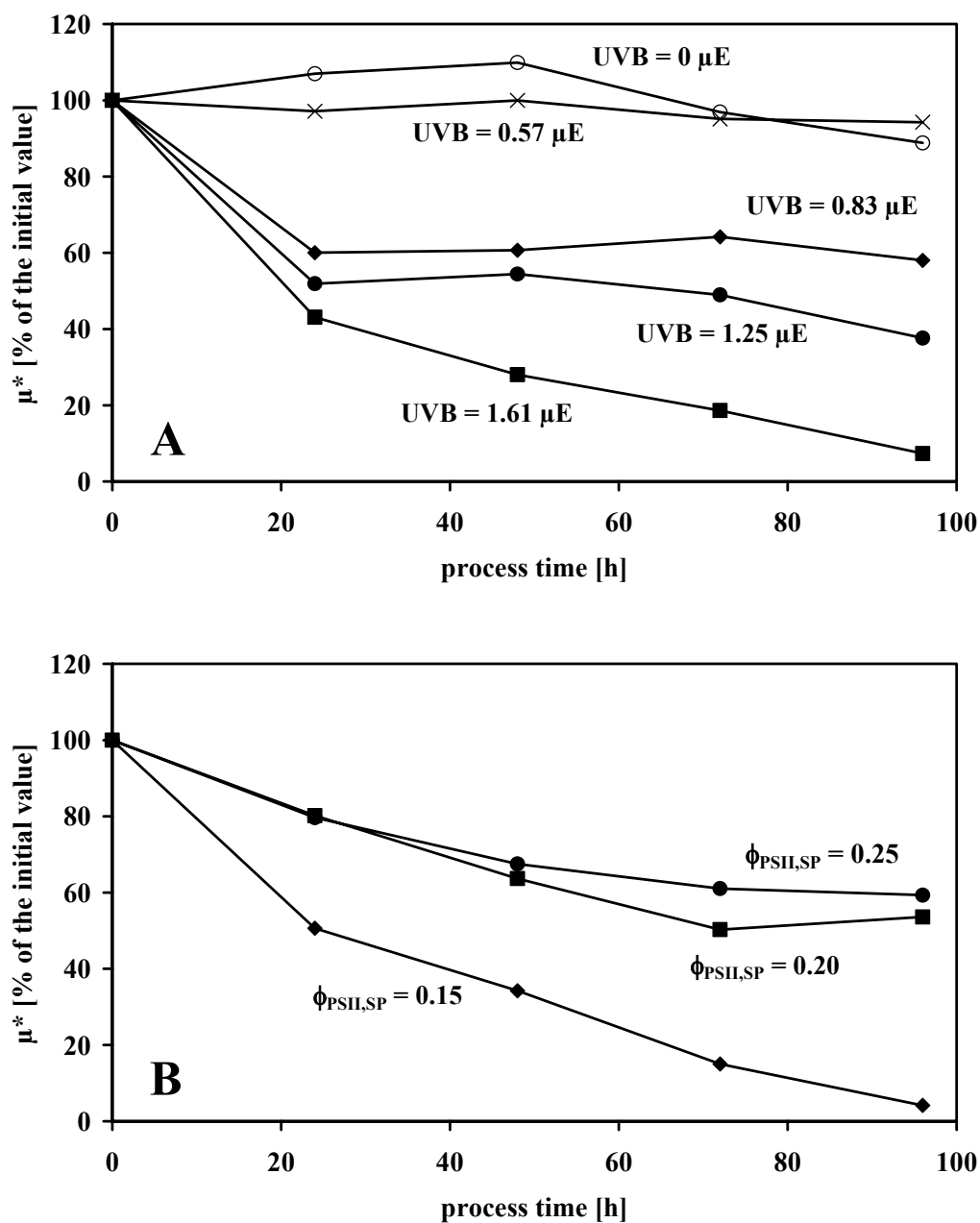


Figure 5.2. Normalised growth rates [μ^*] of the cultivation experiments. The initial values at $t = 0$ are given in Table 5.2. Initial values were measured before UVB-radiation was applied. (A) Turbidostatic control with UVB = 0 $\mu\text{mol photons m}^{-2} \text{s}^{-1}$ (O); UVB = 0.57 $\mu\text{mol photons m}^{-2} \text{s}^{-1}$ (×); UVB = 0.83 $\mu\text{mol photons m}^{-2} \text{s}^{-1}$ (◆); UVB = 1.25 $\mu\text{mol photons m}^{-2} \text{s}^{-1}$ (●); UVB = 1.61 $\mu\text{mol photons m}^{-2} \text{s}^{-1}$ (■). (B) Physiostatic control with the set points $\phi_{\text{PSII,SP}} = 0.25$ (●); $\phi_{\text{PSII,SP}} = 0.2$ (■); $\phi_{\text{PSII,SP}} = 0.15$ (◆).

Table 5.2. Initial values of the growth rates μ (taken at $t = 0$ before UVB-treatment started in the experiments of Fig. 5.2) for all cultivation experiments.

Turbidostat with stepwise changed UVB-intensity [$\mu\text{mol photons m}^{-2}\text{s}^{-1}$]	μ [d^{-1}]	Turbidostat with additional physiostatic control ($\phi_{\text{PSII,SP}}$)	μ [d^{-1}]
0.00	0.69	0.25	0.58
0.57	0.44	0.20	0.71
0.83	0.58	0.15	0.51
1.25	0.60		
1.61	0.66		
Overall average	0.60		
Deviation [%]	15.3		

5.3. Fluorescence signals

The technical set up of the photobioreactor system (Fig. 3.1) enabled the *inline* measurement of the fluorescence signals F and F_M' . By means of these signals, the process control system calculated the photosynthetic efficiency ϕ_{PSII} by means of Eq. 3.3. Fluorescence signals were determined in three kinds of experiments. Fluorescence signals of an UVB-untreated experiment (used as reference), experiments with stepwise changed UVB-intensity (both in the turbidostat), and experiments in which ϕ_{PSII} was controlled (named physiostatic process) are displayed.

5.3.1. Fluorescence signals from a cultivation not irradiated by UVB

In Fig. 5.3. the fluorescence signals of a non UVB-radiated cultivation process are shown. The time courses of the fluorescence signals of this experiment (Fig. 5.3) are significant

different from the time courses of the UVB-influenced fluorescence signals (Figs. 5.4 to 5.11).

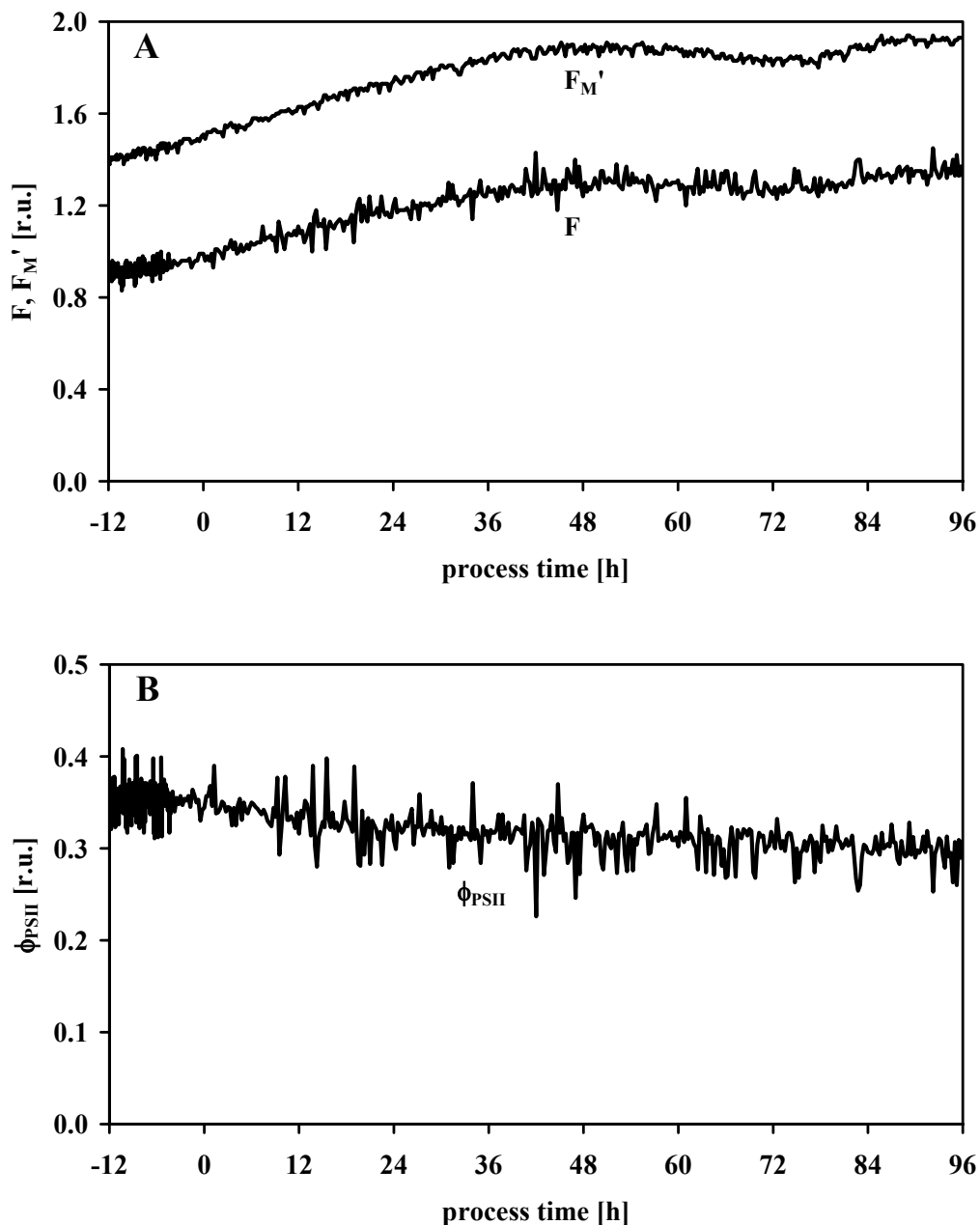


Figure 5.3. Fluorescence signals of the not UVB-radiated cultivation experiment.

r.u. = relative units.

Both F - and F_M' -signal increase in parallel and reach a plateau after 48 h for the next 30 h of the process time. After 78 h a second slower increase of both signals occurred until the end of the experiment (Fig. 5.3A). The time course of ϕ_{PSII} (Fig. 5.3B) indicates that F and F_M' are

not strictly in parallel, because of ϕ_{PSII} decreases slowly during the entire cultivation from 0.35 at the beginning to 0.3 at the end of the process (Fig. 5.3).

5.3.2. Fluorescence signals of cultivation experiments influenced by stepwise changed UVB-intensity in the turbidostat

The effect of stepwise changed UVB-irradiation from 0 to $0.57 \mu\text{mol photons m}^{-2} \text{s}^{-1}$ in a turbidostatic process is shown in Fig. 5.4. After switching on the UVB-radiation ($t = 0 \text{ h}$), ϕ_{PSII} decreases from 0.29 to 0.26 and returns back within 20 h to a value of 0.31. Thereafter, ϕ_{PSII} remains constant at this value until the end of the experiment. Immediately after the beginning of UVB-exposure, the F_M' -signal decreased whereas the F-signal remained constant for the next 6 h and declined afterwards. Both fluorescence signals reached constant values after 36 h of the process time (Fig. 5.4A).

The basic features of the responses described above occur also under higher intensities of the stepwise changes UVB-irradiation (Fig. 5.5 from 0 to $0.83 \mu\text{mol photons m}^{-2} \text{s}^{-1}$, Fig. 5.6 from 0 to $1.25 \mu\text{mol photons m}^{-2} \text{s}^{-1}$, Fig. 5.7 from 0 to $1.61 \mu\text{mol photons m}^{-2} \text{s}^{-1}$). However there are some differences. The short-time answer to irradiation becomes more and more dramatic. The initial decrease in F_M' becomes more and more dominant with increasing UVB-intensity. Another new feature occurring with increasing intensities is the initial upwards peak in the F trace. It reaches a maximum value in Fig. 5.6 at $1.25 \mu\text{mol photons m}^{-2} \text{s}^{-1}$. As a consequence of the rapid changes in F_M' , also ϕ_{PSII} shows a very steep decay immediately after the onset of UVB-irradiation, which becomes stronger with increasing intensities. The long-term effects do not reveal any intensity-dependent occurrence of new features.

The effect of the highest UVB-dose (Fig. 5.8), however, is different from those described above. The initial F-peak is gone, F_M' still shows a rapid response but less steep than in Fig. 5.7. The most remarkable feature is the monotonous decrease of ϕ_{PSII} without any recovery phase as found at lower intensities in Figs. 5.5 to 5.7. Fig. 5.12A gives a synopsis of the responses to different UVB-doses.

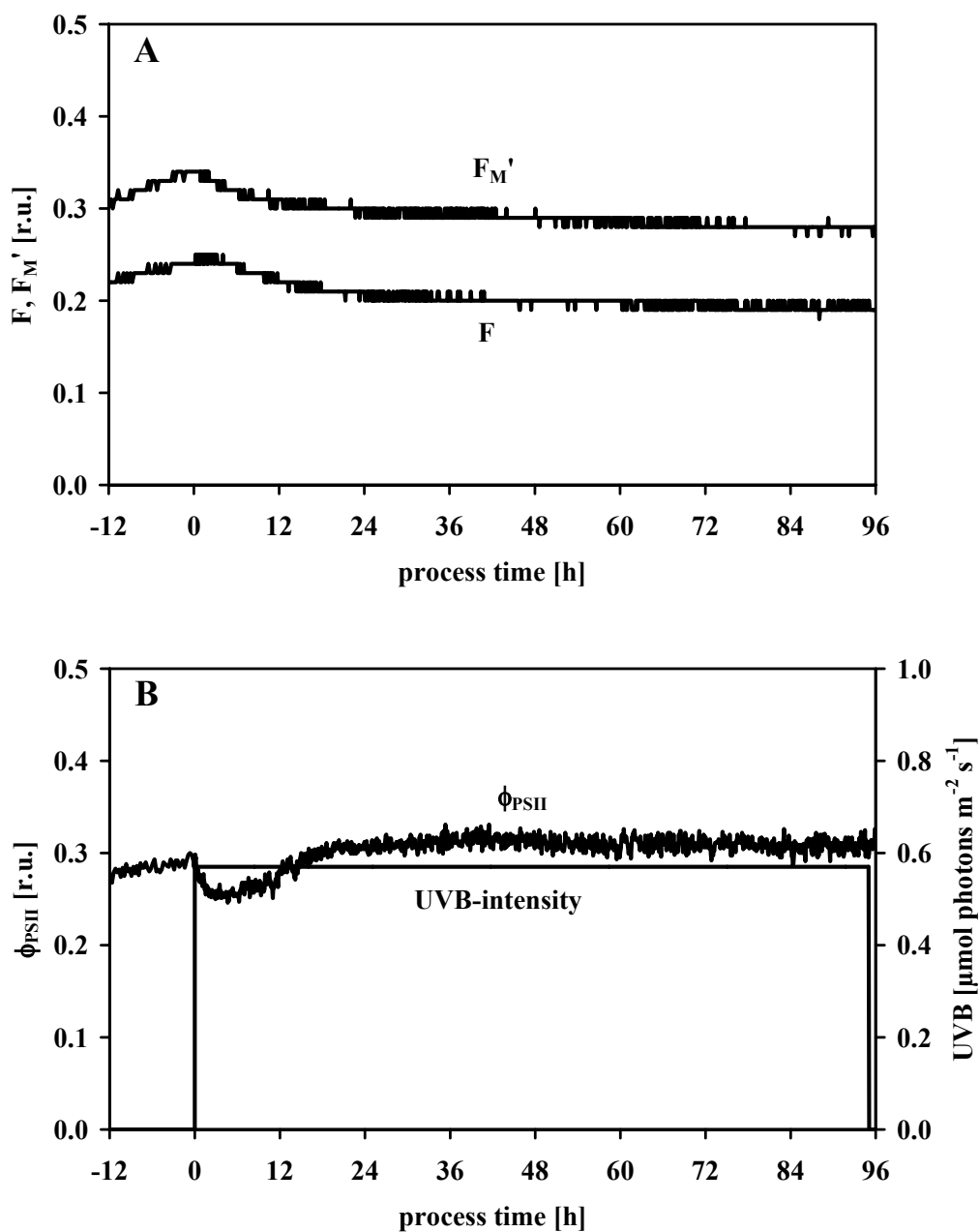


Figure 5.4. Fluorescence signals of a cultivation experiment influenced by stepwise changed UVB-intensity of $0.57 \mu\text{mol photons m}^{-2} \text{s}^{-1}$. r.u. = relative units.

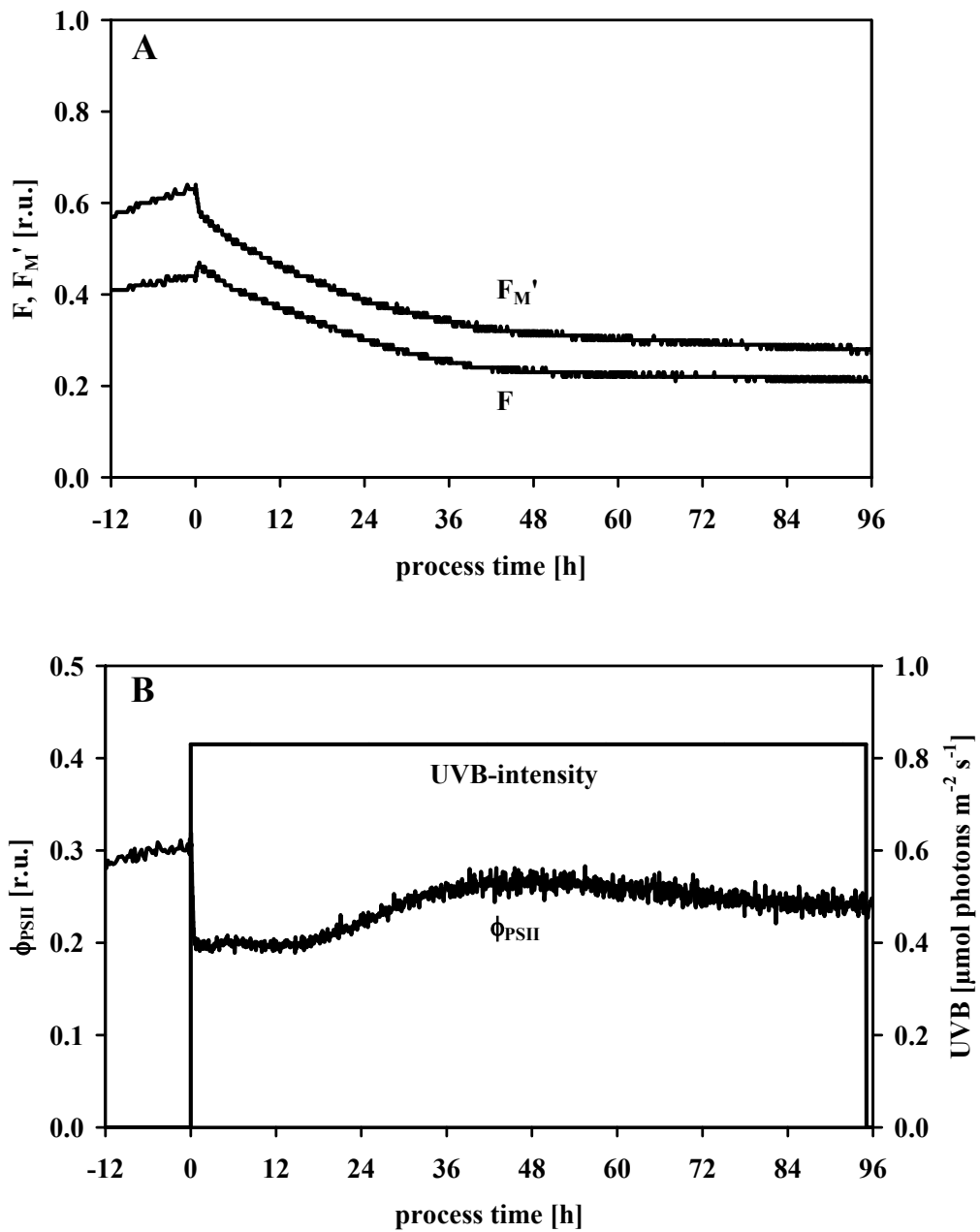


Figure 5.5. Fluorescence signals of a cultivation experiment influenced by stepwise changed UVB-intensity of $0.83 \mu\text{mol photons m}^{-2} \text{s}^{-1}$. r.u. = relative units

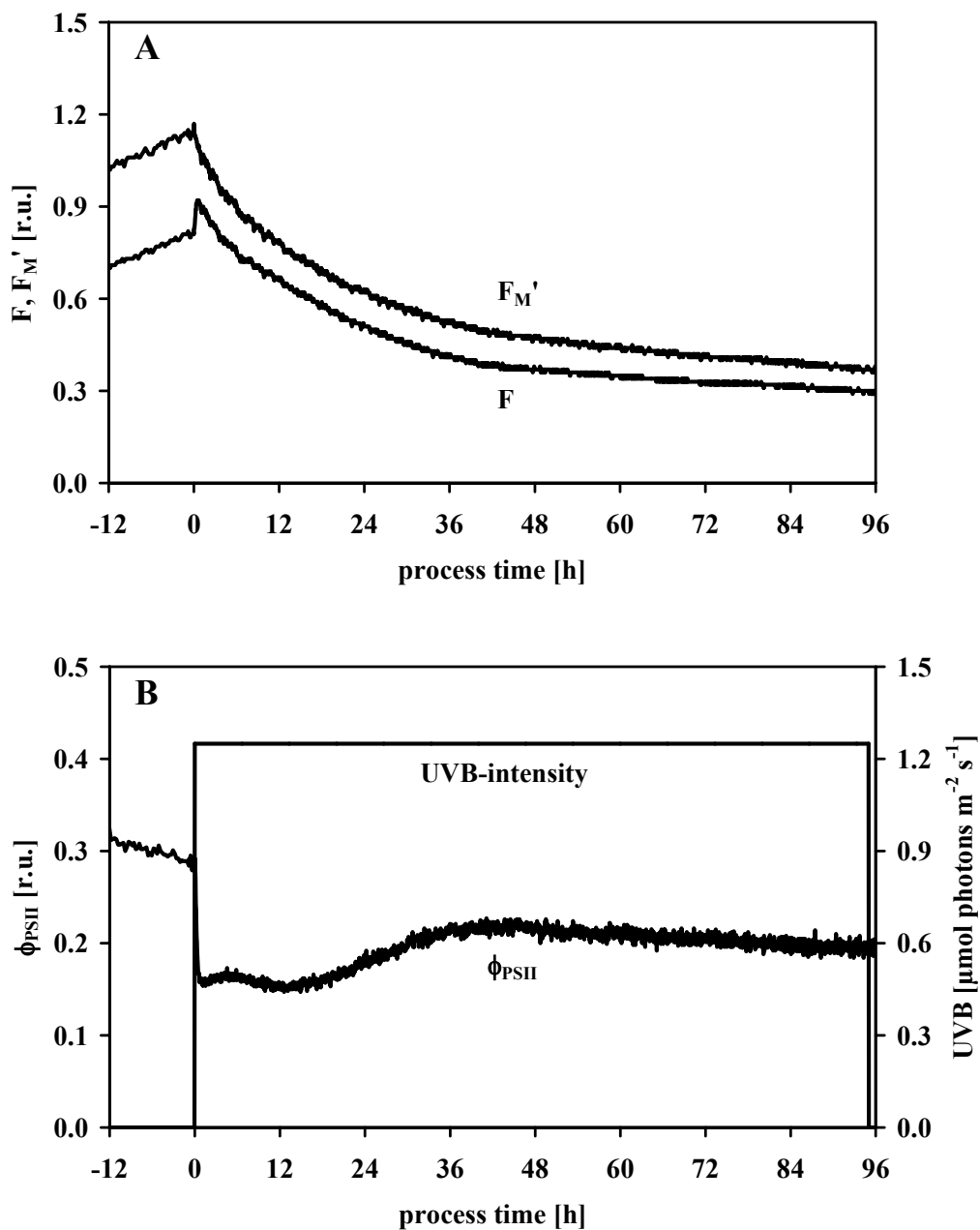


Figure 5.6. Fluorescence signals of a turbidostatic experiment influenced by stepwise changed UVB-intensity of $1.25 \mu\text{mol photons m}^{-2} \text{s}^{-1}$. r.u. = relative units.

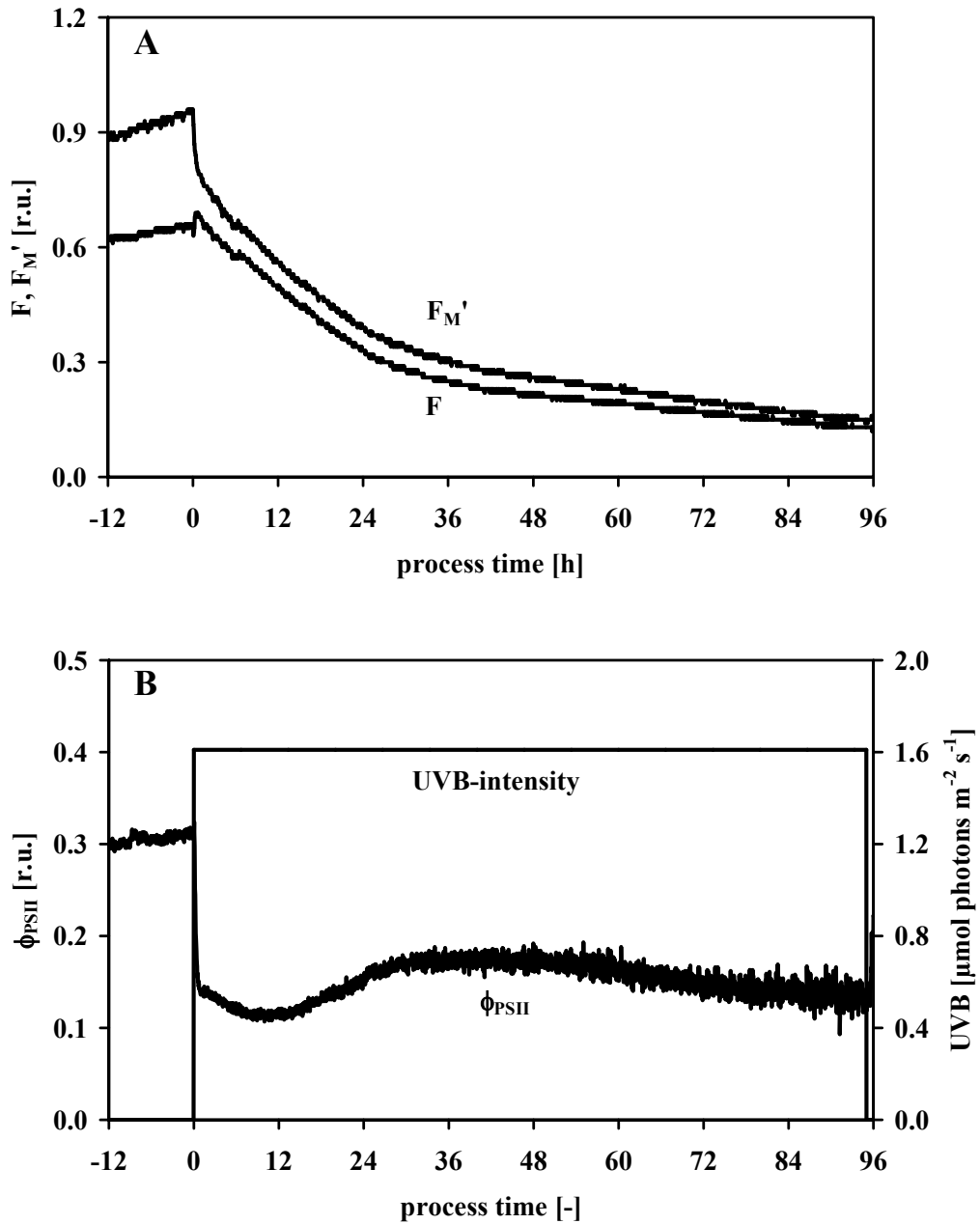


Figure 5.7. Fluorescence signals of a turbidostatic experiment influenced by stepwise changed UVB-intensity of $1.61 \mu\text{mol photons m}^{-2} \text{s}^{-1}$. r.u. = relative units.

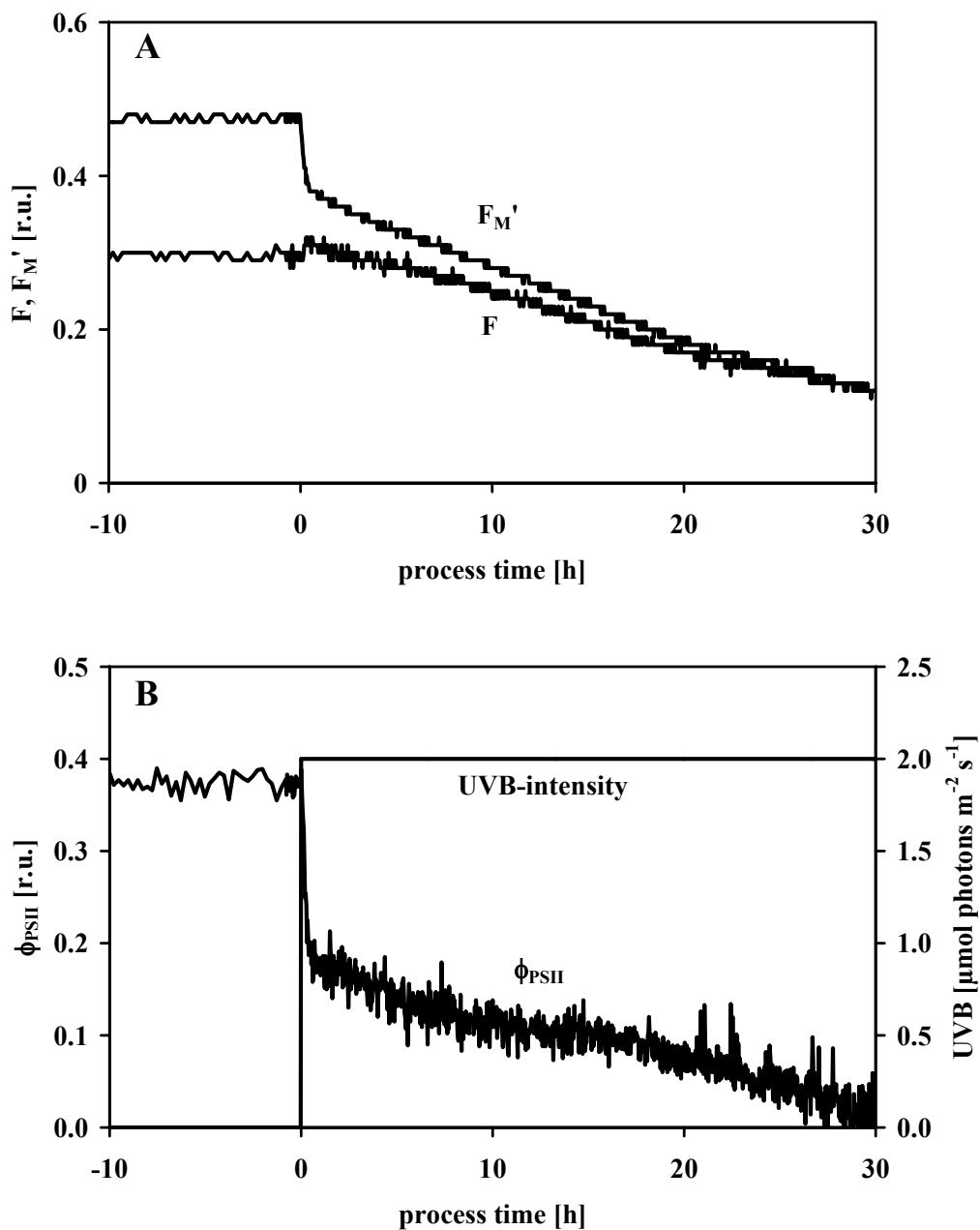


Figure 5.8. Fluorescence signals of a turbidostatic experiment influenced by stepwise changed UVB-intensity from 0 to 2 $\mu\text{mol photons m}^{-2} \text{s}^{-1}$. r.u. = relative units.

5.3.3. Fluorescence signals of physiostatic cultivation experiments

Figure 5.9 shows a physiostatic cultivation process with a preset set point ($\phi_{\text{PSII,SP}}$) of 0.25 ($\phi_{\text{PSII,SP}} = 0.25$). After closing the feed-back loop, ϕ_{PSII} jumps to its set point with 2 h and stays there to the end of the experiment. This indicates the proper function of the physiostatic control loop. In these experiments, information about the biological system is not obtained from ϕ_{PSII} as in the turbidostatic experiments but from the behaviour of UVB-intensity and F and F_M' .

UVB-intensity as the actuating parameter varied between 0.49 (after activating the controller mode) and 0.88 (at 59 to 64 hours of the process time) $\mu\text{mol photons m}^{-2} \text{s}^{-1}$ (Fig. 5.9). The fluorescence signals F and F_M' showed similar time courses like those in the stepwise UVB-changed experiments (Figs. 5.4 to 5.7). F_M' declined immediately and F increased during the first 2 hours. After 2 hours, F and F_M' decreased in a parallel mode and reached constant values after 72 hours of the process time.

An averaged UVB-intensity of $0.79 \mu\text{mol photons m}^{-2} \text{s}^{-1}$ can be calculated from the time interval after the set point had been reached. The variation of UVB-intensity corresponded to a modulation degree of 15 %.

Employing lower set point forces the controller to impose a higher UVB-intensity. For $\phi_{\text{PSII,SP}} = 0.2$ (Fig. 5.10B), it ranged from 0.58 (at the beginning of the physiostatic cultivation) to $1.13 \mu\text{mol photons m}^{-2} \text{s}^{-1}$ at the maximum (between 42 and 43 hours of the process time). Since noise was lower in the record of Fig. 5.10, the typical time course becomes clearer. Again the fluorescence yield ϕ_{PSII} reached the set point after 2 h, and remained constant for the rest of the cultivation. The UVB-intensity reached a first maximum of $0.99 \mu\text{mol photons m}^{-2} \text{s}^{-1}$ after 7 hours, decreased during the next 6 hours and remained at a constant level of $0.91 \mu\text{mol photons m}^{-2} \text{s}^{-1}$ for 10 hours. After 24 hours of the process time the UVB-intensity increased again and a second maximum of the UVB-intensity of $1.13 \mu\text{mol photons m}^{-2} \text{s}^{-1}$ occurred after 43 hours. Thereafter, the UVB-intensity was characterised by a decline until the end of the experiment and reached a final intensity of $1.01 \mu\text{mol photons m}^{-2} \text{s}^{-1}$.

The behaviour of the F and F_M' -signal did not show dramatic differences as compared to the traces obtained with the higher set point in Fig. 5.9. The initial peak in the F -signal occurred under all set points even though noise may hide its occurrence in Fig. 5.10.

Under a set point of $\phi_{\text{PSII,SP}} = 0.15$ (Fig. 5.11) UVB-intensity displayed a pattern similar to the experiment in Fig. 5.10. However, the feed-back controller seems to come to its technical limitations. It could not prevent an overshoot, when the set point was achieved after 5 hours. This overshoot is an effect of the integral action coefficient implemented in the controller (Eq. 4.17) which is close to the critical value of T_N (Eq. 4.19; see chapter 4.2).

The related time course of UVB-intensity (Fig. 5.11B) is similar to that in Fig. 5.10B. It includes a first UVB-intensity maximum of $1.75 \mu\text{mol photons m}^{-2} \text{s}^{-1}$. Then, the controller lowered the UVB-intensity (Fig. 5.11B). The UVB-intensity was adjusted to an intensity of $1.41 \mu\text{mol photons m}^{-2} \text{s}^{-1}$ after 13 hours of the process time. Due to the lowering of the UVB-intensity, ϕ_{PSII} increased again and reached the set point of 0.15. Subsequently the controller increased the UVB-intensity again in order to keep ϕ_{PSII} constant. After 32 hours of the process time the UVB-intensity was set to a second maximum of $2.03 \mu\text{mol photons m}^{-2} \text{s}^{-1}$. This intensity is the maximal adjustable intensity of the UVB-radiation and was present for the next 25 hours in which ϕ_{PSII} remained constant at the set point. At a process time of 58 hours the UVB-intensity was continuously lowered by the controller to a final intensity of $1.39 \mu\text{mol photons m}^{-2} \text{s}^{-1}$. An average UVB-intensity of $1.78 \mu\text{mol photons m}^{-2} \text{s}^{-1}$ with a modulation degree of 18 % occurred regarding the process time when the set point was reached.

Both F- and F_M' -signal showed similar characteristics (Fig. 5.11A) like the experiments above (Figs. 5.9A and 5.10A). The F-signal increased after the physiostatic process was activated and decreased exponentially after 2 hours of the process time. Immediately after the activation of the physiostatic control the F_M' -signal decreased. Both signals achieved a constant value after 72 hours of the process time.

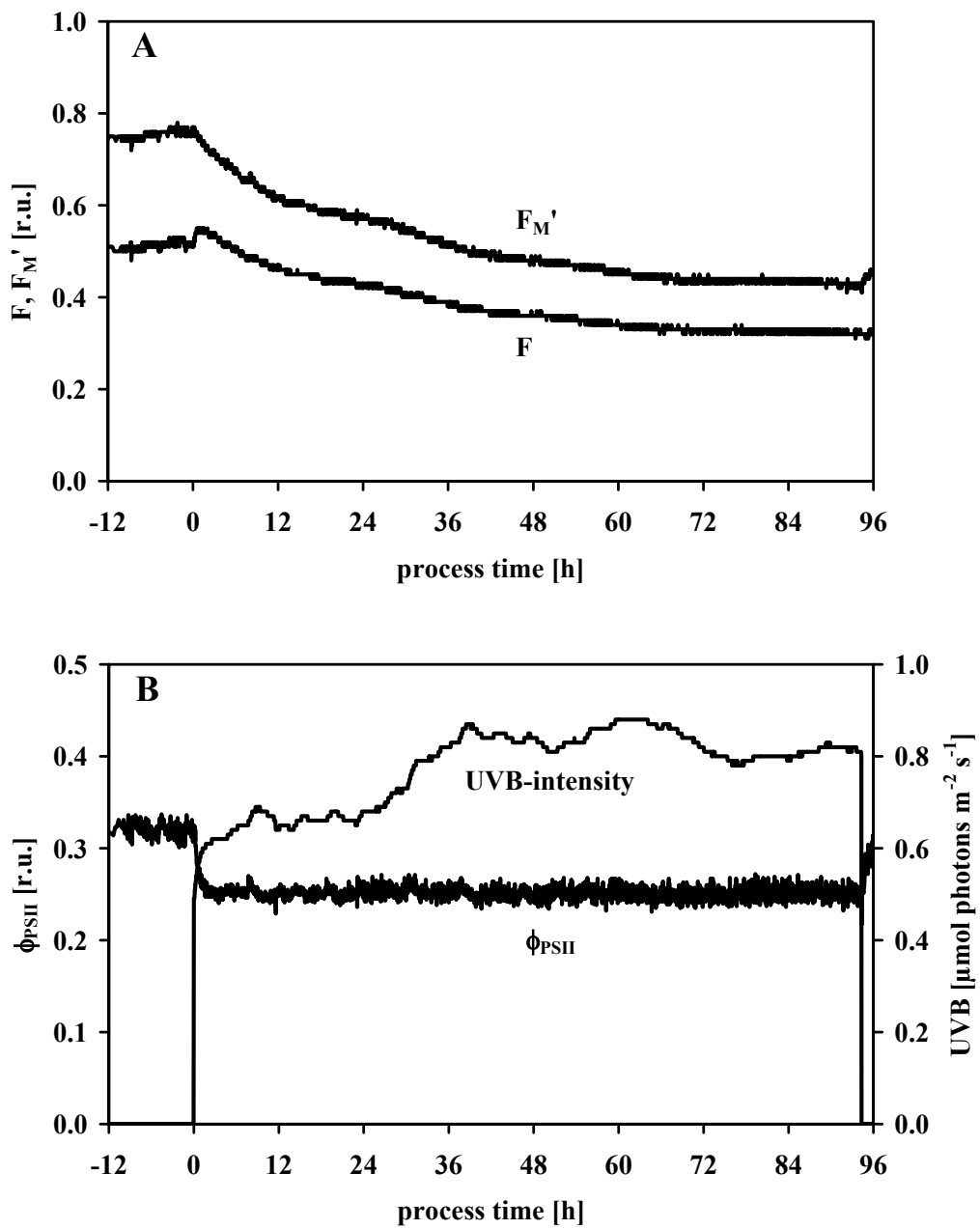


Figure 5.9. Fluorescence signals of a physiostatic cultivation experiment ($\phi_{PSII,SP} = 0.25$).
r.u. = relative units.

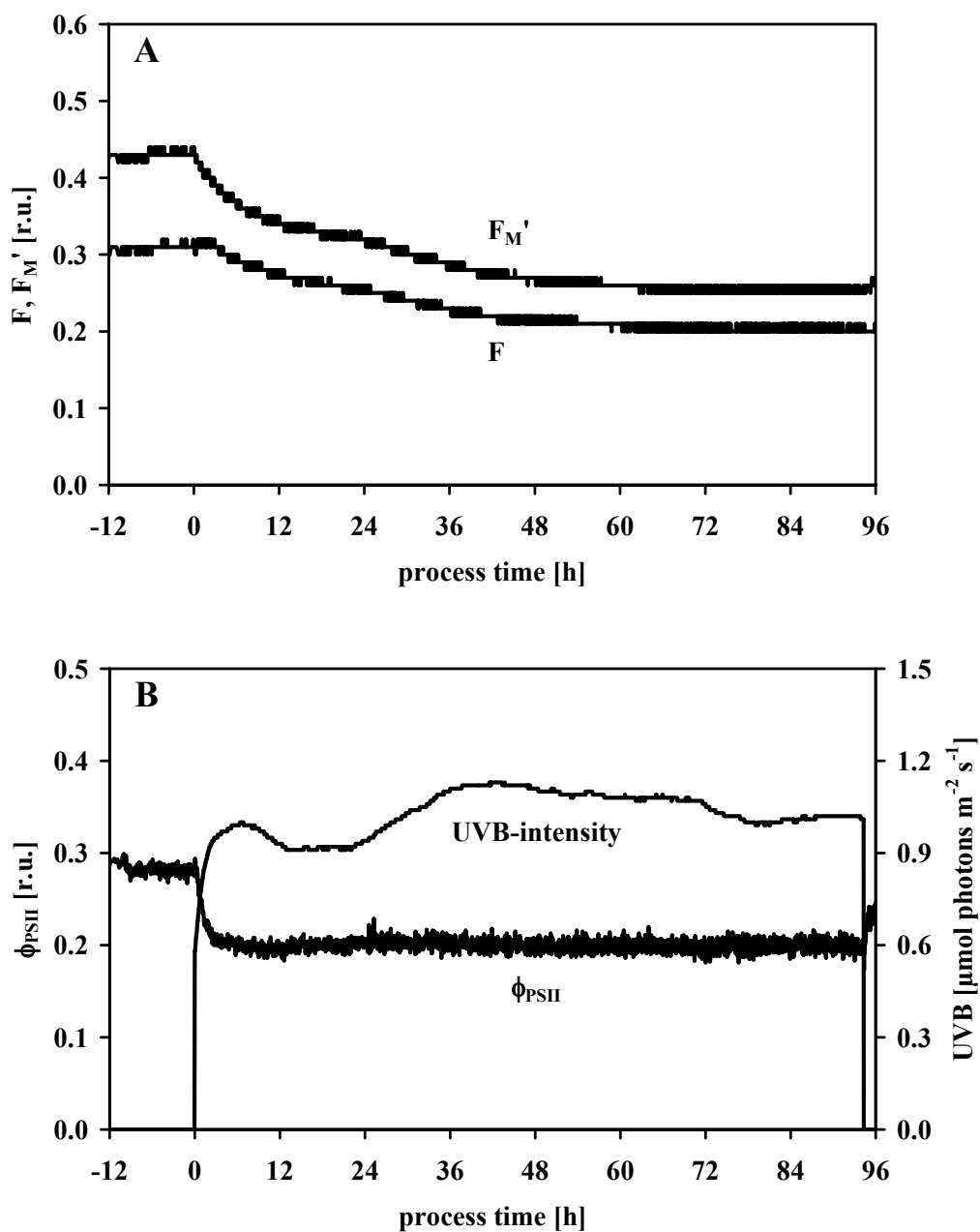


Figure 5.10. Fluorescence signals of a physiostatic cultivation experiment ($\phi_{PSII,SP} = 0.2$).
r.u. = relative units.

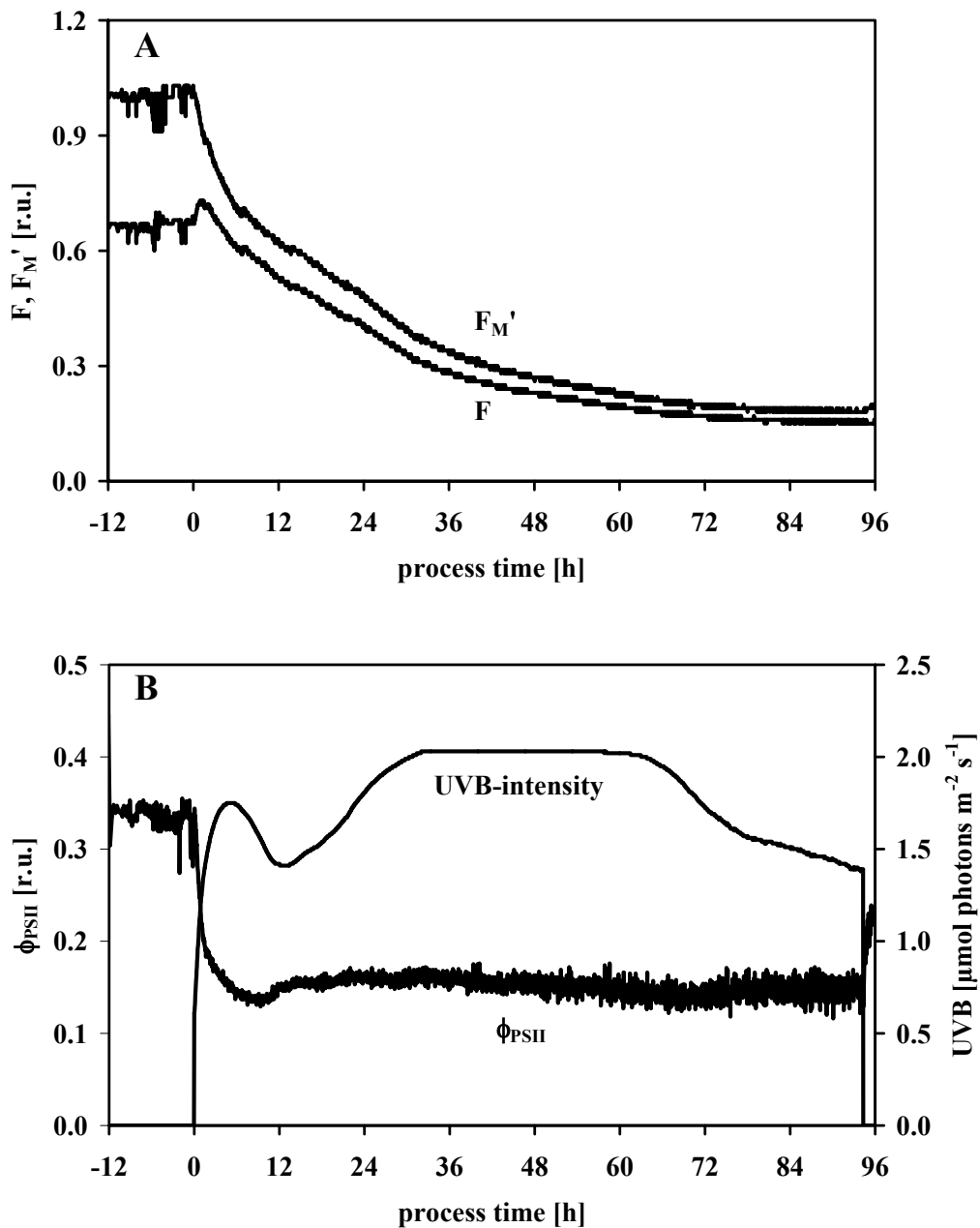


Figure 5.11. Fluorescence signals of a physiostatic cultivation experiment ($\phi_{PSII,SP} = 0.15$).
r.u. = relative units.

Figure 5.12 summarised ϕ_{PSII} courses measured in the turbidostat and physiostat. Figure 5.12A illustrates the basic similarity of ϕ_{PSII} responses induced by stepwise changed UVB-intensities in the turbidostat. Under physiostatic control, ϕ_{PSII} is not expected to have deviations from the rectangular shape. The curve from the lowest set-point indicates that the feed back loop has problems to fulfil its task.

For the discussion of the mechanistic background for the curve shapes observed in the above investigations, typical time courses of ϕ_{PSII} response induced by stepwise changed UVB-intensity in the turbidostat (from Fig. 5.7) and of UVB-intensity in the physiostat (from Fig. 5.10) are compared (Fig. 5.13).

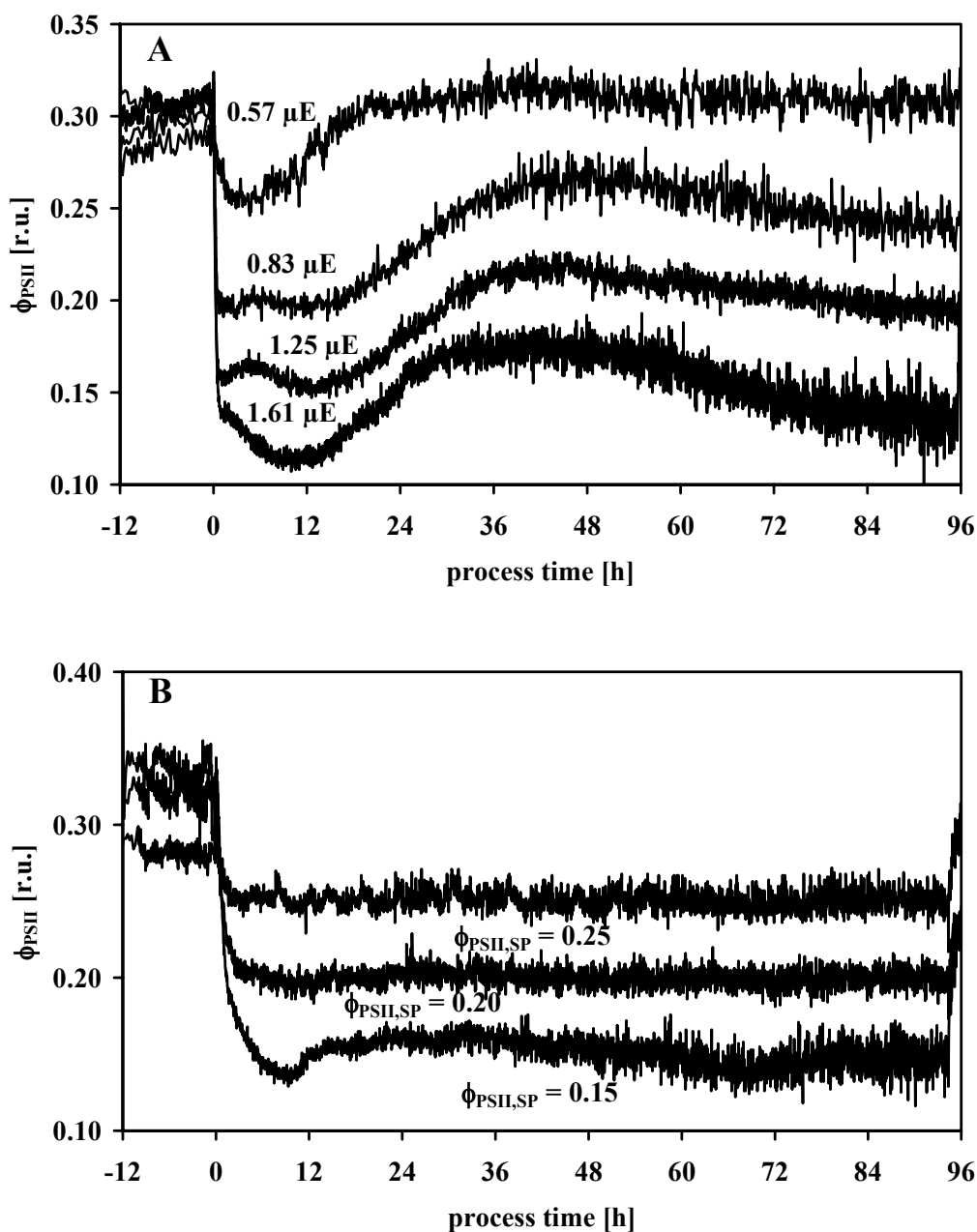


Figure 5.12. Summary of ϕ_{PSII} influenced by stepwise changed UVB-intensity (A) or controlled by the feed-back loop (B).

Since the modulation of the UVB-intensity is necessary for keeping ϕ_{PSII} constant (Figs. 5.9 to 5.11), their time courses should be similar. If only one mechanism is involved the time course should show a parallel or an anti-parallel behaviour. Deviations indicate that different mechanisms are involved. This is discussed in detail in chapter 7.

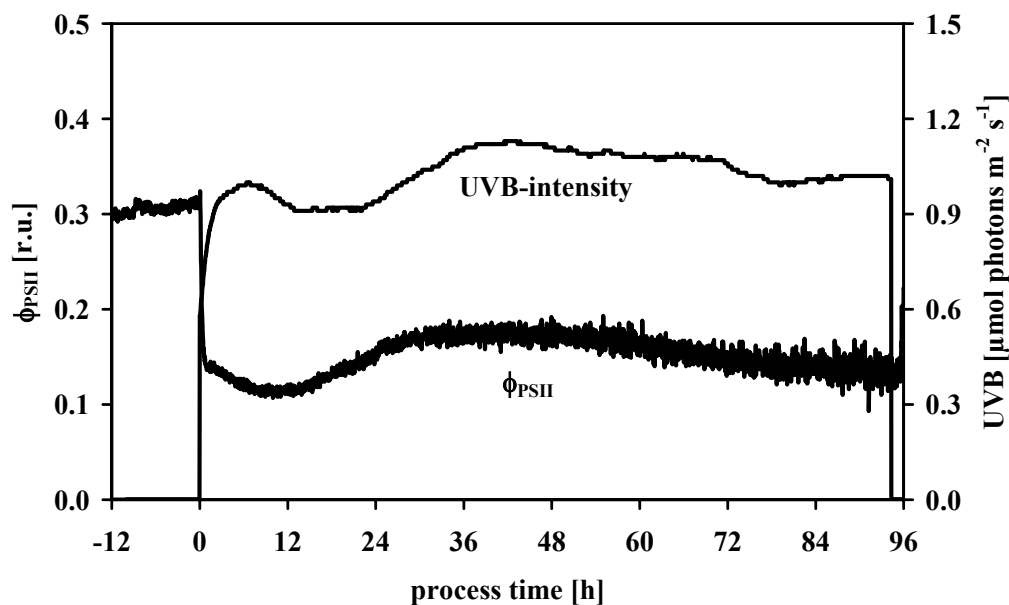


Figure 5.13. Similarity of the time courses of ϕ_{PSII} (uncontrolled) and modulated UVB-intensity for keeping ϕ_{PSII} constant. r.u. = relative units.

5.4. Pigment analyses

By means of the HPLC-method (chapter 3.2.3) pigment composition and the single pigment concentration were measured *offline* by taking samples from the reactors. The determined concentrations were normalised to the biological dry mass.

Since the time courses of the measured pigment concentrations are normalised to the initial value measured before the onset of UVB-irradiation (i.e., they all start with “1”), the real initial values at $t = 0$ are given in Tab. 5.3. The averaged initial values in Tab. 5.3 of each measured pigment are normalised to the biological dry masses. In addition, the related standard deviations are listed.

Table 5.3. Initial values of the pigments chlorophyll *a*, myxoxanthophyll, zeaxanthin, echinenone, and β -carotene. The initial values were measured before UVB-treatment started. All pigment values are normalised to the BDM and given in mg [g BDM]⁻¹. UVB-intensity is in $\mu\text{mol photons m}^{-2} \text{s}^{-1}$. Chl. *a* = chlorophyll *a*; Myxo = myxoxanthophyll, Zea = zeaxanthin; Ech = echinenone, β -Car = β -carotene; Turbido¹ = turbidostat with stepwise changed UVB-intensity [$\mu\text{mol photons m}^{-2} \text{s}^{-1}$]; Turbido² = turbidostat with additional physiostatic control ($\phi_{\text{PSII,SP}}$).

Turbido¹	Chl. A	Myxo	Zea	Ech	β-Car
0.00	11.11 \pm 0.59	0.39 \pm 0.12	0.42 \pm 0.03	0.31 \pm 0.01	0.82 \pm 0.07
0.57	9.51 \pm 0.62	0.51 \pm 0.04	0.32 \pm 0.05	0.42 \pm 0.04	0.65 \pm 0.05
0.83	11.55 \pm 2.54	0.60 \pm 0.12	0.48 \pm 0.08	0.33 \pm 0.23	0.82 \pm 0.12
1.25	8.27 \pm 0.53	0.50 \pm 0.16	0.21 \pm 0.08	0.13 \pm 0.03	0.33 \pm 0.08
1.61	9.43 \pm 0.04	0.50 \pm 0.13	0.28 \pm 0.04	0.25 \pm 0.03	0.73 \pm 0.03
Turbido²	Chl. A	Myxo	Zea	Ech	β-Car
0.25	14.14 \pm 0.88	0.42 \pm 0.06	0.41 \pm 0.03	0.32 \pm 0.03	1.15 \pm 0.06
0.20	10.71 \pm 0.34	0.16 \pm 0.02	0.18 \pm 0.01	0.22 \pm 0.02	0.58 \pm 0.02
0.15	11.40 \pm 1.08	0.25 \pm 0.02	0.31 \pm 0.03	0.25 \pm 0.02	0.75 \pm 0.07
Average	10.77	0.41	0.33	0.28	0.73
Deviation [%]	16.5	35.2	32.2	31.1	32.1

The chlorophyll *a* concentration ranged between a minimum of 8.27 mg [g BDM]⁻¹ and a maximum of 14.14 mg [g BDM]⁻¹. A resulting average of 10.77 mg [g BDM]⁻¹ and a deviation of 16.5 % were calculated. Minimum and maximum of the myxoxanthophyll concentration were measured at 0.16 and 0.6 mg [g BDM]⁻¹. The overall myxoxanthophyll average was 0.41 mg [g BDM]⁻¹ with a belonging deviation of 35.2 %. Zeaxanthin concentration measurements resulted in an overall average of 0.33 mg [g BDM]⁻¹ with a deviation of 32.2 %. Minimum and maximum were at 0.18 and 0.48 mg [g BDM]⁻¹. A maximum of 0.42 mg [g BDM]⁻¹ and minimum of 0.13 mg [g BDM]⁻¹ occurred for the echinenone results. An average of 0.28 mg [g BDM]⁻¹ and a deviation of 31.1 % for all

experimental echinenone measurements were calculated. β -carotene detection delivered a maximum of 1.15 mg [g BDM]⁻¹ and a minimum of 0.33 mg [g BDM]⁻¹. A deviation of 32.1 % was calculated for the average of 0.73 mg [g BDM]⁻¹.

5.4.1. Chlorophyll *a*

The chlorophyll *a* concentrations (depicted in Fig. 5.14A) in turbidostatic experiments without UVB-irradiation and with UVB-intensities of 0.57, 0.83 and 1.25 $\mu\text{mol photons m}^{-2} \text{s}^{-1}$ showed similar results. Final values ranged between 94 % and 60 % compared to the initial values. At the highest UVB-intensity (1.61 $\mu\text{mol photons m}^{-2} \text{s}^{-1}$) the chlorophyll *a* concentration decreased to 40 % of the initial value. All experiments showed continuously decreases during the entire processes.

Also physiostatic experiments (Fig. 5.14B) using set points of 0.25 and 0.2 ($\phi_{\text{PSII,SP}} = 0.25$ and 0.2) resulted in a continuous decrease of the chlorophyll *a* concentrations. Compared to the initial values, chlorophyll concentrations were lowered to 75 % ($\phi_{\text{PSII,SP}} = 0.25$) or 85 % ($\phi_{\text{PSII,SP}} = 0.2$), respectively. A set point of 0.15 ($\phi_{\text{PSII,SP}} = 0.15$) lowered the chlorophyll *a* concentration to 45 % at the end of the experiments.

The results show that the highest UVB-intensity and the lowest set point of ϕ_{PSII} cause a significant decrease of chlorophyll *a* concentration whereas in the other experiments no significant differences between UVB-radiated experiments and the not UVB-radiated experiments are observable (Fig. 5.14A and 5.14B).

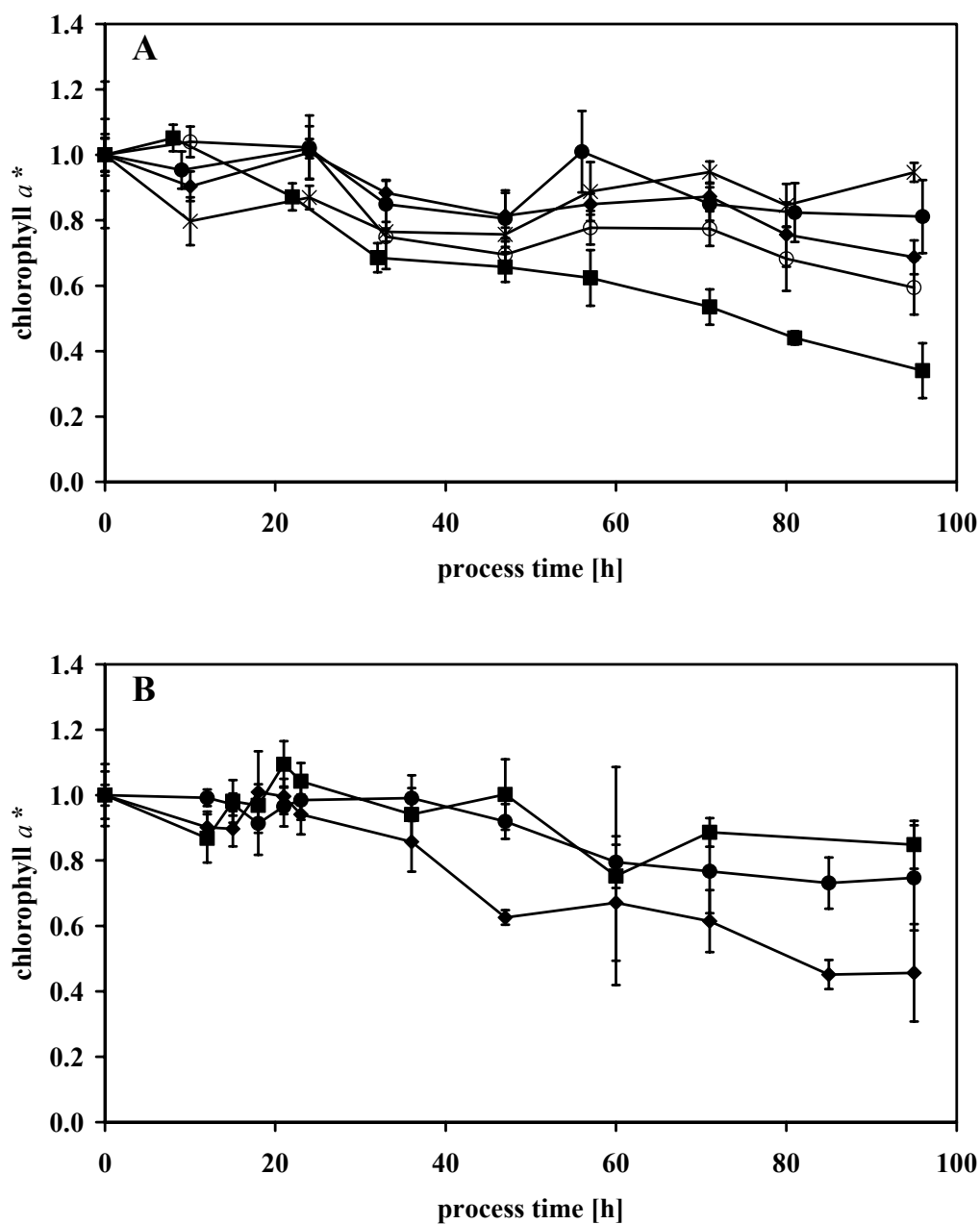


Figure 5.14. Normalised chlorophyll a concentrations (chlorophyll a^*) of the cultivation experiments. **A:** Turbidostat with UVB = 0 $\mu\text{mol photons m}^{-2} \text{s}^{-1}$ (O); UVB = 0.57 $\mu\text{mol photons m}^{-2} \text{s}^{-1}$ (\times); UVB = 0.83 $\mu\text{mol photons m}^{-2} \text{s}^{-1}$ (\blacklozenge); UVB = 1.25 $\mu\text{mol photons m}^{-2} \text{s}^{-1}$ (\bullet); UVB = 1.61 $\mu\text{mol photons m}^{-2} \text{s}^{-1}$ (\blacksquare). **B:** Turbidostat with additional physiostatic control $\phi_{\text{PSII,SP}} = 0.25$ (\bullet); $\phi_{\text{PSII,SP}} = 0.2$ (\blacksquare); $\phi_{\text{PSII,SP}} = 0.15$ (\blacklozenge).

5.4.2. Myxoxanthophyll

In Fig. 5.15A, the concentrations of myxoxanthophyll measured in turbidostatic experiments with and without stepwise applied UVB-intensity are shown. The cultivation experiment employing an UVB-intensity of $0.57 \mu\text{mol photons m}^{-2} \text{s}^{-1}$ showed no significant differences compared to the not UVB-radiated cultivation. The myxoxanthophyll concentrations in both cultivations stayed on the same level during the entire processes. Remarkable changes compared to the initial myxoxanthophyll concentrations did not occur. In contrast, higher UVB-intensities (0.83 , 1.25 and $1.61 \mu\text{mol photons m}^{-2} \text{s}^{-1}$) caused a weak increase in concentration after a process time of 47 hours. UVB-intensities of 0.83 and $1.61 \mu\text{mol photons m}^{-2} \text{s}^{-1}$ reached a maximum (226 % and 244 % compared to the initial values) after a process time of 71 hours and decreased again for the rest of the experiment to final values of 155 % and 122 % respectively. An UVB-intensity of $1.25 \mu\text{mol photons m}^{-2} \text{s}^{-1}$ reached its maximum (244 %) at the end of the process.

A completely different behaviour is evoked in physiostatic processes (Fig. 5.15B). Two remarkable effects become observable. Myxoxanthophyll concentration courses in physiostatic processes (Fig. 5.15B) show a strong increase compared to those in the turbidostat. There is a remarkable feature at the beginning of the exposure to physiostatic controlled UVB-irradiation. After a process time of 12 hours, all concentrations began to increase strongly within the next 12 hours and reached their maximum after 60 to 70 hours.

Employing a set point of 0.25 ($\phi_{\text{PSII,SP}} = 0.25$) revealed a maximum of 234 % after 60 hours. A set point of 0.2 reached a maximum of 600 % after 72 hours of the process whereas the maximum for a set point of 0.15 was 425 % compared to the initial value. Final enhancements for all physiostatic processes were increased in comparison to their initial values of 166 % for $\phi_{\text{PSII,SP}} = 0.25$, 541 % for $\phi_{\text{PSII,SP}} = 0.2$ and 260 % for $\phi_{\text{PSII,SP}} = 0.15$.

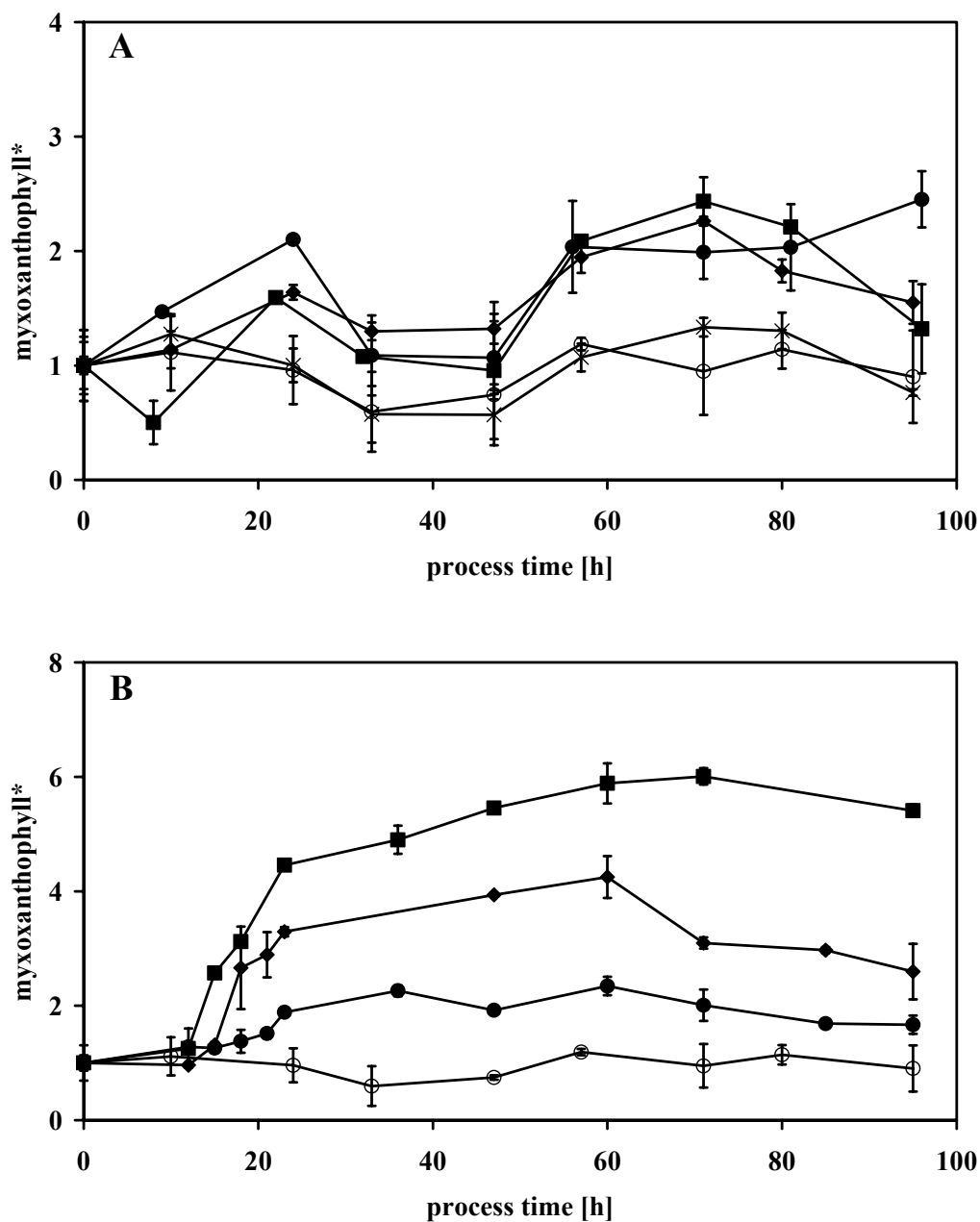


Figure 5.15. Normalised myxoxanthophyll concentrations (myxoxanthophyll*) of the cultivation experiments. The UVB = 0 trace is part of both pictures for the sake of comparison. **A:** Turbidostat with UVB = 0 $\mu\text{mol photons m}^{-2} \text{s}^{-1}$ (O); UVB = 0.57 $\mu\text{mol photons m}^{-2} \text{s}^{-1}$ (x); UVB = 0.83 $\mu\text{mol photons m}^{-2} \text{s}^{-1}$ (♦); UVB = 1.25 $\mu\text{mol photons m}^{-2} \text{s}^{-1}$ (●); UVB = 1.61 $\mu\text{mol photons m}^{-2} \text{s}^{-1}$ (■). **B:** Turbidostat with additional physiostatic control $\phi_{PSII,SP} = 0.25$ (●); $\phi_{PSII,SP} = 0.2$ (■); $\phi_{PSII,SP} = 0.15$ (♦) and UVB = 0 $\mu\text{mol photons m}^{-2} \text{s}^{-1}$ (O).

5.4.3. Zeaxanthin

Zeaxanthin concentrations in turbidostatic processes with and without stepwise changed UVB-intensities are depicted in Fig. 5.16A. Whereas the zeaxanthin concentrations for process without UVB-irradiation remained constant during the process zeaxanthin concentrations of the UVB-irradiated cultivation increased approximately in a linear manner.

Concentration values for three different UVB-intensities (0.57, 0.83 and 1.61 $\mu\text{mol photons m}^{-2} \text{s}^{-2}$) increased to a final enhancement in a range from 295 to 317 % compared to their initial values. An UVB-intensity of 1.25 $\mu\text{mol photons m}^{-2} \text{s}^{-1}$ ended in the highest zeaxanthin enhancement (453 %).

Similar to the effects of the myxoxanthophyll concentrations in physiostatic cultivations the higher efficiency in stimulating pigment concentrations becomes also obvious in the time course of the zeaxanthin concentrations (Fig. 5.16B). Again there was a delay of 12 h before the synthesis was started.

5.4.4. Echinenone

Echinenone concentrations (Fig. 5.17A) for the non UVB-radiated cultivation decreased during the entire process time down to 75 % of the initial value at the end of the cultivation period. UVB-radiated cultivations showed a different picture. All cultivations achieved their maximal echinenone concentration after a process time of 71 to 81 hours. Concentration increased by 55 % (UVB-intensity = 0.57 $\mu\text{mol photons m}^{-2} \text{s}^{-1}$) and 89 % (UVB-intensity = 0.83 $\mu\text{mol photons m}^{-2} \text{s}^{-1}$). The two other intensities led to similar increases (56 and 62 %). At the end of the cultivations, echinenone concentrations of all UVB-radiated experiments (Fig. 5.17A) dropped below their maxima and obtained values between 107 % (UVB-intensity = 0.57 $\mu\text{mol photons m}^{-2} \text{s}^{-1}$) and 160 % (UVB-intensity = 0.83 $\mu\text{mol photons m}^{-2} \text{s}^{-1}$) of their initial values.

In Fig. 5.17B, echinenone enhancements of the physiostatic processes are presented. Again, a delay of 12 hours was found in all experiments followed by a fast increase. Between 60 and 71 hours the maximal enhancements were reached. Employing a set point of 0.25 led to a maximal increase by 51 % whereas maxima of 193 % ($\phi_{\text{PSII,SP}} = 0.15$) and 216 % ($\phi_{\text{PSII,SP}} = 0.2$) for the other two physiostatic processes occurred. Afterwards, echinenone remained

constant for $\phi_{\text{PSII,SP}} = 0.2$. For $\phi_{\text{PSII,SP}} = 0.15$ and $\phi_{\text{PSII,SP}} = 0.25$ echinenone decreased down to 133 % and 147 % of their initial values. Nevertheless, the enhancement of echinenone (Fig. 5.17B) is less pronounced than the enhancements of myxoxanthophyll and zeaxanthin (Figs. 5.15B and 5.16B) in the physiostatic processes.

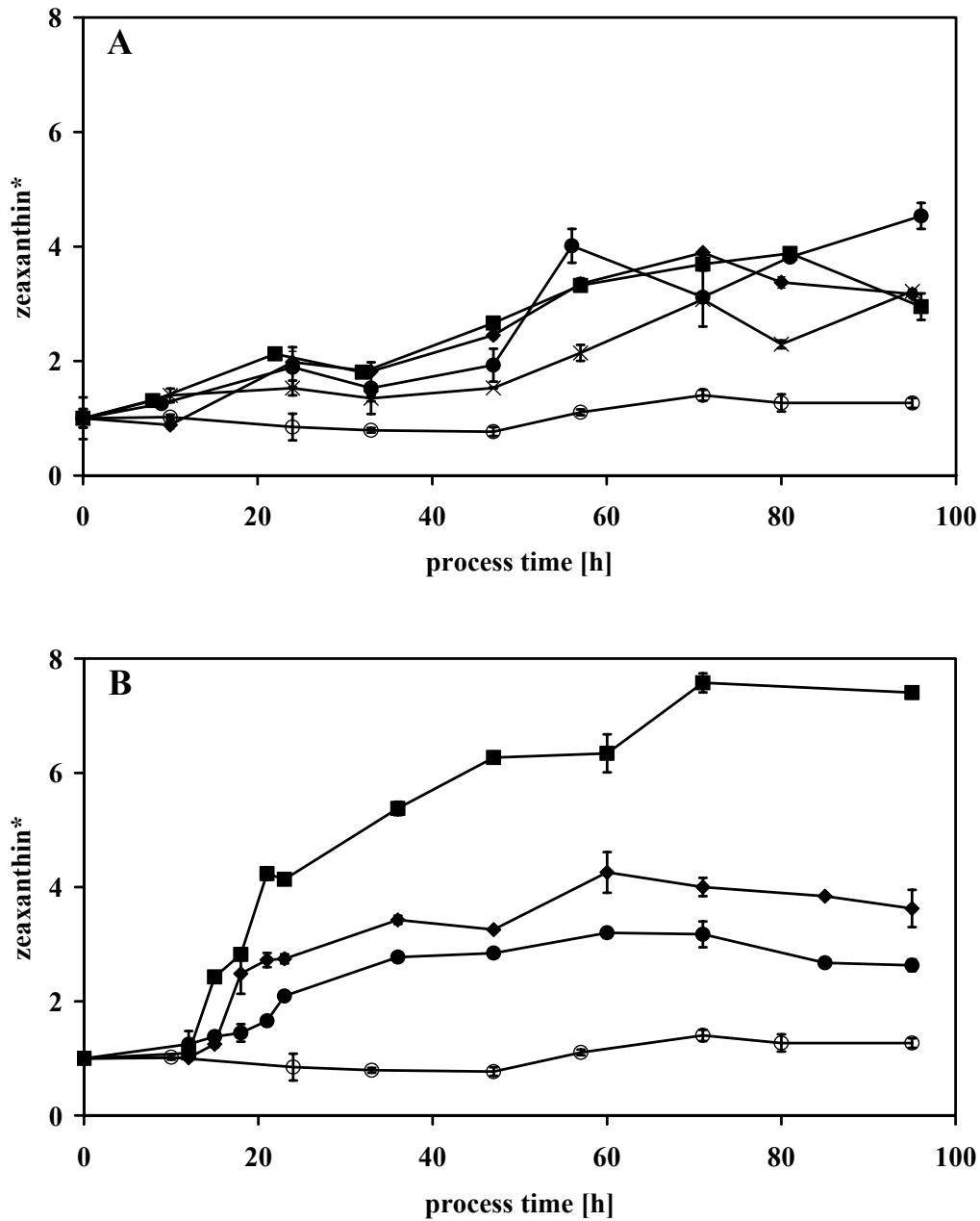


Figure 5.16. Normalised zeaxanthin concentrations (zeaxanthin*) of the cultivation experiments. The UVB = 0 trace is part of both pictures for the sake of comparison. **A:** Turbidostat with UVB = 0 $\mu\text{mol photons m}^{-2} \text{s}^{-1}$ (O); UVB = 0.57 $\mu\text{mol photons m}^{-2} \text{s}^{-1}$ (x); UVB = 0.83 $\mu\text{mol photons m}^{-2} \text{s}^{-1}$ (\blacklozenge); UVB = 1.25 $\mu\text{mol photons m}^{-2} \text{s}^{-1}$ (\bullet); UVB = 1.61 $\mu\text{mol photons m}^{-2} \text{s}^{-1}$ (\blacksquare). **B:** Turbidostat with additional physiostatic control $\phi_{PSII,SP} = 0.25$ (\bullet); $\phi_{PSII,SP} = 0.2$ (\blacksquare); $\phi_{PSII,SP} = 0.15$ (\blacklozenge) and UVB = 0 $\mu\text{mol photons m}^{-2} \text{s}^{-1}$ (O).

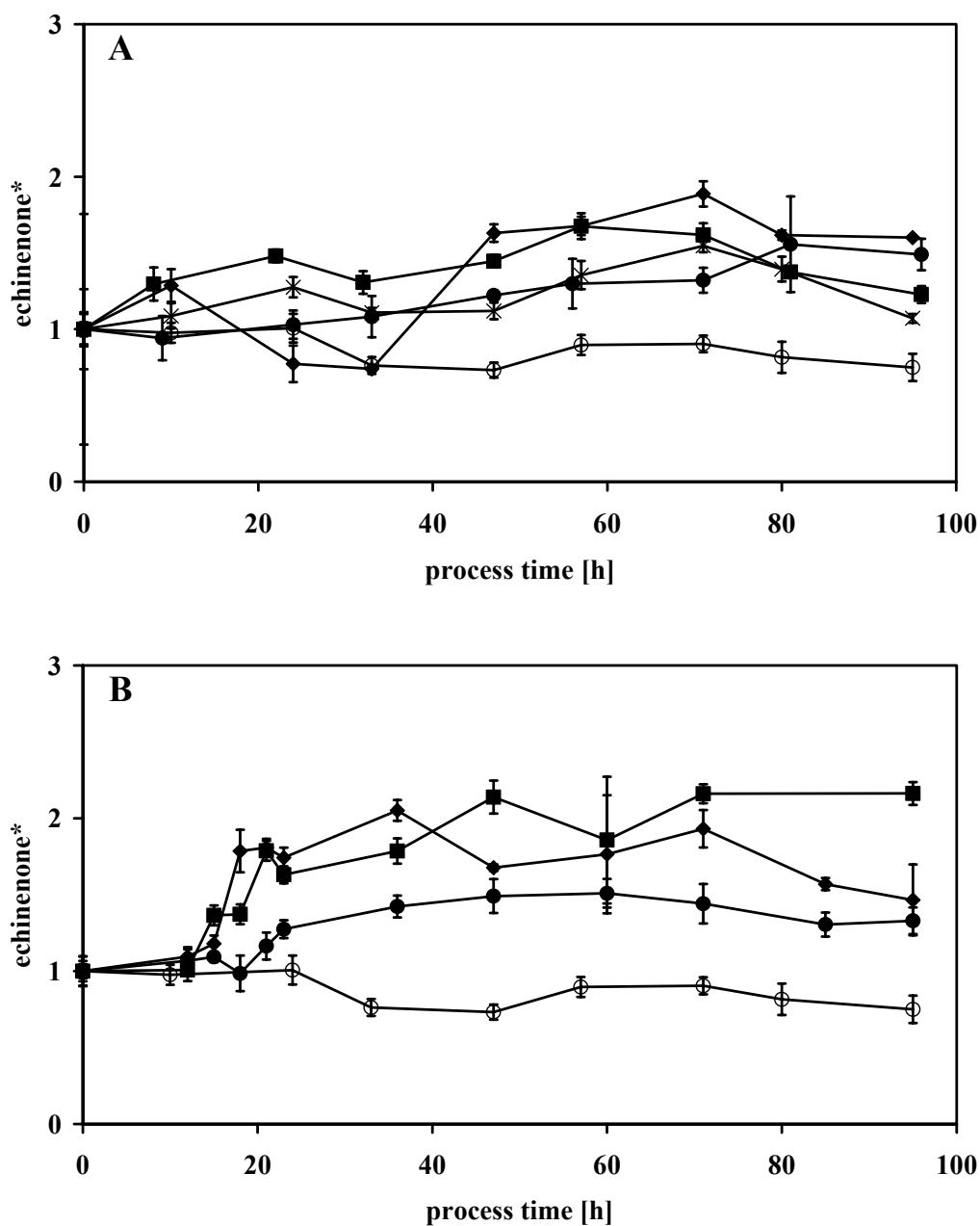


Figure 5.17. Normalised echinenone concentrations (echinenone*) of the cultivation experiments. The UVB = 0 trace is part of both pictures for the sake of comparison. **A:** Turbidostat with UVB = 0 $\mu\text{mol photons m}^{-2} \text{s}^{-1}$ (O); UVB = 0.57 $\mu\text{mol photons m}^{-2} \text{s}^{-1}$ (\times); UVB = 0.83 $\mu\text{mol photons m}^{-2} \text{s}^{-1}$ (\blacklozenge); UVB = 1.25 $\mu\text{mol photons m}^{-2} \text{s}^{-1}$ (\bullet); UVB = 1.61 $\mu\text{mol photons m}^{-2} \text{s}^{-1}$ (\blacksquare). **B:** Turbidostat with additional physiostatic control $\phi_{\text{PSII,SP}} = 0.25$ (\bullet); $\phi_{\text{PSII,SP}} = 0.2$ (\blacksquare); $\phi_{\text{PSII,SP}} = 0.15$ (\blacklozenge) and UVB = 0 $\mu\text{mol photons m}^{-2} \text{s}^{-1}$ (O).

5.4.5. β -Carotene

The non UVB-radiated process showed a decrease of β -carotene at the end of the process to 65 % of its initial value. Employing an UVB-intensity of $1.25 \mu\text{mol photons m}^{-2} \text{s}^{-1}$ increased β -carotene at the end by 33 %. At an UVB-intensity of $1.61 \mu\text{mol photons m}^{-2} \text{s}^{-1}$, β -carotene decreased until the end of the experiment below its initial value after reaching a maximal increase by 35 % at 71 hours. Moderate UVB-irradiation of 0.57 and $0.83 \mu\text{mol photons m}^{-2} \text{s}^{-1}$ increased β -carotene to 185 and 180 % respectively after 71 hours process time. Subsequently the β -carotene concentrations decreased again. This resulted in a final increase of 165 % ($0.57 \mu\text{mol photons m}^{-2} \text{s}^{-1}$) and 156 % ($0.83 \mu\text{mol photons m}^{-2} \text{s}^{-1}$) of β -carotene respectively. Considering the scattering behaviour of the traces it is difficult to come to a final conclusion of whether there is a significant effect of UVB-irradiation in the turbidostat.

Again, the effects become much more clear in the physiostatic process. After the already well-known lag of 12 h, β -carotene contents increases between 12 and 24 hours process time where the main changes occurred. After 24 hours of process time, β -carotene remained in a constant range between 113 and 107 % for 62 hours for the physiostatic process with an adjusted set point of 0.25 ($\phi_{\text{PSII,SP}} = 0.25$). At the end of the process, β -carotene decreased below its initial value to 90%. The lower set point of 0.2 ($\phi_{\text{PSII,SP}} = 0.2$) provoked a β -carotene increase to 223 % after 47 hours of the process time and 210 % of the initial value at the end of the process. The lowest set point ($\phi_{\text{PSII,SP}} = 0.25$) led to a rapid β -carotene increase between 12 and 24 hours process time. Within these 12 hours, β -carotene increase to 165 %. Afterwards the β -carotene concentration slowly decreased until the end of the experiment to 108 %.

Unlike the changes of myxoxanthophyll and zeaxanthin (Figs. 5.15B and 5.16B) and similar to the time course of echinenone (Fig. 5.17B) the UVB-induced enhancement of β -carotene (Fig. 5.18B) is less pronounced.

Summarising the above findings it has to be stated that the physiostatic process is much more efficient in increasing pigment concentrations. This holds especially for myxoxanthophyll and zeaxanthin (Figs. 5.15B and 5.16B). In turbidostatic processes influenced by stepwise changed UVB-intensities only zeaxanthin showed a significant increase of synthesis (Fig. 5.16A).

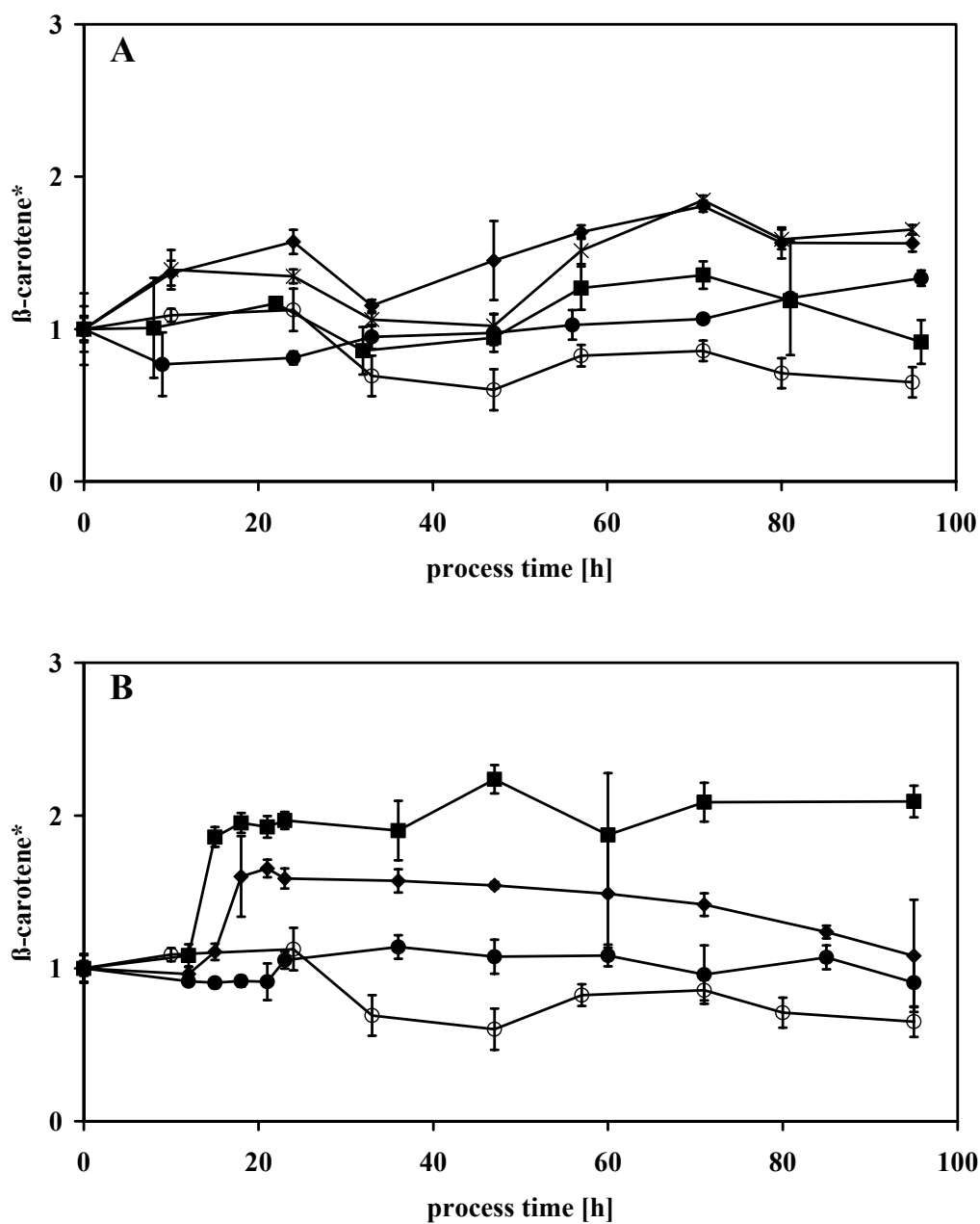


Figure 5.18. Normalised β -carotene concentrations (β -carotene*) of the cultivation experiments. The UVB = 0 trace is part of both pictures for the sake of comparison. **A:** Turbidostat with UVB = 0 $\mu\text{mol photons m}^{-2} \text{s}^{-1}$ (O); UVB = 0.57 $\mu\text{mol photons m}^{-2} \text{s}^{-1}$ (\times); UVB = 0.83 $\mu\text{mol photons m}^{-2} \text{s}^{-1}$ (\blacklozenge); UVB = 1.25 $\mu\text{mol photons m}^{-2} \text{s}^{-1}$ (\bullet); UVB = 1.61 $\mu\text{mol photons m}^{-2} \text{s}^{-1}$ (\blacksquare). **B:** Turbidostat with additional physiostatic control $\phi_{\text{PSII,SP}} = 0.25$ (\bullet); $\phi_{\text{PSII,SP}} = 0.2$ (\blacksquare); $\phi_{\text{PSII,SP}} = 0.15$ (\blacklozenge) and UVB = 0 $\mu\text{mol photons m}^{-2} \text{s}^{-1}$ (O).

5.4.6. Phycobilisomes

The concentration of the phycobilisomes was determined spectrophotometrically after extraction of the samples of the reactors. Because the absorption spectrum is very broad (Fig. 5.19), the area between 550 and 640 nm was calculated (chapter 3.2.3). Since only relative changes were of interest this area was used for the estimation of the influence of UVB-radiation on the cyanobacterial phycobilisome complex.

In Fig. 5.19, a typical absorption spectrum of the phycobilisomes extract is shown. The absorption has a maximum at a wavelength of 630 nm and a long tail towards the shorter wavelengths. Wavelengths longer than 650 nm showed no influence whether or not phycobilisomes were present.

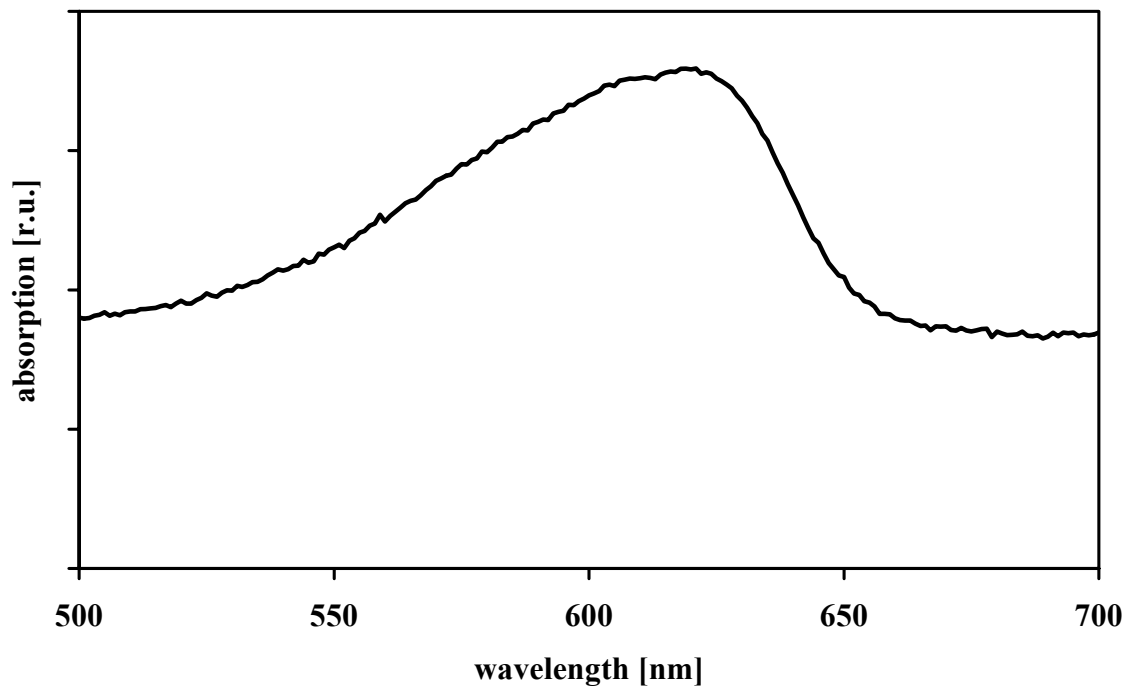


Figure 5.19. Wavelength scan of the phycobilisomes extract. This absorption spectrum was obtained from *Synechocystis* sp. PCC 6803 as described in chapter 3.2.3.6.

Again, the presented time courses in Fig. 5.20 are normalised for the sake of better comparison. Thus, the initial values of phycobilisomes are listed in Table 5.4 for the turbidostatic and physiostatic experiments. Phycobilisome concentration as measured by the area of the absorption spectrum between 550 nm and 640 nm ranged between a minimum of

6.43 area [g BDM]⁻¹ and maximum of 10.55 area [g BDM]⁻¹. The average over all experiments was 8.09 area [g BDM]⁻¹ with a standard deviation of 18.5 %.

Table 5.4. Initial values of the phycobilisomes concentrations (A_{Phyco}) determined for all cultivation experiments before UVB-treatment started.

Turbidostat with stepwise changed UVB-intensity [$\mu\text{mol photons m}^{-2}\text{s}^{-1}$]	Initial phycobilisomes concentration [$A_{\text{Phyco}} / \text{g BDM}$]
0.00	7.80 ± 0.74
0.57	7.40 ± 0.56
0.83	6.65 ± 1.57
1.25	8.40 ± 0.48
1.61	10.01 ± 0.53

Turbidostat with additional physiostatic control ($\phi_{\text{PSII,SP}}$)	Initial phycobilisomes concentration [$A_{\text{Phyco}} / \text{g BDM}$]
0.25	6.43 ± 0.69
0.20	7.48 ± 0.51
0.15	10.55 ± 1.02

Overall average	8.09
Deviation [%]	18.5

Time courses of the phycobilisome measurements are presented in Fig. 5.20A and Fig. 5.20B. In Fig. 5.20A the non UVB-radiated cultivation showed an increase to 150 % of phycobilisomes content until the end of the experiment. Phycobilisome contents in the turbidostat influenced by stepwise changed UVB-radiation petered out in approximately exponential manner (Fig. 5.20A). Applying an UVB-intensity of 0.57 $\mu\text{mol photons m}^{-2} \text{s}^{-1}$ provoked a decrease of the phycobilisomes to 45 % of the initial value. Higher intensities of 0.83 and 1.25 $\mu\text{mol photons m}^{-2} \text{s}^{-1}$ caused a similar decrease to 24.75 and 22.77 % of the

initial values but differed in the degradation rates (see below). The highest UVB-intensity of $1.61 \mu\text{mol photons m}^{-2} \text{ s}^{-1}$ removed the phycobilisomes nearly completely. A remaining phycobilisomes content of 6.65 % appeared.

Phycobilisome contents of physiostatic cultivation experiments decayed with an exponential degradation (Fig. 5.20B). Independently of the employed set point, final values ranged between 20.02 % ($\phi_{\text{PSII,SP}} = 0.25$) and 10.34 % ($\phi_{\text{PSII,SP}} = 0.15$). The set point of 0.2 ($\phi_{\text{PSII,SP}} = 0.2$) led to a decrease to 18.31 % of the initial value.

The results presented in the Fig. 5.20 show the sensitivity of the phycobilisomes against UVB-radiation which is more pronounced than the sensitivity of e.g. chlorophyll *a* (Fig. 5.14).

By means of Eq. 3.5, the degradation rate of the phycobilisomes was calculated. Figure 5.21 depicts a typical fit for the determination of the degradation rate. The fits delivered different degradation rates for different UVB-intensities in the turbidostatic experiments.

Fitted degradation rates versus employed UVB-intensity are shown in Fig. 5.22. The figure shows a linear relationship between degradation rate and used UVB-intensity.

Furthermore, the extrapolated regression line predicts the prompt degradation of the phycobilisomes in the cells employing an UVB-intensity of $2.2 \mu\text{mol photons m}^{-2} \text{ s}^{-1}$ under the conditions used in the cultivation experiments.

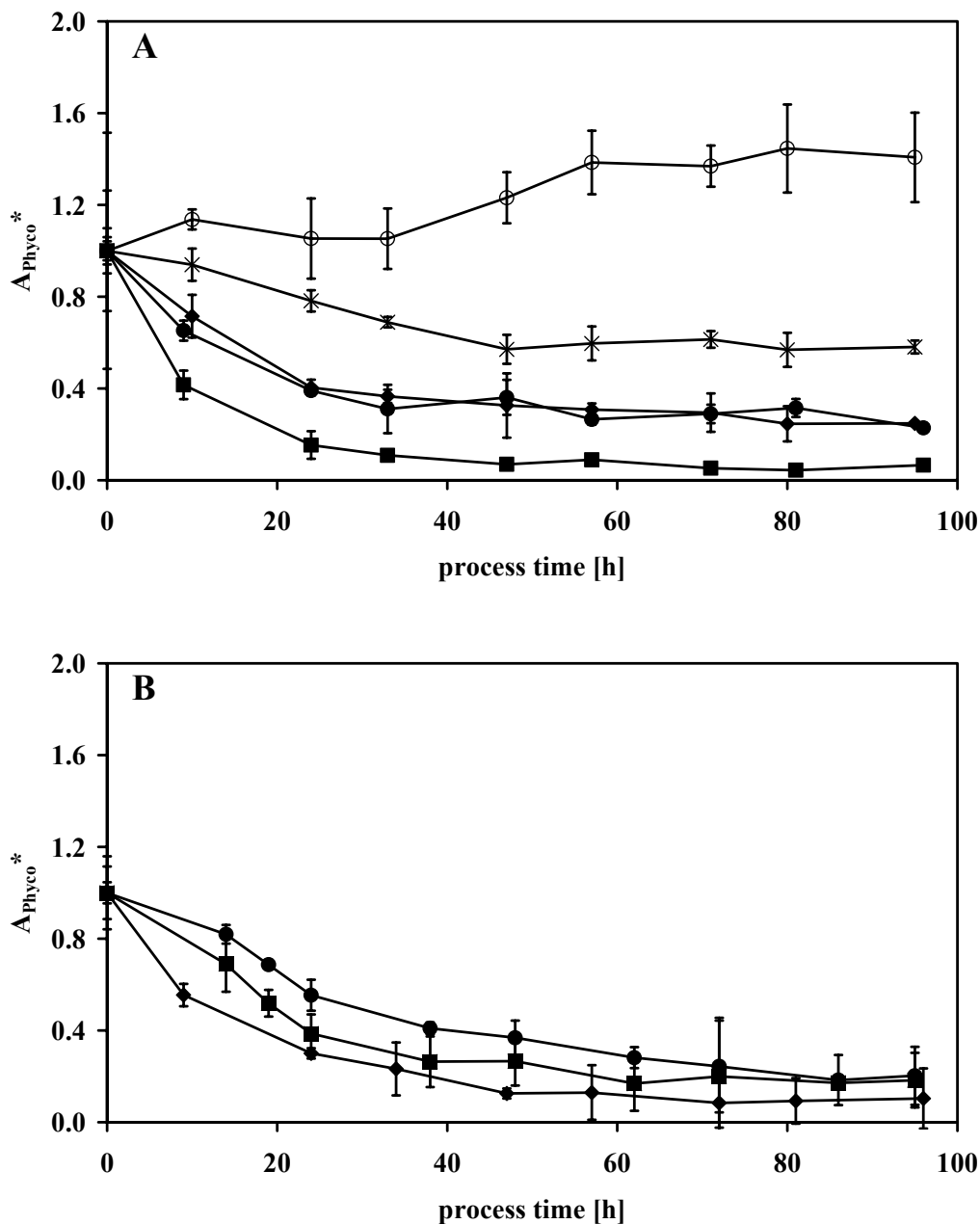


Figure 5.20. Normalised phycobilisome concentrations (A_{Phycos}) of the cultivation experiments. **A:** Turbidostat with UVB = 0 $\mu\text{mol photons m}^{-2} \text{s}^{-1}$ (O); UVB = 0.57 $\mu\text{mol photons m}^{-2} \text{s}^{-1}$ (x); UVB = 0.83 $\mu\text{mol photons m}^{-2} \text{s}^{-1}$ (\blacklozenge); UVB = 1.25 $\mu\text{mol photons m}^{-2} \text{s}^{-1}$ (\bullet); UVB = 1.61 $\mu\text{mol photons m}^{-2} \text{s}^{-1}$ (\blacksquare). **B:** Turbidostat with additional physiostatic control $\phi_{\text{PSII,SP}} = 0.25$ (\bullet); $\phi_{\text{PSII,SP}} = 0.2$ (\blacksquare); $\phi_{\text{PSII,SP}} = 0.15$ (\blacklozenge).

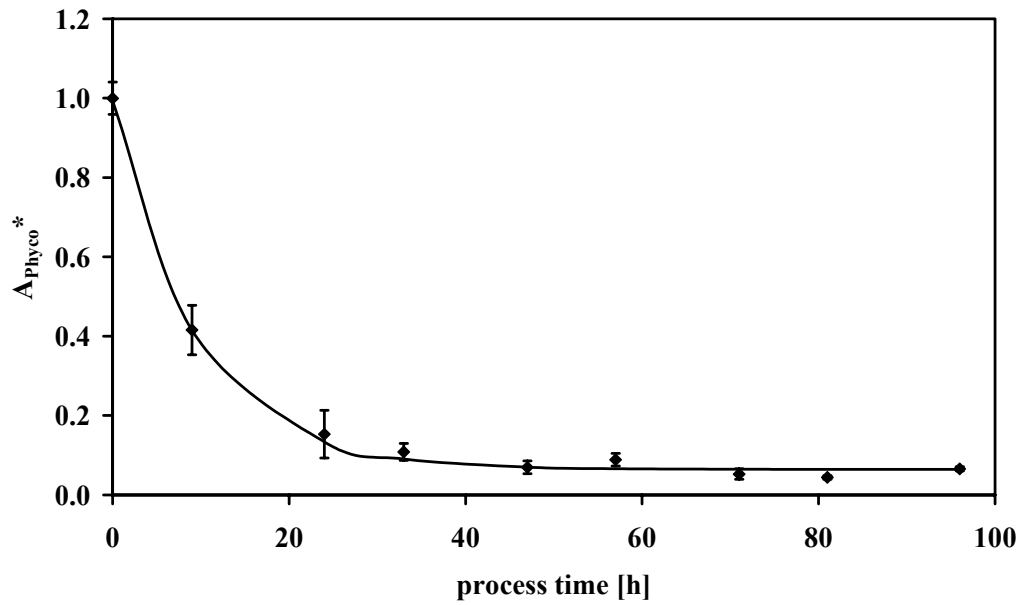


Figure 5.21. Typical fit for determination of the degradation rate using Eq. 3.5.

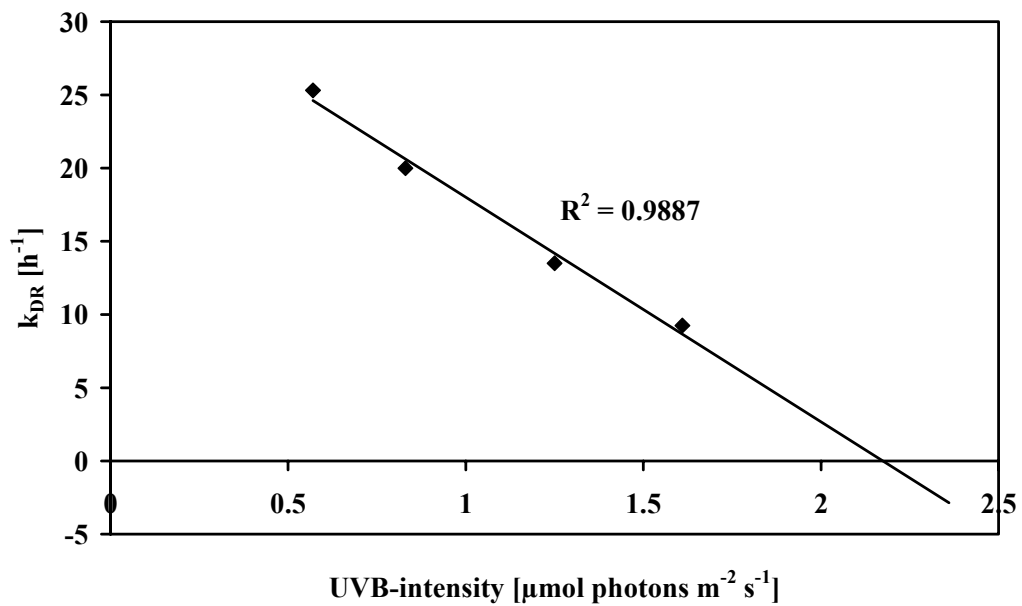


Figure 5.22. Relationship between degradation rate (k_{DR}) and employed UVB-intensity.

5.5. Optimum curves of the carotenoid and xanthophylls

Fig. 5.23A and Fig. 5.23B show the UVB-induced average changes (in the turbidostat and in the physiostat) of the pigments myxoxanthophyll, zeaxanthin, echinenone and β -carotene for the last 24 hours of each experiment. Without UVB-intensity pigments remained at the initial level (Fig. 5.23A, not repeated here).

In the turbidostat under moderate UVB-intensities of 0.57 and 0.83 $\mu\text{mol photons m}^{-2} \text{s}^{-1}$, β -carotene and echinenone yielded maximal changes (1.69-fold and 2.25-fold). At higher intensities, both β -carotene and echinenone decreased and reached constant values of 1.41-fold (echinenone) and 1.15-fold (β -carotene) above the initial values.

Zeaxanthin and myxoxanthophyll were maximally enhanced using an UVB-radiation of 1.25 $\mu\text{mol photons m}^{-2} \text{s}^{-1}$. Zeaxanthin increased to 382 % of its origin value and decreased at an higher UVB-intensity of 1.61 $\mu\text{mol photons m}^{-2} \text{s}^{-1}$ to 351 % of the initial value. Maximal myxoxanthophyll enhancement, 2.3-fold of the initial value, occurred at 1.25 $\mu\text{mol photons m}^{-2} \text{s}^{-1}$. This enhancement decrease to 1.89 employing an UVB-radiation of 1.61 $\mu\text{mol photons m}^{-2} \text{s}^{-1}$.

Experiments in the physiostat showed pigment changes dependent on the adjusted set point (Fig. 5.23B). The four pigments increased to a maximum under a set point of 0.2 ($\phi_{\text{PSII,SP}} = 0.2$). β -Carotene and echinenone reached nearly identical increases of 2-fold above their initial values. Myxoxanthophyll increased to 571 % compared to the origin value whereas zeaxanthin adapted to a maximum enhancement of 749 %. With set points of 0.15 and 0.25, β -carotene enhancements ranged on the same level (125 % and 98 %). Similar β -carotene and echinenone changes using set points of 0.15 and 0.25 reached enhanced values of 165 % and 136 % of their initial values increase.

Myxoxanthophyll increased by 189 % under a set point of 0.25, a lower set point of 0.15 caused an increase by 282 %. At a set point of 0.25 zeaxanthin concentration was enhanced to 289 % of the origin value as a lower set point of 0.15 caused an increase by 282 %.

The comparison of pigment changes induced by UVB in the turbidostat (Fig. 5.23A) and in the physiostat (Fig. 5.23B) shows the advantage of a physiostatic process when the aim of a cultivation is the upregulation of some pigments (e.g. myxoxanthophyll and zeaxanthin).

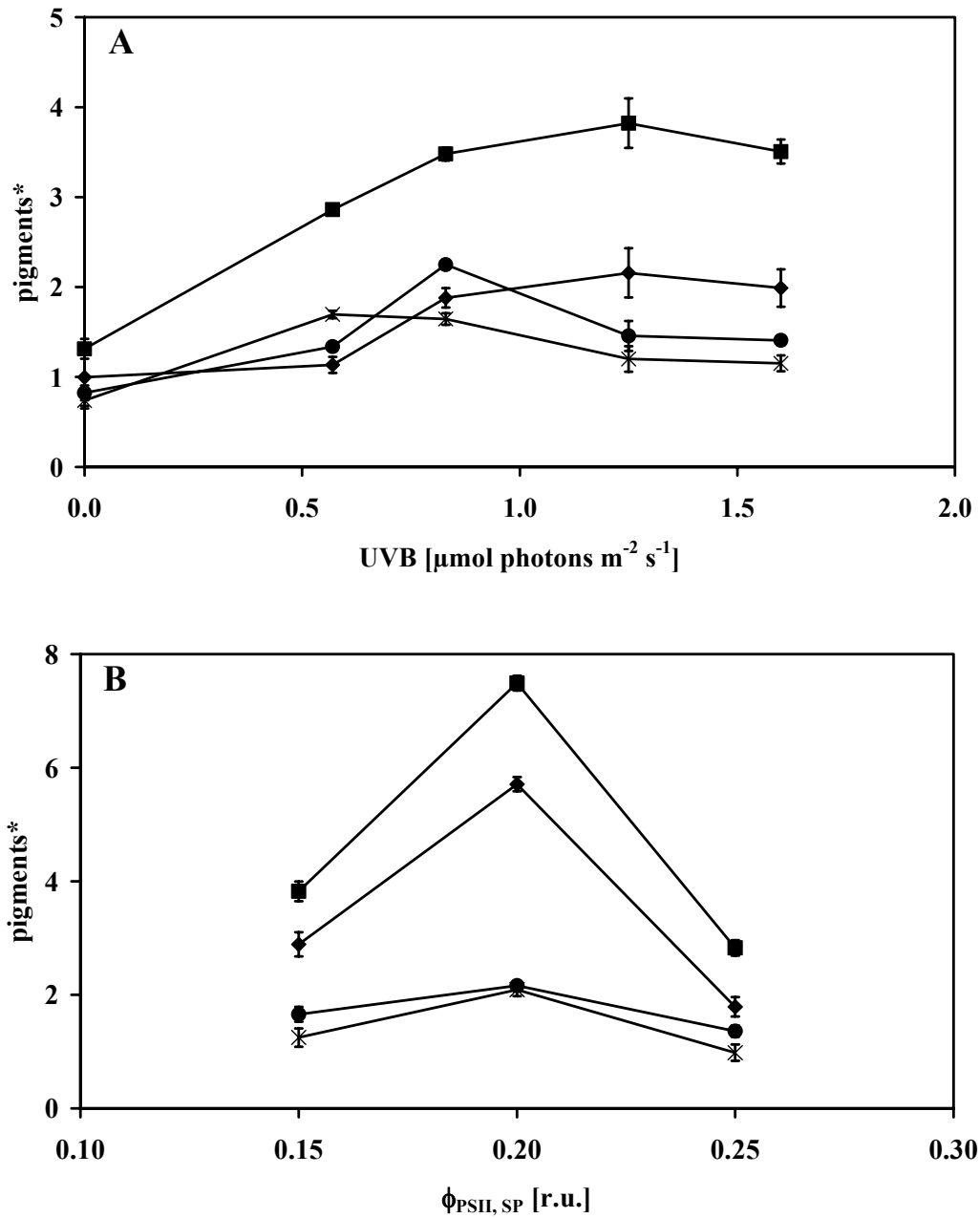


Figure 5.23. Normalised pigment changes (pigments*) at the end of the cultivation experiments (72 – 96 h) induced by either stepwise changed UVB-intensities or modulated UVB-intensities. Myxoxanthophyll (◆); Zeaxanthin (■); Echinenone(●); β -Carotene(×) (A) Turbidostat with stepwise changed UVB-intensity. (B) Turbidostat with additional physiostatic control ($\phi_{\text{PSII,SP}}$). r.u. = relative units.

5.6. Mycosporine-like amino acids (MAAs; here shinorine)

The HPLC-method (chapter 3.2.3) revealed two peaks in the chromatogram. The first one was identified as the injection peak, and the second one was unknown in the first investigations. Therefore, three 10 mL freeze-dried reactor samples were sent to a commercial laboratory (TeLA GmbH, Bremerhaven, Germany). The analyses revealed shinorine as a cellular component of *Synechocystis* sp. PCC 6803. Therefore, it was possible to assign the unknown peak in the HPLC-chromatogram to shinorine.

For testing influences of UVB-radiation on the shinorine content, three cultivation experiments were used. Two of them were conducted in the turbidostat with ($1.25 \mu\text{mol photons m}^{-2} \text{s}^{-1}$) and without UVB-irradiation, the third one in the physiostat ($\phi_{\text{PSII,SP}} = 0.2$). The HPLC-intern analysis program calculated the shinorine area. These data were normalised to the related biological dry mass. Since the time courses are normalised to “1”, the initial values taken before irradiation are listed in Table 5.5. Initial areas between 115288 [-] and 172304 [-] were found.

Table 5.5. Shinorine area normalised to the related biological dry mass. The values were measured before the UVB-treatments started.

Turbidostat with stepwise changed UVB-intensity [$\mu\text{mol photons m}^{-2} \text{s}^{-1}$]	$A_{\text{Shinorine}} / \text{g BDM}$
0.00	124424 ± 17890
1.25	172304 ± 12650
Turbidostat with additional physiostatic control ($\phi_{\text{PSII,SP}}$)	$A_{\text{Shinorine}} / \text{g BDM}$
0.20	115288 ± 25490

Figure 5.24 shows the temporal development in the three experiments. The not UVB-radiated samples varied between 91 % and 128 % of the initial values. At the end of the

cultivation, the shinorine concentration reached the same value as the initial value at the beginning of the experiment. Shinorine concentrations influenced by stepwise changed UVB-radiation in the turbidostat showed also variations in the same range from 89 % to 110 %. The highest range was obtained from the physiological controlled cultivation. A range from 93 % to 138 % occurred. For all investigated cultivation experiments, no significant trends were detectable, and the shinorine concentrations remained constant during the entire experiments.

The results show that in *Synechocystis* sp. PCC 6803 UVB-radiation do not lead to an enhanced synthesis of shinorine. This finding is different from those in other microorganisms.

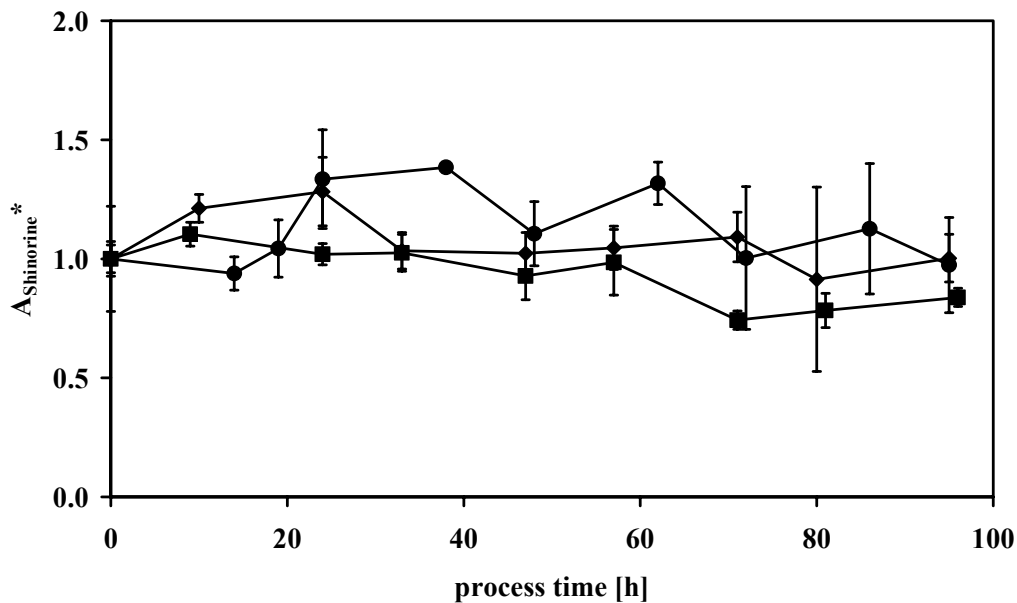


Figure 5.24. Normalised shinorine ($A_{\text{Shinorine}^*}$) time courses of the three experiments measured in the turbidostat with stepwise changed UVB-irradiation of $1.25 \mu\text{mol photons m}^{-2} \text{s}^{-1}$ (■), without UVB-radiation (◆) or in the physiostat with $\phi_{\text{PSII,SP}} = 0.2$ (●).

5.7. α -Tocopherol measurements

Freeze-dried samples from the reactors were analysed *offline* in order to determine the α -tocopherol concentrations. By means of the HPLC-method (chapter 3.2.3) clear differences were evoked by different experimental conditions.

Again, the initial concentrations of α -tocopherol (taken before irradiation) are listed in Table 5.6. A minimum and maximum of 1.99 and 7.79 mg [g BDM]⁻¹, respectively, appeared. This wide range causes the high deviation of 44.7 % for a overall average of 4.78 mg [g BDM]⁻¹.

In Fig. 5.25A, time courses of α -tocopherol concentrations are shown for the experiments with and without UVB-irradiation in the turbidostat. α -Tocopherol concentrations varied during the entire cultivation process without UVB-illumination between a minimum of 67 % (at the end of the cultivation) and a maximum of 152 % (after 71 hours) of the initial value.

Exposure to an UVB-intensity of 0.57 $\mu\text{mol photons m}^{-2} \text{s}^{-1}$ decreased the α -tocopherol concentration in the turbidostat within 47 hours to 95 % of the initial value. Thereafter, the concentration increased to a maximum of 150 % of the origin value and reached a final value of 120 % at the end of the cultivation. Higher doses of UVB-radiation did not evoke significantly different behaviour. The initial dip around 20 h was more pronounced, and the trace related to an exposure to 0.83 $\mu\text{mol photons m}^{-2} \text{s}^{-1}$ decreased down to 45 % at the end of the cultivation process. However, the data display a strong scatter which prevents that effects of this kind have to be taken too serious. The most likely statement is that the α -tocopherol concentrations with UVB-irradiation show a weak increase after an transient decrease rather than the more or less monotonous decrease in the case of non-UVB-irradiated cells.

Table 5.6. Averaged initial values of α -tocopherol measurements before UVB-treatment started.

Turbidostat with stepwise changed UVB-intensity [$\mu\text{mol photons m}^{-2}\text{s}^{-1}$]	Initial α-tocopherol concentration [$\mu\text{g / g BDM}$]
0.00	1.99 ± 1.07
0.57	1.80 ± 0.43
0.83	4.60 ± 3.20
1.25	4.96 ± 0.69
1.61	4.22 ± 0.18
Turbidostat with additional physiostatic control ($\phi_{\text{PSII,SP}}$)	Initial α-tocopherol concentration [$\mu\text{g / g BDM}$]
0.25	5.99 ± 0.71
0.20	7.79 ± 1.70
0.15	6.89 ± 1.26
Overall average	4.78
Deviation [%]	44.7

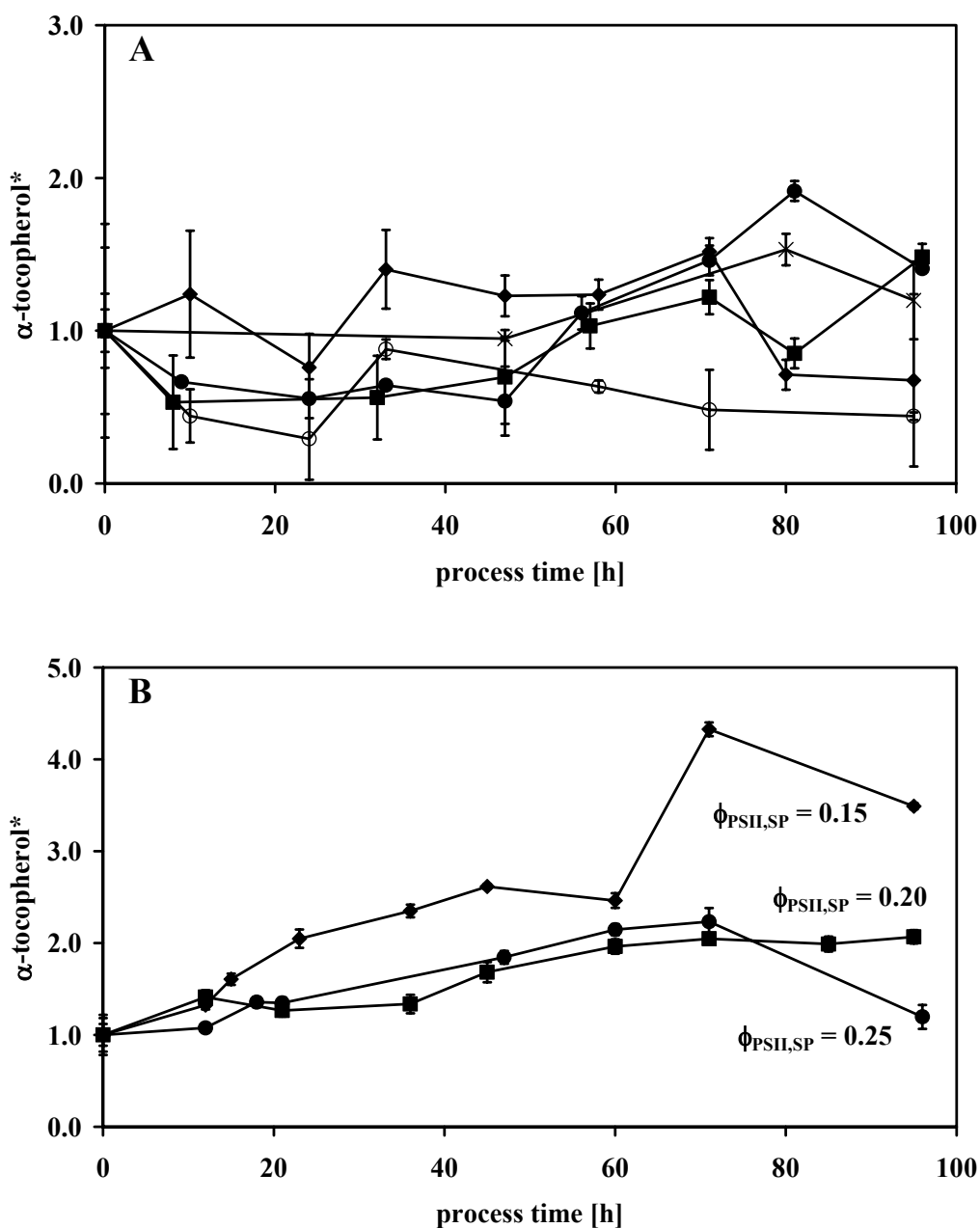


Figure 5.25. Normalised α -tocopherol measurements (α -tocopherol*) of the cultivation experiments. **A:** Turbidostat with UVB = 0 $\mu\text{mol photons m}^{-2} \text{s}^{-1}$ (O); UVB = 0.57 $\mu\text{mol photons m}^{-2} \text{s}^{-1}$ (\times); UVB = 0.83 $\mu\text{mol photons m}^{-2} \text{s}^{-1}$ (\blacklozenge); UVB = 1.25 $\mu\text{mol photons m}^{-2} \text{s}^{-1}$ (\bullet); UVB = 1.61 $\mu\text{mol photons m}^{-2} \text{s}^{-1}$ (\blacksquare). **B:** Turbidostat with additional physiostatic control $\phi_{\text{PSII,SP}} = 0.25$ (\bullet); $\phi_{\text{PSII,SP}} = 0.2$ (\blacksquare); $\phi_{\text{PSII,SP}} = 0.15$ (\blacklozenge).

The results of the physiostatic experiments are presented in Fig. 5.25B. After switching on the controlling mode, α -tocopherol concentrations in all physiostatic experiments increased and reached maxima after 72 hours process time (i.e. about 230 % for

the set points $\phi_{\text{PSII,SP}} = 0.20$ and 0.25). From this point until the end of the experiment, α -tocopherol concentration remained constant for $\phi_{\text{PSII,SP}} = 0.2$ at about 205 % of the initial value. In the case of the other set points more or less significant decreases occur. Experiments with a set point of 0.15 ($\phi_{\text{PSII,SP}} = 0.15$) led to the higher enhancements of α -tocopherol concentrations with an maximum of 430 % after 72 hours and a final value the end of the cultivation process of 349 % of the value before exposure to UVB.

In the physiostatic cultivations it becomes obvious that UVB-radiation enhances the amount of α -tocopherol in *Synechocystis* sp. PCC 6803. This enhancement of the α -tocopherol concentration in physiostatic processes leads to the assumption that α -tocopherol plays an important role in protecting *Synechocystis* sp. PCC 6803 against UVB-radiation as discussed in chapter 7.

5.8. Antioxidative potential (AOP)

With respect to the pilot studies of chapter 4.1 the antioxidative potential (AOP) was *offline* determined using the DPPH-method described in chapter 3. The measurement of the AOPs was used for the determination of the integral efficiency of the methanol soluble antioxidants in *Synechocystis* sp. PCC 6803.

Since also here the time courses of the changes in AOP under UVB-irradiation are normalised to “1”, the real values of the AOP taken before the onset of irradiation are listed in Table 5.7. The values are in good agreement with the determined slope of *Synechocystis* sp. PCC 6803 of the pilot studies presented in Chapter 4.1. In these initial values, a maximum of $24.45 \mu\text{mol DPPH} [\text{g BDM}]^{-1}$ and minimum of $17.45 \mu\text{mol DPPH} [\text{g BDM}]^{-1}$ were found. The overall average was $20.5 \mu\text{mol DPPH} [\text{g BDM}]^{-1}$ with a standard deviation of 11.3 %.

The time courses measured in the turbidostat with and without UVB-irradiation are presented in Fig. 5.26A. AOP data from the non UVB-illuminated cells showed a decrease down to 11 % of the initial value at the end of the cultivation. Exposure to UVB-irradiation in the turbidostat showed moderate increases of reduced DPPH. It is hardly possible to find a clear effect of the intensity, because of the scattering behaviour. The final values at the end of the experiment ranged between 181 and 226 % of the initial values. Even though there is no

significant influence of intensity, there is a significant increase over the AOP of the non-irradiated cells. Thus, it may be concluded that the intensities are already saturating for stimulating the antioxidative potential of methanol soluble antioxidants. It may be argued that the capacity of the methanol is saturated (as described in chapter 4.1.2 and 4.1.3). However, then a clear influence of intensity should be seen at the beginning of the exposure to UVB when the increases of the amounts of antioxidants are still small.

Table 5.7. Averaged initial values of the antioxidative potential (AOP) determined by the DPPH-measurements for the cultivation experiments before UVB-treatments started.

Turbidostat with stepwise changed UVB-intensity [$\mu\text{mol photons m}^{-2}\text{s}^{-1}$]	Initial antioxidative potential [$\mu\text{mol DPPH / g BDM}$]
0.00	21.42 \pm 0.68
0.57	24.45 \pm 0.52
0.83	22.11 \pm 0.73
1.25	17.45 \pm 0.16
1.61	18.49 \pm 0.59
Turbidostat with additional physiostatic control ($\phi_{\text{PSII,SP}}$)	Initial antioxidative potential [$\mu\text{mol DPPH / g BDM}$]
0.25	18.42 \pm 0.95
0.20	21.43 \pm 0.74
0.15	20.40 \pm 2.07
Overall average	20.52
Deviation [%]	11.3

The stimulation of the synthesis of methanol soluble antioxidants is much more evident in the physiostatic processes (Fig. 5.26B). For all set points, a strong increase up to 260 % is observed. The high set-points of $\phi_{\text{PSII,SP}} = 0.2$ and 0.25 ended in a plateau of about

equal height. The trace with the lower set point ($\phi_{\text{PSII,SP}} = 0.15$) started to decay after 60 h exposure time, before it reached a maximum which was in the same range as the final values of the other two set points. Maybe, the decay indicates a severe damage of the system.

The initial slope of the responses to UVB-exposure is quite different. There is no lag time for the lowest set point (with the highest UVB-intensity) and a delay of up to 20 h for the highest set-point. All curves reach the major step to the maximum quite fast within 30 to 40 h. The behaviour in the physiostatic processes is similar to that of myxoxanthophyll and zeaxanthin. They all show the major part of the increase in the physiostatic processes between 12 and 24 h after UVB-exposure. Also the differences of the responses under turbidostatic and physiostatic control (Fig. 5.26) resemble those found for myxoxanthophyll and zeaxanthin (Fig. 5.15 and Fig. 5.16). This may be taken as a hint that the AOP is mainly furnished by these two pigments. This, however, is discussed in more detail in chapter 7.

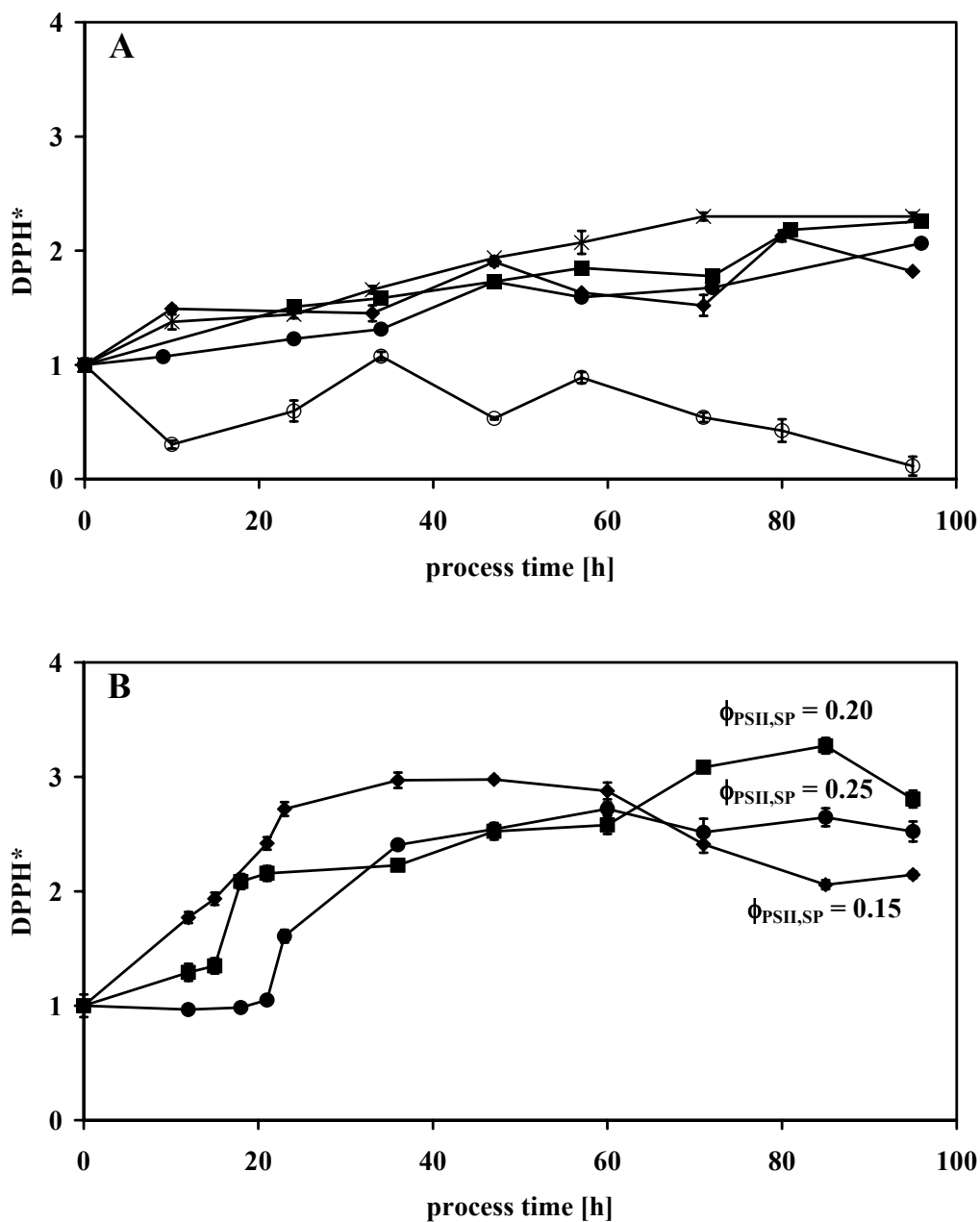


Figure 5.26. Time courses of the normalised AOPs (DPPH*) after the exposure to UVB-irradiation. **A:** Turbidostat with UVB = 0 $\mu\text{mol photons m}^{-2} \text{s}^{-1}$ (O); UVB = 0.57 $\mu\text{mol photons m}^{-2} \text{s}^{-1}$ (x); UVB = 0.83 $\mu\text{mol photons m}^{-2} \text{s}^{-1}$ (\blacklozenge); UVB = 1.25 $\mu\text{mol photons m}^{-2} \text{s}^{-1}$ (\bullet); UVB = 1.61 $\mu\text{mol photons m}^{-2} \text{s}^{-1}$ (\blacksquare). **B:** Turbidostat with additional physiostatic control $\phi_{\text{PSII,SP}} = 0.25$ (\bullet); $\phi_{\text{PSII,SP}} = 0.2$ (\blacksquare); $\phi_{\text{PSII,SP}} = 0.15$ (\blacklozenge).

6. Discussion of the pilot studies

In this chapter a discussion of the pilot studies is given. The discussion deals with the AOP-measuring method and the physiostatic pilot study. The overall discussion is presented in chapter 7.

6.1. Discussion of the AOP-measuring method

A method capable of determining antioxidant potential (AOP) should use a wavelength whose absorbance is mainly influenced by the DPPH radical and not by interference as caused by antioxidants (Bondet et al., 1997), e.g. carotenoids, polyunsaturated fatty acids (PUFAs), α -tocopherol. By means of the experiments presented in Fig. 4.1, a key to such an approach was found. This key is the peculiarity of the behaviour at the wavelength of 550 nm, namely that the absorbance change reflects the chemical state of the DPPH radicals (oxidized or reduced state) without interference by α -tocopherol. Therefore, this wavelength enables a straightforward analysis and interpretation of the measured absorbance decrease.

The effect of α -tocopherol in Fig. 4.1 on the absorbance at wavelengths different from 550 nm has to be taken serious. The problem which is illustrated in Fig. 4.1 was also found by Britton (1995). He found that wavelength signals below 530 nm are strongly influenced by carotenoids. In general, the problem may not arise from α -tocopherol (or carotenoids) alone, also other methanolic soluble compounds from microorganisms like PUFAs as well as some proteins are known to exhibit antioxidative potential (Fang et al., 2002). This could lead to a misinterpretation of the measured absorbance decrease when a wavelength is chosen which is influenced by both DPPH radical and the absorptive properties of the extract (as by carotenoids).

In addition to the selection of a proper wavelength (which may not exclude all possible interferences), a major part of this kind of interference can be eliminated by running the absorbance measurement against a reference cuvette filled with the same extract

concentration as in the measuring cuvette. This was done throughout the investigations presented here

The experiments of Figs. 4.2A and 4.3A indicate some caveats regarding the extraction by methanol. At low concentrations, Figs. 4.2A and 4.3A show a linear decrease of DPPH absorption saturation of the absorbance decrease when plotted vs. extract concentration. This is a very encouraging result providing evidence that only the amount of antioxidants in the extracts are measured independent of the amount of added DPPH. However, the saturation regions have to be avoided. This saturation can be explained by the limited capacity of methanol to extract the antioxidants from the aliquots of freeze-dried microorganisms. Finding equal decreases in the saturating region for both DPPH concentrations indicates that only the amount of antioxidants which were extracted (and not what was in the aliquots) were measured by this procedure. The independence on DPPH concentration leads to the conclusion that the volume of the applied methanol is not able to extract the complete content of carotenoids and PUFAs from the investigated microorganisms samples.

The above explanation based on limited capacity of methanol extraction is supported by the effect of α -tocopherol on the absorbance measurements. Fig. 4.2B and Fig. 4.3B show that the remaining absorbance in Figs. 4.2A and 4.3A is caused by DPPH radicals, which were left over after the antioxidants in the extracts were used up. Adding α -tocopherol, the remaining DPPH were reduced, and thus the absorbance at 550 nm reached values close to zero.

Summarising the results of Figs. 4.2A and 4.3A, the great benefit of this approach becomes obvious namely that the slope in Figs. 4.2A and 4.3A is a direct measure of the antioxidative potential of the investigated sample of microorganisms. Thus, this slope yields a useful tool for the direct comparison of different extracts with respect to their antioxidant potential. However, the saturation region has to be avoided.

In the experiments reported here, there are two important features which make the method powerful. One is the selection of the most adequate wavelength, the other one is the usage of the slopes in Figs. 4.2A and 4.3A (i.e. repeating the experiment with different extract concentrations). The evaluation by means of the slope can also be employed when a different wavelength is employed, which may be more suitable for other microorganisms or chemicals. Another result of Figs. 4.2A and 4.3A is already mentioned above, i.e., the independence of

the slope on DPPH concentration. This provides an important advantage over the determination of the antioxidative capacity based on the EC_{50} value (Table 4.1).

The method investigated here has an important restriction, i.e., methanolic extraction excludes the detection of the antioxidative potential of water soluble antioxidative substances, e.g. ascorbat, glutathion, phycocyanin (Romay et al., 1998). Thus, carotenoids, fatty acids, and α -tocopherol are the most likely candidates causing the decrease of DPPH absorbance.

By using methanol as extract solvent all methanolic soluble components from a microorganisms sample will be collected in the methanolic extract phase. It is therefore not possible to say which component of the investigated microorganisms is mainly responsible for the reduction of the DPPH radicals.

The compositions of carotenoids and fatty acids in microorganisms samples are individual and vary from species to species (Wada & Murata, 1990; Yongmanitchai & Ward, 1991; Allakhverdiev et al., 1999; Kosakowska et al., 2004). Furthermore the individual composition of these two components within one microorganisms species is influenceable by environmental conditions (Cifuentes et al., 2003; Gomez et al., 2003; Hoshida et al., 2005).

The estimation of the influence of environmental conditions on the antioxidative potential requires a highly instrumented photobioreactor system. This system should enable the cultivation of the microorganisms under strictly defined conditions (Marxen et al., 2005).

Usually, the DPPH absorbance is measured at a wavelength of 515 - 520 nm (Bandoniene et al., 2002; Pavlov et al., 2002; Gazi et al., 2004). Due to the modification (choosing a wavelength of 550 nm), the AOP-measuring method was successfully tested (Figs. 4.2A and 4.3A) and offers a novel analytical approach in the biotechnology.

6.2. Discussion of the physiostatic pilot studies

Figure 4.4 shows a close of *offline* measured biological dry mass with *inline* measured optical density (Fig. 4.4). Additionally, Fig. 4.4 shows a similar correlation of *inline* measured optical density with *offline* measured photometric samples. Thus, the *inline* measurement of the optical density can be used for turbidostatic processes.

6.2.1. Performance of the physiostat

The system was used for investigating the effect of different UVB-intensities (modulation of the UVB-amplitudes) and different UVB-frequencies on ϕ_{PSII} . This system theoretical approach resulted in the determination of two time constants and amplitude factors by means of frequency response analysis (Fig. 4.10). It is remarkable that the first time constant ($\tau_1 = 0.9$ min) is nearly nineteen-times faster than the second time constant ($\tau_2 = 17.04$ min).

The knowledge of the time constants and amplitude factors (Table 4.4) enabled the identification of the transfer function (Eq. 4.17) of the system “microorganisms” which was to be controlled. It was therefore possible to calculate controller parameters for a reliable control loop. The calculation allowed a new process strategy named physiostat which provided the control of the physiological state of microorganisms under defined conditions.

The crucial feature of the physiostat was the control loop for the actual photosynthetic efficiency of PSII (ϕ_{PSII}). The amplification of the control loop was not independent because of the integral component of the PI-controller. The technical set-up of the photobioreactor system allowed strictly defined cultivation conditions. The selected adjustments of the operating conditions (e.g. pH-value, temperature, optical density, PAR-intensity, see Material and methods) enabled the successful implementation of the physiostat. Changes in some of the conditions may lead to different biological behaviour, so that a new frequency analysis may probably become necessary.

The controller parameters ($K_P = -1$, $T_N = 0.3$ min) used here conformed ϕ_{PSII} to the set point ($\phi_{\text{PSII, SP}}$, Fig. 4.14) within two hours which were 2.6 % of the total process time (78 h).

The physiostat provides a new process strategy for the controlled synthesis of biologically active compounds or for the characterisation of different stress influences, as demonstrated here for UVB-radiation.

6.2.2. Biological approach for explaining the time constant τ_2 (17.04 min)

The crucial challenge of determined time constants is the allocation to specific processes. The time constants τ_1 (0.9 min) and τ_2 (17.04 min) were determined by fitting (Eq. 4.16) of characteristic fluorescence responses provoked by UVB-radiation. Therefore τ_1 and τ_2 are related to fluorescence effects induced by UVB-radiation.

The findings presented in Figs. 4.5 and 4.7 indicate a changing of the cyanobacterial apparatus (PSII and phycobilisomes) involved in the generating of fluorescence. An approach for explaining the fluorescence characteristics (Figs. 4.5 and 4.7) is given by Sinha et al. (1995) and Zolla et al. (2002). The pigment matrix of cyanobacteria is influenced by UVB-radiation. Photometric and spectrophotometric measurements of the antenna systems show a decrease of the phycocyanin (participate in the structure of the phycobilisomes) absorption after exposure to UVB-radiation. This decline reduces the energy transfer from the antenna systems to the chlorophyll *a* molecules of the reaction centres. Thus, the chlorophyll fluorescence intensity of F and F_M' decreases and are in agree with the findings presented in Figs. 4.5 and 4.7.

A more detailed description about the effects of UVB-radiation on the composition of the pigment matrix of cyanobacteria is given by Lao & Glazer (1996). Phycobiliproteins in intact phycobilisomes from *Anabaena* sp. PCC 7120 were UVB-radiated. Besides the calculation of the photodestruction quantum yield, the relative fluorescence of the fluorescence emission were monitored during UVB-illumination at 680 nm (which reflects the phycobilisomes core) and at 640 nm (resulting from fluorescence emission of the phycobilisomes rod). The emission of the core decreased exponentially whereas the emission of the rod in Fig. 4B of Lao & Glazer (1996) showed a similar fluorescence pattern as ϕ_{PSII} in Fig. 4.5 and Fig. 4.7 presented here.

The time course of the relative fluorescence of the phycobilisomes in living cells as well as in purified form induced by UVB-illumination is also described by Lao & Glazer (1996). Within 150 min, the fluorescence of the purified phycobilisomes decreases exponentially to a minimum. The fluorescence signal of the phycobilisomes in living cells also fall exponentially within 250 min to a minimum. Both time constants of these exponential decreases (Fig. 6 in Lao & Glazer, 1996) are located in a temporal range (between 10 and 40 min) close to that of the slow time constant ($\tau_2 = 17.04$ min) of the investigations

described here. It is therefore possible that this time constant represents the process of photodamage of the phycobilisomes in *Synechocystis* sp. PCC 6803.

It has to be mentioned that Lao & Glazer (1996) worked with purified phycobilisomes or rather with phycobilisomes in whole cells. They used a different strain of cyanobacteria and different UVB-intensities. Nevertheless, their results seem to be in close relation to the results presented here.

A further effect of UVB-radiation on the photosynthesis apparatus is the degradation of the D1 reaction center protein (Vass et al., 1996; Chaturvedi & Shyam, 2000). In contrast to some other cyanobacteria (e.g. *Synechococcus*, Campbell et al., 1998), *Synechocystis* sp. PCC 6803 has only one form of the D1 protein (Máté et al., 1998). This protein is encoded by the genes *psbAII* and *psbAIII* (Máté et al., 1998). UVB-radiation induces differential transcriptions of these genes (Máté et al., 1998; Huang et al., 2002). Under unstressed conditions, mainly the *psbAII* gene is active whereas under UVB-radiation the *psbAIII* gene is activated. This turnover occurs within 90 min (Máté et al., 1998). Furthermore in *Synechococcus* sp. PCC 7942, the transcripts of the gene *cpcB1A1* (beneath *cpcB2A2* responsible for encoding nonpigmented linker proteins of phycocyanin) decreases under UVB exposure within 15 min and returns to the initial level within the next 45 - 90 min of UVB-exposure (MacDonald et al., 2003). This time domain corresponds with the chlorophyll fluorescence pattern in Figs. 4.5. and 4.7. The decrease of the transcripts of the gene *cpcB1A1* within 15 min is close to the time constant τ_2 (17.04 min) determined here.

7. Discussion of the cultivation experiments

In this chapter, the results of the turbidostatic and physiostatic processes are inspected in order to find out whether the physiostatic approach yields a better UVB-induced stimulation of the synthesis of commercially relevant agents. Furthermore, the peculiarities of these approaches are considered to obtain information about the mechanistic backgrounds.

7.1. Biological dry mass (BDM) and growth rate (μ)

Biological dry mass and growth rate are not in the focus of the investigations presented here. However, they can serve as important indicators of whether the turbidostat works correctly (which is employed in the turbidostatic but also in the physiostatic processes, see chapter 3). Furthermore, BDM has to be measured in order to provide a normalisation for the presentation of the synthesis of investigated products.

In turbidostatic processes, the BDM-values are kept constant. Thus, the measurement of BDM by OD measurements does not provide information about growth behaviour. However, the constancy is a means of checking the proper performance of the turbidostatic control loop. This is verified by Fig. 5.1 showing that the BDM set points are kept constant during 100 h of process time with a scatter of 2.5 % to 5 % (Table 5.1).

There seems to be a small influence of UVB-irradiation of about 10% in Table 5.1 and Fig. 5.1. This is unexpected, since BDM is regulated by means of the measured OD value. Thus, it may be speculated that there is an effect of UVB-irradiation on pigment concentrations. This offset exists already before the onset of irradiation. In addition, there is no significant temporal trend in Fig. 5.1.

Whereas BDM in the reactor stays constant under control of the feed-back loop (Fig. 5.1) in turbidostatic processes, the growth rate (μ) can be calculated from the added volume of fresh medium during a defined time interval (Eq. 3.4). This fresh medium is added by the feed

back loop in order to keep BDM (optical density) constant. Without external influence, the turbidostat reaches steady state conditions. This offer a precise calculation of μ .

Here, an averaged growth rate of 0.6 d^{-1} (Table 5.2) as initial value was calculated before UVB-illumination started. This value has to be compared with the results of other workers. Wada & Murata (1989) cultivated *Synechocystis* sp. PCC 6803 in a batch process (i.e., without feed-back control to keep BDM constant) using photoautotrophic medium. Taking samples at the exponential growth phase and measuring *offline* the optical density at a wavelength of 730 nms they calculated a growth rate of 1.7 d^{-1} (at a temperature of $34 \text{ }^{\circ}\text{C}$) and 1.2 d^{-1} (at a temperature of $22 \text{ }^{\circ}\text{C}$). These values are higher than the averaged growth rate in this study. However, the calculated value of μ in exponential phases has to be higher than in turbidostatic process because the cell numbers of the parent generation does not increase but stays constant in a turbidostatic process under the assumptions that pigment amount per cell stays constant (this is assumed here in most cases).

Cultivating *Synechocystis* sp. PCC 6803 in a BG11 medium at $30 \text{ }^{\circ}\text{C}$ with a PAR-light of $40 \text{ } \mu\text{mol photons m}^{-2} \text{ s}^{-1}$ resulted also in a higher growth rate of 2 d^{-1} (optical density at 730 nm measured *offline*, Tichy & Vermaas, 1999) than those in Table 2 (0.6 d^{-1} , Eq. 3.4).

Again these experiments cannot be taken as an indication that the cells in the investigations here are not healthy. Besides the absence of a turbiostatic control the experimental conditions are unknown. Tichy & Vermaas (1999) did not mentioned the adjusted pH-value or at which phase of the cultivation samples were taken. The comparison with the above data shows that the growth rates in Table 5.2 are somewhat lower, but this difference can be explained by experimental conditions.

The growth rate μ in the turbidostat under the influence of stepwise changed UVB-intensities or in the physiostat showed a significant reduction of μ (Fig. 5.2).

Ehling et al. (1997) and He et al. (2002) proposed that reducing cell replication is caused by the metabolic cost of increased synthesis of cellular compounds and biomolecules used for the repair of UVB-induced damages or replacement of damaged biomolecules. The conclusions of Ehling et al. (1997) and He et al. (2002) can be validated by the findings of this study. In the experiments presented in this study, the increase of specific cellular components like e.g. carotenoids, xanthophylls or α -tocopherol (Fig. 5.15 – 5.18; 5.25) and the decrease of the growth rates (Fig. 5.2) proceeded concomitantly.

A second effect may reduce growth rate under UVB-irradiation. Ehling-Schulz et al. (1997) reported negligible effects of short-time (1 to 1.5 days) UVB-exposure of cyanobacterium *Nostoc commune* in terms of dry weight. Longer UVB-exposure led to a two- to threefold increase of dry weight per cell. Since the turbidostatic process keeps biological dry mass constant cell numbers have to decrease. This may lead to a lower replication rate and thus to a lower μ without providing any evidence for a reduced vitality of the cells under turbidostatic control.

7.2. Fluorescence signals F , F_M' and ϕ_{PSII}

As in many other studies, (Geider et al., 1998; Lippemeier et al., 2001; Hammes et al., 2006; Hoffmann et al., 2006; Schubert et al., 2006) chlorophyll fluorescence is used to monitor physiological changes in the microalgae. It is the principle of the physiostat to keep ϕ_{PSII} constant, thus most of the changes in fluorescence do not become obvious. However, the feedback loop has to compensate changes which occur during the experiment by changes in UVB-irradiation. Thus, it has to be known what kind of changes in chlorophyll fluorescence can occur during such an experiment.

Firstly, the behaviour in cultivations not subject to UVB-irradiation was investigated. Even without UVB-irradiation or other obvious changes in environmental parameters, the courses of the fluorescence signals F and F_M' increase for about 60 h (Fig. 5.3) and then end in a plateau. The photosynthetic flux, (ϕ_{PSII} , Fig. 5.3A) as calculated from F and F_M' in Fig. 5.3B decreases monotonously, indicating that the increase of F_M' is slightly stronger than that of F . This effect which results from the decrease of the chlorophyll a content (shown in Fig. 5.14A) and the increase of the phycobilisomes content (Fig. 5.20A). Since fluorescence from the phycobilisomes contribute to the measured fluorescence signal (Rakhimberdieva et al., 2004), but shows less sensitivity to quenching by photosynthetic activity, an increase of phycobilisomes occurring concomitantly with a decrease of chlorophyll a leads to a decrease of ϕ_{PSII} .

Under UVB-irradiation, the time courses of both ϕ_{PSII} and the single fluorescence signals F and F_M' show a different behaviour (Figs. 5.4 to 5.11). The comparison between Fig.

5.3 and Figs. 5.4 to 5.11 indicates that the measured fluorescence changes of the UVB-treated experiments are induced by this radiation source and are no measuring artefacts or induced by other hidden parameters.

The highly resolved fluorescence measurements reveal several remarkable points in UVB-influenced cultivation experiments. One of them is the prompt decrease of F_M' and the increase of F (although sometimes F remains constant (Figs. 5.4 and 5.10)). After starting UVB-treatments these effects became observable in the most of the experiments (regarding all UVB-treated cultivation experiments, see Figs. 5.4 to 5.11) and were also observed by Giacometti et al. (1996) which illuminated *Synechocystis* sp. PCC 6803 with a PAR-light intensity of $50 \mu\text{mol photons m}^{-2} \text{s}^{-1}$ and employed a UVB-intensity of $25 \mu\text{mol photons m}^{-2} \text{s}^{-1}$. Due to the light adapted state of the cells (for nomenclature see v. Kooten & Snel, 1990) the detected fluorescence signals F and F_M' in this study can be related to the fluorescence signals F_0 and F_M mentioned by Giacometti et al. (1996).

Giacometti et al. (1996) investigated the fluorescence pattern of intact cells upon UVB-radiation and interpreted an increase of F_0 as a lower efficiency of the reaction centers in trapping excitation energy. The lower efficiency of the reaction centers is related to both the destruction of the plastoquinone pool in the Q_A site and the degradation of the D1 protein (which leads to a disruption of the PSII assembly). In both cases excitons accumulate and the internal chlorophylls of CP43 and CP47 would increase F_0 . This conclusion of Giacometti et al. (1996) is supported by the findings of Ihalainen et al. (2005) who proposed a non-photochemical function of CP43 under high light conditions by virtue of its ability to dissipate energy. The conclusions and findings of Giacometti et al. (1996) and Ihalainen et al. (2005) deliver possible explanations for the observed increase of F measured in the experiments presented here (Fig. 5.4 to 5.11).

A prompt decrease of F_M upon UVB-radiation is interpreted by Giacometti et al. (1996) as an indicator for the formation of stable fluorescence quenchers (e.g. zeaxanthin, orange carotenoid protein, see below) responsible for non-photochemical quenching which increase when cells are exposed to UVB-radiation (Giacometti et al., 1996). The propose of Giacometti et al. (1996) of stable fluorescence quenchers is supported by the role of zeaxanthin (Baroli et al., 2003) and the recently observed function of an orange carotenoid protein (OCP) (Wilson et al., 2006). This corresponds to the increase found in Fig. 5.16.

Under photooxidative stress, higher plants and some microorganisms are protected at least particularly by zeaxanthin (Bilger & Björkman, 1994; Pfündel & Bilger, 1994; Bilger et al., 1995), generated in the xanthophyll cycle. Besides its function in quenching singlet oxygen ($^1\text{O}_2^*$) or free radicals, zeaxanthin protects PSII from photoinduced damages by thermal dissipation of singlet ($^1\text{Chl}^*$) or triplet excited chlorophylls ($^3\text{Chl}^*$). This energy dissipation leads to an increase in non-photochemical fluorescence quenching. In phycobilisome containing species like cyanobacteria or rhodophyta, the xanthophyll cycle is absent (Schubert et al., 2006). In spite of these findings, there is evidence that in the absence of a functional xanthophyll cycle *de novo* synthesised zeaxanthin protects photosynthetic active cells from photodamage by direct quenching of $^1\text{O}_2^*$ and/or free radicals (Baroli et al., 2003), by a decrease of the PSII light harvesting antenna size, and by liberating additional zeaxanthin into the lipid phase of the thylakoid membrane (Baroli et al., 2003). A decrease of the PSII light harvesting antenna size induced by zeaxanthin is not an important protection mechanism in cyanobacteria, because the light harvesting complex is built by phycobilisomes (which are not affected by zeaxanthin). Nevertheless, the enhanced synthesis of zeaxanthin determined in this study (Fig. 5.16) indicates a protective role of zeaxanthin in UVB-radiated cells of *Synechocystis* sp. PCC 6803.

Besides zeaxanthin, another protecting agent has to be considered in order to explain the UVB-effects on chlorophyll fluorescence in Fig. 5.4 to 5.11. In *Synechocystis* sp. PCC 6803 the orange carotenoid protein (OCP) is encoded by the *slr1963* gene (Wu & Krogmann, 1997). Wilson et al. (2006) showed that these proteins are involved in non-photochemical fluorescence quenching in *Synechocystis* sp. PCC 6803 under high light conditions. The investigated quenching mechanism induced by the OCP seems to be neither dependent on a transthylakoid pH gradient nor on excitation pressure from the antenna on PSII or on changes in the redox state of the plastoquinone pool (Wilson et al., 2006). Rather the OCPs are induced by blue light and quench phycobilisome fluorescence. This fluorescence quenching was interpreted as a lesser energy transfer from the phycobilisomes to PSII and PSI in cyanobacteria (Wilson et al., 2006). The linker-membrane protein of the phycobilisomes was suggested as a possible candidate which interacts with the OCPs (Wilson et al., 2006). Up to now, there is no ensured information about structural changes of the OCPs or about mechanisms of energy dissipation. This effect requires blue light, but it is feasible that the even higher photon energy of UVB can exert a similar effect. Effects of this kind are known

from other studies, dealing with structural changes. Wilson et al., (2006) speculated about carotenoid isomerisation induced by blue light, conformational changes of the chromophore, proton or electron transfer, or modified energy dissipation. For instance, direct interaction of the carotenoid with the phycobilin chromophore, and interaction of the OCPs with the phycobilisome cores cause alteration of the phycobilisomes structure. By means of the above mechanisms, the OCPs may function as light sensors, as mediator of quenching, as and quenchers themselves. These effects are reported for blue light. Even though UVB-radiation was not tested this quenching mechanism might also occur when cells are exposed to this radiation source.

A further remarkable point of the fluorescence signals are the time courses of ϕ_{PSII} (Figs. 5.4 to 5.7). In the cultivation experiments in the turbidostat with stepwise changed UVB-intensities, ϕ_{PSII} firstly decreased and then reached an approximately constant value after 12 h of the process time. Afterwards, ϕ_{PSII} recovered again and increased for the next 20 to 24 h of the process time (Figs. 5.4 to 5.7).

The time course of ϕ_{PSII} (Figs. 5.4 to 5.7) was also observed by He et al. (2002). They investigated the influence of UVB-radiation on *Anabaena* sp. employing a constant UVB-intensity. Determination of the photosynthetic activity by measuring F and F_M' (He et al., 2002) revealed a time course with a similar pattern to the time course of ϕ_{PSII} determined here. They proposed that the recovery of ϕ_{PSII} is closely correlated with the *de novo* synthesis of new D1 and D2 proteins and replacement of damaged ones.

In addition, damage and repair of DNA strands also show a similar time course like the time course of ϕ_{PSII} (He et al., 2002). Therefore the repair of damaged DNA strands may also contribute to the recovery of ϕ_{PSII} (He et al., 2002).

Assuming that the suggestions of He et al. (2002) are also valid in this study, the recovery of the UVB-induced changes in ϕ_{PSII} (Figs. 5.9 to 5.11) may be interpreted in terms of both the synthesis of new and replacement of damaged D1 and D2 proteins and the repair of DNA. The modulation of the UVB-intensity limits the repair and replacement processes at a level in such a way that the set point of ϕ_{PSII} can be reached (Figs. 5.9 to 5.11).

The overall decrease of both F and F_M' (Figs. 5.4 to 5.11) is related to the degradation of the phycobilisomes (Fig. 5.20), the main light harvesting complex in cyanobacteria (MacColl, 1998). This degradation leads to a decreased transfer of light energy to chlorophyll *a*, the reaction center of PSII and responsible for the variable fluorescence signals F and F_M' .

Nevertheless it seems that cells compensate both the degradation of the phycobilisomes and the suppression of the processes responsible for recovering of ϕ_{PSII} at least particularly by increased synthesis of both other cellular pigments and α -tocopherol which is described below.

The feed-back driven modulation of UVB-intensities of physiostatic processes counteract the recovering of ϕ_{PSII} by increasing UVB-intensities (Figs. 5.9 to 5.11). This counteracting lead to the presumption that the increasing UVB-intensities, necessary for keeping ϕ_{PSII} in a defined state, suppress one or more cellular processes responsible for recovering of ϕ_{PSII} .

7.3. Pigments (chlorophyll *a*, carotenoids, xanthophylls, and phycobilisomes)

Developing a strategy for increasing the synthesis of pigments is one of the goals of the investigations here. The approach is based on the assumption that in all photosynthetic active cells pigments are essential components for supplying PSII with light energy but also for protecting PSII against stress conditions (Young et al., 1997; Steiger et al., 1999; Wang et al., 2003). Thus the influence of UVB-radiation as a stressor on the synthesis of these components has become one of the main topics in photosynthesis research (Pfundel & Bilger, 1994; Ehling-Schulz et al., 1997; Niyogi et al., 1997; Götz et al., 1999).

7.3.1. Chlorophyll *a*, carotenoids, and xanthophylls

In the UVB-untreated cultivation, the chlorophyll *a* content decreased slightly (Fig. 5.14) whereas the carotenoid and xanthophyll contents remained either constant (myxoxanthophyll, Fig. 5.15; zeaxanthin, Fig. 5.16) or decreased slightly (echinenone, Fig. 5.17; β -carotene, Fig. 5.18). Also under moderate UVB-intensities of 0.57, 0.81 and 1.25 $\mu\text{mol photons m}^{-2} \text{s}^{-1}$ (Fig. 5.14A) in the turbidostat, the chlorophyll *a* content remained unaffected. The same holds in the physiostat using higher set points of ϕ_{PSII} of 0.25 and 0.2 (Fig. 5.14B).

Only the highest UVB-intensity of $1.61 \mu\text{mol photons m}^{-2} \text{s}^{-1}$ or the lowest set point of ϕ_{PSII} of 0.15 (which causes the highest UVB-intensity) provokes a decrease of chlorophyll *a* (Figs. 5.14A and 5.14B). This is in contrast to other results (He et al., 2002) who describe a time course of the chlorophyll *a* content similar to the time course of ϕ_{PSII} . Here, this could not be validated. The time courses of chlorophyll *a* and ϕ_{PSII} do not show similarities (Figs. 5.4 – 5.7 compared to Fig. 5.14A). This indicates that other components are also involved in the modulation of ϕ_{PSII} .

A better correspondence to the results of other workers (e.g. Lagarde et al., 2000) is found for the initial values of carotenoids and xanthophylls before UVB-irradiation (Table 5.3). The strong influence of UVB-radiation on these compounds is presented in Figs. 5.15 to 5.18. Cultivation experiments in the turbidostat influenced by stepwise changed UVB-radiation (Figs. 5.15A to 5.18A) and the physiostatic process with the highest set point ($\phi_{\text{PSII,SP}} = 0.25$; Figs. 5.15B to 5.18B) reach similar final results in the pigments enhancements. Employing lower set points of ϕ_{PSII} (0.2 and 0.15) a significant increase of the pigments concentrations over those in the turbidostatic process is found (Figs. 5.15B to 5.18B).

Nevertheless, the cultivation experiments using UVB-irradiation either in the turbidostat or in the physiostat revealed six remarkable points.

1. In the turbidostat zeaxanthin undergoes the greatest changes whereas minor changes of the other components are observable.
2. The zeaxanthin concentration increases in turbidostat experiments with stepwise changed UVB-intensities. However, the final zeaxanthin concentrations (Fig. 5.16A) ended in the same range. Therefore, the synthesis of zeaxanthin may saturate already at very low UVB-intensities.
3. In physiostatic processes, the contents of all investigated substances increased mainly between 12 and 24 h of the process time in an approximately exponential manner whereas in the turbidostat exposed to stepwise changed UVB-intensities zeaxanthin changes showed a linear increase.
4. In contrast to the turbidostatic processes using stepwise changed UVB-intensities, physiostatic processes caused a significant increase of myxoxanthophyll content.

5. Myxoxanthophyll and zeaxanthin contents reached the greatest changes in the physiostatic cultivation experiments.
6. In the physiostatic experiments, echinenone and β -carotene reached a high level within 24 h and then stayed approximately constant..

These points demonstrate the high potential of physiostatic experiments which will provide an additional means when the aim of a cultivation is the enhanced synthesis of interesting substances like myxoxanthophyll and zeaxanthin (Cifuentes et al., 2003; Eonseon et al., 2003; Spolaore et al., 2005).

Considering the results listed above, myxoxanthophyll and zeaxanthin might be the major components protecting *Synechocystis* sp. PCC 6803 from UVB-radiation whereas β -carotene and echinenone are secondary components in terms of UVB-protection. This is confirmed by the results of other researchers reporting on the protection potential of myxoxanthophyll against high light conditions (Steiger et al., 1999) and zeaxanthin as a very effective protection component against UVB-radiation (Götz et al., 1999) and light stress (Pfündel & Bilger, 1994; Schäfer et al., 2006).

Lagarde et al. (2000) published data obtained from genetically manipulated *Synechocystis* sp. PCC 6803. The genetic manipulation was employed in order to over express the production of zeaxanthin and other pigments. The aim of this investigation (Lagarde et al.; 2000) was not the maximal production of zeaxanthin but the demonstration of the application of genetic manipulation. The achieved yields (Lagarde et al., 2000) and the differences between genetic manipulated and wild types of *Synechocystis* sp. PCC 6803 (Lagarde et al., 2000) are below the values obtained here. In their investigations (Lagarde et al., 2000), myxoxanthophyll increased 2.64-fold in the manipulated strain compared to the wild type. Zeaxanthin increased in the genetic manipulated strain 2.52-fold compared to the wild type.

In the physiostat, higher values were obtained (Figs. 5.15B and 5.16B). The maximum change of myxoxanthophyll was 5.71-fold and of zeaxanthin change was 7.49-fold. The changes occurred during a process using a ϕ_{PSII} set point of 0.2, which was determined as the optimum condition for pigment synthesis (Fig. 5.23B).

The comparison of physiostatic processes with the turbidostatic process shows the significant advantage of the physiostatic process strategy. The maxima in Fig. 5.23B for upregulation of myxoxanthophyll (or zeaxanthin) in a physiostatic process with a set point of

0.2 ($\phi_{\text{PSII,SP}} = 0.2$, Fig. 5.23B) was 2.7-fold (or 2-fold) higher than in the turbidostatic process (Fig. 5.23A).

Searching for a reason for the higher efficiency of the physiostat, it has to be taken into account that the feed-back control hinders the cell to compensate the effects of chlorophyll fluorescence by increased synthesis of protecting pigments. The absence of the success of the synthesis may stimulate the cells to increase the synthesis of both myxoxanthophyll and zeaxanthin. Thus, the experiments of chapter 5 result in two messages. Firstly, UVB-radiation has a high potential when the aim of the cultivation of *Synechocystis* sp. PCC 6803 is the enhanced synthesis of interesting substances usable for commercial application. Secondly, the physiostatic processes is more efficient than the turbidostat exposed to stepwise changed UVB-experiments. The physiostatic process using UVB-radiation as actuating variable offers a serious alternative over genetic manipulation for the cultivation of phototrophic microorganism when the aim of the cultivation is an enhanced yield of active agents like myxoxanthophyll and zeaxanthin.

7.3.2. Phycobilisomes

Figure 5.20 shows the degradation of phycobilisomes induced by UVB-radiation. This effect of UVB-irradiation on phycobilisomes is one of the most investigated UVB-damage on cyanobacteria ((Lao & Glazer, 1996; Araoz & Häder, 1997; Richaud et al., 2001; Zolla et al., 2002)). The interest in these effects may arise from the feature that phycobilisomes are a peculiarity of cyanobacteria. They constitute the main harvesting complexes located on the surface of the thylakoids and transfer the absorbed energy to PSII (Campbell et al., 1998). The important pigments of phycobilisomes are allophycocyanin (AP), phycocyanin (PC) and phycoerythrin (PE). In *Synechocystis* sp. PCC 6803, investigated here, AP and PC are the dominant pigments whereas PE is not present (Riethmann et al., 1988; Zolla & Bianchetti, 2001). In this study, no distinction in terms of AP and PC is made.

Figure 5.20 shows the results which have to be discussed here. The phycobilisome content of a cultivation not exposed to UVB-irradiation increased during the experimental course (Fig. 5.20A), but in contrast to UVB-radiated cultivations (in the turbidostat or physiostat) the phycobilisome contents decreased (Fig. 5.20A and 5.20B). This difference

between the experiments with and without UVB-irradiation indicates that the degradation of the phycobilisomes is caused by the employed UVB-radiation.

Furthermore, the fitting of the degradation rate for the phycobilisomes degradation induced by stepwise changed UVB-intensities by means of Eq. 3.5 leads to the results presented in Fig. 5.22. A linear relationship between UVB-intensity and degradation rate is found (Fig. 5.22). Figure 5.22 predicts a complete destruction of the phycobilisomes because the degradation rate approaches zero when cells are illuminated with an UVB-intensity of $2.25 \mu\text{mol photons m}^{-2} \text{s}^{-1}$. This conclusion was tested by illuminating *Synechocystis* sp. PCC 6803 with an UVB-intensity of $2 \mu\text{mol photons m}^{-2} \text{s}^{-1}$ (Fig. 5.8). ϕ_{PSII} decreased within 30 h close to zero. This can be interpreted as an evidence for complete degradation of the phycobilisomes.

The measured phycobilisome degradations in Fig. 5.20 caused by UVB-radiation agree with published results. Zola et al. (2002) investigated the UVB-influence on both, whole cells of *Synechocystis* sp. PCC 6803 and isolated phycobilisomes from this organism. When exposed to UVB-radiation for 4 h, the supramolecular organisation of linker proteins, rod subcomplexes and core are destroyed. Mainly the loss of β -PC and the rod linker occur. The phycobilisome proteins are able to absorb light arrived from the UV-range (Zolla & Bianchetti, 2001). However, the rod linker does not own a high aromatic amino acid content, which contribute to wavelengths absorption in the UV-range (Zola et al., 2002). Therefore Zolla et al. (2002) propose two possible reasons: 1. the presence of a particular functional group in this rod and/or 2. the location of this rod close to the source of reactive species by damaging radiation.

Furthermore Zolla et al. (2002) suggested three explanations for the loss of β -PC:

1. β -PC contains two bilin pigments whereas the other phycobilisomes contain only one.
2. β -PC is the most frequent protein in the cell.
3. In contrast to AP, β -PC is located at the periphery of the phycobilisomes.

Pandey et al. (1997) showed further effects of UVB-radiation on the phycobilisomes of *Synechococcus* sp. PCC 7942. In contrast to the findings of Zolla et al. (2002) here UVB-radiation affected both β -PC and α -PC and all linker proteins in *in vivo* cells. Additionally a strong decrease of PC/AP ratio was determined. UVB-investigations (Pandey et al., 1997)

using isolated phycobilisomes *in vitro* showed that only the linkers connecting the core of the phycobilisomes to the thylakoid membranes and the linkers of the rod structure were affected. A slight decrease of β -PC and no effects on α -PC were observed.

Furthermore, Pandey et al. (1997) suggest that the main site of UVB-damage is the linker connecting the phycobilisomes core to the thylakoid membranes. Destroying of this polypeptide leads to a dissociation of the phycobilisomes complex and the loss of the constituent polypeptides.

Nevertheless, independent from the suggested damaging mechanism(s), the degradation of the phycobilisomes observed here (Fig. 5.20) confirms the finding of Lao & Glazer (1996), Pandey et al. (1997), and Zolla et al. (2002) that phycobilisomes are negatively affected by UVB-radiation.

Cells have to compensate at least particularly this degradation by increased synthesis of other pigments for both protection against UVB-radiation and supply of the reaction centres with light energy. These pigments seem to be zeaxanthin and myxoxanthophyll according to Figs. 5.15B and 5.16B.

7.4. Mycosporine-like amino acids (MAAs; here shinorine)

Many research groups reported on the ability of microorganisms to accumulate MAA-contents when exposed to UVB-radiation (Portwich & Garcia-Pichel, 1999; Shick et al., 1999; Sinha et al., 1999; Sinha et al., 2003) or high PAR-radiation (Figueroa et al., 2003) using MAAs as protecting compounds. Nevertheless, only few reports on the synthetic pathway, mechanism and cellular protection role of MAAs for cyanobacteria under UVB-radiation are available (He et al., 2002).

Since now no literature is known regarding the occurrence of shinorine in *Synechocystis* sp. PCC 6803 the MAA-measurements (Fig. 5.24) were interpreted in terms changes in shinorine as cellular component (see chapter 5.6), according to the analysis described in chapter 3.2.3.

Nevertheless, no influences on the content of shinorine were detected with or without UVB-radiation (Fig. 5.24). This result suggests that in *Synechocystis* sp. PCC 6803 shinorine

has no active or important part in protecting cells from UVB-inducible damages. Even though it could be shown in chapter 5.6 that *Synechocystis* sp. PCC 6803 synthesise shinorine *de novo* but its function within the cells remains unclear.

Although some MAAs exhibit also antioxidative activities (e.g. mycosporine-glycine) shinorine showed no antioxidative activity (Dunlap & Yamamoto, 1995). Shinorine could fulfil a potential role as osmolyte (Oren, 1997) in *Synechocystis* sp. PCC 6803.

7.5. α -Tocopherol

The role of α -tocopherol in biological systems is not related to a single function and the major function is still unclear (Trebst et al., 2002; Maeda et al., 2005; Kruk et al., 2005; Krieger-Liszkay & Trebst, 2006). Nevertheless, the natural antioxidative properties of α -tocopherol are interesting for commercial application (Cahoon et al., 2003; Valentin & Qi, 2005).

Figure 5.25 indicates that the production of α -tocopherol can be stimulated by UVB-radiation and that this works better in the physiostat than in the turbidostat. The initial concentrations of α -tocopherol (Table 5.6.) are below the values found by other authors (Dähnhardt et al., 2002). But the observed differences in the time courses of α -tocopherol between UVB-exposed and non-exposed cells (Fig. 5.25) enable the allocation of α -tocopherol as protecting component against UVB-radiation.

In order to find out in which way UVB-radiation may induce the enhanced synthesis of α -tocopherol and to speculate about a possible function of α -tocopherol in *Synechocystis* sp. PCC 6803 the following observations concerning different light conditions are to be considered.

At high light intensities effects on the acceptor and the donor side of PS II have been reported. Trebst et al. (2002) investigated the influence of high and low light intensities on the cellular content of α -tocopherol in *Chlamydomonas reinhardtii* and its relationship to acceptor side-related damage. Under high light intensities, an enhanced triplet formation of the reaction center of PS II (P680) occurs, due to the overreduction of the plastoquinone pool and of the plastoquinone acceptors Q_A and Q_B . This triplet formation generates singlet oxygen

which leads to a degradation of the D1 protein of PSII (Janssen et al., 1999). If the cell is unable to compensate this effect the PSII proteins disappear, pigments uncouple from PSII, and chlorophyll photodynamic bleaching occurs (Trebst et al., 2002). α -Tocopherol counteracts this deleterious effect by direct quenching of the generated singlet oxygen by oxidation (Trebst et al., 2002; Kruk et al., 2005). This reaction is irreversible and therefore the cells have to regenerate α -tocopherol (e.g. using ascorbate; Smirnov, 2000) permanently to sustain a protection mechanism against the energised oxygen (Smirnov, 2000). Also He & Häder (2002) found that UVB-radiation causes the formation of $^1\text{O}_2$, even though Haged & Vass (1996) described a different reaction.

Donor side related photoinhibition at high light intensities was investigated by (Barber & Andersson, 1992). If the donation of electrons to PSII is not in balance with the withdrawal of electrons from PSII the lifetime of the highly oxidised P680^+ will increase. Due to its oxidising potential electrons from the ambient molecules can be extracted. These changes of the biochemical environment could lead to a degradation of the D1 protein (Shipton & Barber, 1991). In contrast to acceptor side photoinhibition, no singlet oxygen is involved in this donor side process (Barber & Andersson, 1992). Also Barbato et al. (1992) argue that the primary target of UVB-radiation is the donor side of PSII. The main target of UVB-radiation at the donor side of PSII is the Mn cluster (Giacometti et al., 1996; Vass et al., 1996). It is important for considerations of UVB-induced effects on the synthesis of α -tocopherol that degradation of the Mn cluster does not lead to enhanced formation of $^1\text{O}_2$ (see above).

A third effect occurring at low light intensities is suggested by Keren et al. (1997). They described a so-called 'low-light' mechanism responsible for photoinhibition of PSII. At $30 \mu\text{mol photons m}^{-2} \text{s}^{-1}$ (Keren et al., 1997), charge recombination between the quinone acceptors Q_A^- and Q_B^- and the oxidised states S_2 and S_3 of the water splitting enzyme on the donor side of PSII lead to the formation of triplet chlorophyll, which is responsible for $^1\text{O}_2$ -formation (Keren et al., 1997).

The following considerations exclude a major role of the above three mechanisms for the synthesis of α -tocopherol which were proposed for the effect of visible light (PAR). An differential effect of PAR light can be excluded. Although the employed PAR-intensity ($200 \mu\text{mol photons m}^{-2} \text{s}^{-1}$) might be assumed as high light conditions the PAR-intensity was equal in all turbidostatic cultivations. Therefore a differential high light induced synthesis of α -

tocopherol can not be related to the employed PAR-intensity. Instead a major role of reactive oxygen species (ROS) is to be considered.

The formation of ROS is dependent on the UVB-dose and the formation of ROS increases with increasing UVB-dose (He & Häder, 2002). If the synthesis of α -tocopherol is a protective response of *Synechocystis* sp. PCC 6803 against $^1\text{O}_2$ the highest stepwise changed UVB-intensity of $1.61 \mu\text{mol photons m}^{-2} \text{s}^{-1}$ should lead to the highest α -tocopherol concentration in the UVB-experiments with constant UVB-intensities. But as shown in Fig. 5.25A, no significant differences in α -tocopherol content were found between the single experiments employing stepwise changed UVB-radiation.

Furthermore Haged & Vass (1996) proposed that under UVB-illumination damages of the photosynthetic apparatus is rather caused by the generation of free radicals and not by singlet oxygen. These radicals may induce relevant damages on both photosynthetic apparatus and membranes (Marshall et al., 2005; Lesser, 2006).

Maeda et al. (2005) specified the conclusions of Haged & Vass (1996) and claimed that α -tocopherol was not required in *Synechocystis* sp. PCC 6803 for detoxification or tolerance against O_2^- or $^1\text{O}_2$. Rather α -tocopherol is an important component for protecting the cell membranes against lipid peroxidation (Havaux et al., 2003). It is an established fact that UVB-radiation induces lipid peroxidation in cyanobacterial membranes (He & Häder, 2002; He et al., 2002). Thus, due to the conclusions of Maeda et al. (2005), an enhanced α -tocopherol synthesis in *Synechocystis* sp. PCC 6803 may function as a protecting system against UVB-induced lipid peroxidation.

Furthermore, in physiostatic processes the synthesis of α -tocopherol is more pronounced than in turbidostatic processes influenced by stepwise changed UVB-radiation (Fig. 5.25). The optimum in physiostatic processes is 2-fold higher (Fig. 5.25B) than the optimum of reached in turbidostatic processes (Fig. 5.25A). Unlike the pigment changes of myxoxanthophyll and zeaxanthin, the optimum of α -tocopherol is found in a physiostatic process with an employed set point of 0.15 ($\phi_{\text{PSII,SP}} = 0.15$; Fig. 5.25B). This difference is discussed below.

But, besides the overall higher upregulation of pigments and α -tocopherol in physiostatic processes compared to cultivation experiments affected by stepwise changed UVB-intensities, a further advantage of physiostatic processes becomes obvious. It is possible by adjusting the adequate set point ($\phi_{\text{PSII,SP}} = 0.2$ or 0.15) to choose between an enhanced

synthesis of pigments or α -tocopherol. Depending on which substance is of interest it is possible to yield an enhanced production of this substance. This makes the physiostatic process strategy interesting for a commercial application.

7.6. Antioxidative potential (AOP)

The antioxidative potential (AOP) was measured by means of the modified DPPH-method (chapter 3.1). In contrast to the specific determinations above, the change in DPPH absorption reflects the integral effect of several antioxidants, namely of all those which can be extracted by methanol.

Whereas in the non UVB-treated cultivation the AOP slightly decreases (Fig. 5.26A), an increase of the AOPs occurred in turbidostatic experiments influenced by stepwise changed UVB-radiation or in the physiostat (Fig. 5.26). This indicates that UVB-irradiation is an adequate means of stimulating the synthesis of antioxidants.

In order to find the mechanisms behind this effect it has to be considered what is mentioned above. The increased AOPs of UVB-treated cells reflects the changes in the intrinsic antioxidative properties of carotenoids, xanthophylls and α -tocopherol. (Miller et al., 1996; Cahoon et al., 2003).

The investigations of Steiger et al. (1999) are based on the antioxidative properties of purified carotenoids and xanthophylls. Under photooxidative conditions myxoxanthophyll reached the highest AOP which is 3.2-fold higher than that of β -carotene and zeaxanthin Steiger et al. (1999). The AOPs of these two substances were similar. Echinenone was found to have the lowest AOP, 6-fold lower than the AOP of myxoxanthophyll and 2-fold lower than the AOPs of β -carotene and zeaxanthin.

Using a radical oxidative measuring method (which is similar to the measuring method of the AOP used in this study) the AOPs of the single components show that myxoxanthophyll is still the component with the highest AOP (Steiger et al., 1999). The AOP of zeaxanthin is 1.4-fold below that of myxoxanthophyll and 1.2-fold higher than the AOP of β -carotene. The AOP of echinenone reached a value 2.2-fold below the AOP of myxoxanthophyll. Miki (1991) determined the thiobarbituric acid (TBA)-method and reported

that the AOP of zeaxanthin is 2.4-fold higher than the AOP of β -carotene and 7.4-fold higher than the AOP of α -tocopherol. β -Carotene has an AOP 3.1-fold higher than the AOP of α -tocopherol. Determination of the AOP using a radical generating method is close to the process conditions occurring in UVB-treated cells because UVB-radiation causes the formation of free radicals (Higed & Vass, 1996). Furthermore, the employed method for determination of the AOPs includes also the determination of radicals (DPPH radicals, see chapter 3.1).

The AOPs of single carotenoids and xanthophylls determined by Steiger et al. (1999) might seem to be important agents for interpreting the AOPs of the cultivation experiments determined in this study. Considering the aspects mentioned above lead to the assumption that in this group of substances (carotenoids, xanthophylls and α -tocopherol) myxoxanthophyll and zeaxanthin might be the major candidates which may contribute mainly to the determined AOPs of *Synechocystis* sp. PCC 6803. An inspection of the results in section 5.4 (pigment analysis) supports this assumption:

1. In all turbidostatic experiments using stepwise changed UVB-radiation, the AOPs show similar final results (Fig. 5.26A), and an upregulation of the zeaxanthin contents ended in the same range for these experiments (Fig. 5.16A).
2. In the physiostatic experiments differences between the AOPs were determined. Obviously physiostatic cultivation with pronounced high upregulation of myxoxanthophyll and zeaxanthin (Fig. 5.15B and Fig. 5.16B) provoked an increased AOP (Fig. 5.26B).
3. In physiostatic processes, the AOPs (Fig. 5.26B) and the increase of myxoxanthophyll and zeaxanthin (Figs. 5.15B and 5.16B) reached higher values in all experiments compared to the values determined in the turbidostatic processes influenced by different stepwise changes in UVB-intensities (Figs. 5.15A; 5.16A and 5.26A).

But several points indicate that the AOPs are not generated primarily by the intrinsic antioxidative properties of the investigated components (carotenoid, xanthophylls and α -tocopherol) because:

1. The AOP of a physiostatic process ($\phi_{\text{PSII,SP}} = 0.25$; Fig. 5.26B) is higher than the AOPs of all processes influenced by stepwise changed UVB-intensities (Fig. 5.26A) although myxoxanthophyll and zeaxanthin changes were approximately in the same range in both process types (Fig. 5.15 and Fig. 5.16).
2. The AOP of $\phi_{\text{PSII,SP}} = 0.15$ decreases after the half of the process time (Fig. 5.26B) in contrast to the time courses of zeaxanthin (Fig. 5.16B) and α -tocopherol (Fig. 5.25B).
3. The time course of myxoxanthophyll in a physiostatic process with $\phi_{\text{PSII,SP}} = 0.15$ shows a decrease after 60 h of the process time (Fig. 5.15B) and the final value is above the final value of myxoxanthophyll in a physiostatic process with $\phi_{\text{PSII,SP}} = 0.25$ (Fig. 5.15B). But the AOP of this process ($\phi_{\text{PSII,SP}} = 0.15$) is below the AOP of the compared physiostatic process ($\phi_{\text{PSII,SP}} = 0.25$; Fig. 5.26B).

These discrepancies lead to the conclusion that in *Synechocystis* sp. PCC 6803 additional substances besides the detected ones contribute to the AOP. These substances have to be methanol soluble, nonenzymatic and able to scavenge free radicals. Possible candidates are polyunsaturated fatty acids which fulfil the above criteria (Fang et al., 2002).

Nevertheless, the AOPs of physiostatic processes are 1.5-fold higher than in processes influenced by stepwise changed UVB-radiation (Fig. 5.26). Although upregulated agents like myxoxanthophyll, zeaxanthin or α -tocopherol, which are known to have antioxidative potential, may not be the main substances responsible for the determined AOPs, the physiostatic process deliver a promising strategy when the aim of the cultivation is an enhanced overall AOP of the cells (e.g. if cells are used for dietary supplement (Belay, 2002; Bhosale & Bernstein, 2005)).

7.7. Hypothesis for the explanation of pigment and α -tocopherol synthesis in two different physiostatic processes ($\phi_{\text{PSII,SP}} = 0.2$ and $\phi_{\text{PSII,SP}} = 0.15$)

In experiments without UVB-radiation pigment concentrations show minor changes. Employing a stepwise changed UVB-intensity causes an upregulation of the zeaxanthin

concentrations independent of the UVB-intensity (see chapter 7.3.1). In physiostatic processes the synthesis of pigments (mainly myxoxanthophyll and zeaxanthin, Figs. 5.15B and 5.18B) and α -tocopherol (Fig. 5.26B) are closely related to the adjusted set point of $\phi_{\text{PSII,SP}}$. In the case of the pigments this is illustrated in Fig. 5.23.

In order to find the mechanism(s) behind the different performance in the physiostat, the time courses of fluorescence signals (Figs. 5.4 to 5.7) are compared with the time courses of pigments (Figs. 5.15A to 5.18A) and α -tocopherol (Fig. 5.25A). This leads to the hypothesis that the recovery process of ϕ_{PSII} plays an important role.

In physiostatic processes, the mechanisms leading to a recovery of $\phi_{\text{PSII,SP}}$ (Figs. 5.8 to 5.11) are disturbed because of the feed-back loop. Eliminating the effects of these recovery processes on photosynthetic flux ϕ_{PSII} , abolishes putative cellular feed-back signals in the repair mechanisms and force the cells to switch their synthesis steps towards the enhanced synthesis of pigments (Figs. 5.15B to 5.18B) and α -tocopherol (Fig. 5.25B).

Interestingly, in the physiostatic process with the lowest set point of 0.15 the highest upregulation of α -tocopherol occurred. The highest upregulation of myxoxanthophyll and zeaxanthin occurred in a physiostatic process employing a set point of 0.2 ($\phi_{\text{PSII,SP}} = 0.2$, Figs. 5.15B and 5.16B).

Considering the biological functions of both pigments and α -tocopherol might be an explanation for these effects:

Carotenoids are located in thylakoid and outer membranes in cyanobacteria (Jürgens & Mäntele, 1991). Their main intracellular function is the trapping of light and the transfer of the light energy to the reaction centre (P680) of PSII. In addition, they quench singlet ($^1\text{P680}$) and triplet formation ($^3\text{P680}$) of P680 (Götz et al., 1999; Steiger et al., 1999) and protect PSII from oxidative damage (Baroli et al., 2003).

Besides its function in protecting PSII from oxidative damage (Trebst et al., 2002), α -tocopherol plays also an important role in protecting against lipid peroxidation of cellular membranes (Havaux et al., 2003; Maeda et al., 2005).

The α -tocopherol concentration in the physiostatic process with the set point of 0.2 ($\phi_{\text{PSII,SP}} = 0.2$) might be high enough to compensate UVB-induced lipid peroxidation of the cellular membranes. Therefore cells may continue to synthesise pigments for an enhanced protection of PSII but also to compensate the loss of phycobilisomes for supplying PSII with light energy.

In the physiostatic process with the lowest set point of 0.15 ($\phi_{\text{PSII,SP}} = 0.15$) the highest averaged UVB-intensity was applied ($1.78 \mu\text{mol photons m}^{-2} \text{s}^{-1}$, see chapter 5.3.3). This may induce high levels of free radicals which cause an enhanced lipid peroxidation. Cells may counteract these negative effect by enhanced synthesis of α -tocopherol. This enhanced synthesis may be done at the expense of the upregulation of pigments on the same or higher level as in physiostatic process with a set point of 0.2 ($\phi_{\text{PSII,SP}} = 0.2$). The preference of the cells for the protection of the lipid membranes may result from the fact that excessive lipid peroxidation would lead to the dissociation of cellular membranes and in the send to the death of the cells. This may be a more urgent strategy for the survival of the cells than protecting PSII which can be repaired later when the cell is still alive by virtue of increased α -tocopherol synthesis.

8. Outlook

This work revealed new insights in the mechanisms protecting *Synechocystis* sp. PCC 6803 against UVB-radiation. Nevertheless these insights evoked new questions which constitute new challenges for further investigations.

Recent research results provided evidence for an important role of the orange carotenoid protein (OCPs) in non-photochemical quenching mechanisms in cyanobacteria. This leads to the following questions: Do these OCPs also contribute to quenching of phycobilisomes fluorescence when cells are exposed to UVB-radiation? How is the interaction of the OCPs with the recovery process of ϕ_{PSII} ?

Another question is the composition of the AOPs of *Synechocystis* sp. PCC 6803. Which substances participate and to what extent? Possible candidates are the fatty acids.

The enhanced synthesis of α -tocopherol is probably coupled to an increased synthesis of ascorbate which is necessary for detoxification of reactive oxygen species and re-reduction of α -tocopherol. Therefore determination of ascorbate should be one issue in future experiments. The measurement of the lipid peroxidation should also be in the focus in order to reveal a possible relationship between the occurrence of α -tocopherol, ascorbate and lipid peroxidation.

An ambitious object is the determination of DNA-photolyase, an enzyme which specifically repairs UVB-induced DNA-damages. The synthesis of this protein might be inducible by UVB-synthesis.

The results of the investigations revealed open questions of the UVB-protection mechanisms in *Synechocystis* sp. PCC 6803.

But also the developed physiostatic process requires further investigations. These investigations are necessary for a better understanding of the background of this process. Frequency analysis, physiostatic process and process influenced by stepwise changed UVB-intensities were conducted under identical conditions (e.g. PAR-light, temperature, pH-value). But what happens under changing conditions? Is the physiostatic process still feasible if e.g. the PAR-light intensity is changed? Do temperature and pH-value influence the performance

of the physiostatic process? Are the determined time constants τ_1 and τ_2 reproducible if the environmental conditions change and if, how do they dependent on these conditions?

On the other hand physiostatic processes with *Synechocystis* sp. PCC 6803 show a high upregulation of cellular components (myxoxanthophyll, zeaxanthin, α -tocopherol). These results make the process strategy interesting for commercial applications. Other photosynthetic microorganisms which synthesise *de novo* interesting substances should also be in the focus for further physiostatic processes. Promising candidates are e.g. *Dunaliella salina* for β -carotene synthesis, *Nannochloropsis* sp. for eicosapentaenoic acid (EPA), or *Haematococcus pluvialis* for astaxanthin. These microorganisms could increase their synthesis rates when exposed to certain environmental conditions (Cifuentes et al., 2003; Gomez et al., 2003; Jimenez & Niell, 2003, Hoshida et al., 2005). Therefore cultivation in a physiostatic processes might be a promising process strategy.

It is not constrainingly necessary that the actuating variable is UVB-radiation. Also other parameters (e.g. PAR-light, nutrients, temperature) influence fluorescence signals (Torzillo et al., 1996; Geider et al., 1998; Lippemeier et al., 2003) and can probably be used. For the sake of easier implementation, it is recommended to use stepwise changed conditions in the turbidostat firstly and analyse the fluorescence signal in terms of reproducibility. In case of reproducibility the approach as demonstrated in this study (e.g. frequency analysis, determination of time constants) is recommended in order to establish a correct physiostatic process.

9. Summary

The photobioreactor system presented here consisted of four identical single reactors. Each reactor was equipped with identical control systems (e.g. pH-value, temperature) and illumination sources (PAR-light and UVB-radiation).

Generally, turbidostatic control was employed in all experiments presented here. Turbidostatic processes are characterised by keeping the optical density of the cell suspension constant. This should ensure that cell growing is compensated in order to receive steady state conditions in the photobioreactors, thus avoiding nutrient or light limitations.

In pilot studies, the photobioreactor system was used for the investigation of the temporal behaviour of the fluorescence signals emitted from *Synechocystis* sp. PCC 6803 when the cells were exposed to different intensities or frequencies of UVB-irradiation. The knowledge obtained from these pilot studies was used for the development of a feed back loop which enabled the design of a new process strategy (named physiostat). This new strategy allowed the cultivation of *Synechocystis* sp. PCC 6803 in a defined physiological state by controlling the actual photosynthetic efficiency ϕ_{PSII} . The actuating variable of the feedback loop was UVB-radiation.

The main issue of the investigations was the comparison of UVB-induced pigment synthesis under only turbidostatic or under additional physiostatic control. Pigment concentrations were measured *offline* by spectral analysis and/or HPLC. In turbidostatic processes, cells of the cyanobacterium *Synechocystis* sp. PCC 6803 were exposed to different stepwise changed UVB-intensities. In the physiostatic processes different set points of photosynthetic efficiency ϕ_{PSII} were chosen. One turbidostatic process without UVB exposure was used as a reference to ensure that observed effects are induced by UVB-radiation and are not intrinsic effects of *Synechocystis* sp. PCC 6803 caused by unknown stimuli.

In addition, antioxidative potential of microorganisms was measured with a modified method based on DPPH radical quenching.

The cultivation experiment provided several remarkable results. The main points are:

- ϕ_{PSII} shows a recovery process under constant UVB-radiation.

- Under constant UVB-intensities a linearly relationship between degradation rate of the phycobilisomes and employed UVB-intensity is detectable.
- Feed-back driven UVB-radiation in physiostatic processes may suppress repair and replacement processes responsible for recovering of ϕ_{PSII} in turbidostatic UVB-treated processes. Cells respond to this suppression by enhanced synthesis of carotenoids, xanthophylls and α -tocopherol.
- α -tocopherol is inducible by UVB-radiation.
- In physiostatic processes, upregulation of carotenoid, xanthophyll and α -tocopherol was faster than in cultivations processes affected by constant UVB-intensities in only turbidostatic processes.
- The increase of the overall antioxidative potential induced in UVB-irradiated cells is more pronounced in physiostatic processes.

These results indicate that physiostatic processes using UVB-radiation as actuating variable offer an promising cultivation method for an enhanced synthesis of substances interesting for commercial application. In some cases, this may be a replacement for genetic manipulation.

In Table 9.1, the effects of UVB-radiation on the cyanobacterium *Synechocystis* sp. PCC 6803 and their interpretations are summarised.

Table 9.1: Overview of the UVB-induced effects on *Synechocystis* ps. PCC 6803 occurring in turbidostatic processes. The cells were exposed either to a stepwise change in UVB-intensities in purely turbidostatic processes or to feed-back driven UVB-intensities with additional physiostatic control.

Int. dep. / indep. = effects dependent / independent to the applied UVB-intensity

Set point dep. = effects dependent to the applied set point

¹ effected when exposed to high UVB-intensities

² effected when cells were cultivated at low set points of ϕ_{PSII}

³ exponential increase

⁴ linear increase

⁵ still increasing after 24 h of the process time

⁶ remained constant after 24 to 36 h of the process time

	Turbidostat with stepwise changed UVB-intensity		Turbidostat with additional physiostatic control	
	Influence	Remarks	Influence	Remarks
BDM	No	-	No	-
μ	Strong	Int. dep.	Strong	Set point dep.
F, F _{M'}	Strong	Int. dep.	Strong	Set point dep.
Chl. <i>a</i>	No ¹	Int. dep.	No ²	Set point dep.
Myxoxanthophyll	Weak	Int. indep.	Strong ^{3,5}	Set point dep.
Zeaxanthin	Weak ⁴	Int. indep.	Strong ^{3,5}	Set point dep.
Echinenone	Weak	Int. indep.	Weak ^{3,6}	Set point dep.
β -carotene	Weak	Int. indep.	Weak ^{3,6}	Set point dep.
Phycobilisomes	Strong	Int. dep.	Strong	Set point dep.
MAA (Shinorine)	No	-	No	-
α -tocopherol	Weak	Int. indep.	Strong	Set point dep.
AOP	Strong ⁴	Int. indep.	Strong ^{3,6}	Set point dep.

10. Zusammenfassung

Das hier vorgestellte Photobioreaktor System besteht aus vier identischen Einzelreaktoren. Jeder Reaktor wurde mit identischen Regelungssystemen (z.B. pH-Wert, Temperatur) und Bestrahlungsquellen (PAR-Licht und UVB-Strahlung) ausgestattet

Grundsätzlich wurden alle Experimente turbidostatisch geregelt. Turbidostatische Prozesse zeichnen sich durch die Konstanthaltung der optischen Dichte der Zellsuspension aus. Dies sichert die Kompensation des Zellwachstums, um konstante Bedingungen (Vermeidung von Nährstoff- oder Lichtlimitierungen) im Photobioreaktor zu erreichen.

In Pilotstudien wurde das zeitliche Verhalten der von *Synechocystis* sp. PCC 6803 ausgestrahlten Fluoreszenzsignale untersucht, wenn Zellen unterschiedlichen Intensitäten und Frequenzen von UVB-Strahlung ausgesetzt wurden. Das Wissen dieser Pilotstudien wurde für die Entwicklung eines rückgekoppelten Regelkreises verwendet, der die Einführung einer neuen Prozessstrategie ermöglichte. Diese neue Strategie wurde Physiostat genannt. Sie ermöglichte die Kultivierung von *Synechocystis* sp. PCC 6803 in einem definiertem physiologischen Zustand, indem die photosynthetische Effizienz ϕ_{PSII} geregelt wurde. Die Stellgröße des Regelkreises war die UVB-Strahlung.

Hauptanliegen der Untersuchungen war der Vergleich der UVB-induzierten Pigmentsynthese zwischen turbidostatischer Regelung und einer zusätzlichen physiostatischen Regelung. Die Pigmente wurde *offline* mittels Spektralanalyse und/oder HPLC gemessen. In turbidostatischen Prozessen wurden Zellen des Cyanobakteriums *Synechocystis* sp. PCC 6803 unterschiedlichen, sprungförmig geänderten UVB-Intensitäten ausgesetzt. In den physiostatischen Prozessen wurden unterschiedliche Sollwerte der photosynthetischen Effizienz ϕ_{PSII} gewählt. Ein turbidostatischer Prozess ohne UVB-Bestrahlung wurde als Referenz verwendet, um sicherzustellen, dass die beobachteten Effekte durch UVB-Strahlung induziert wurden und keine intrinsischen Effekte von *Synechocystis* sp. PCC 6803 sind.

Zusätzlich wurde das antioxidative Potential von Mikroorganismen mittels einer modifizierten, auf der Reduzierung von DPPH Radikalen basierenden Methode gemessen.

Die Kultivierungsexperimente lieferten einige bemerkenswerte Punkte. Die wichtigsten sind:

- ϕ_{PSII} zeigt einen Erholungsprozess unter konstanter UVB-Bestrahlung.
- Unter konstanten UVB-Intensitäten ist ein lineares Verhältnis zwischen der Abbaurrate der Phycobilisomen und eingesetzter UVB-Intensität feststellbar.
- Rückgekoppelt angesteuerte UVB-Strahlung in physiostatischen Prozessen unterdrückt vermutlich Reparatur- und Austauschprozess, die für die Erholung von ϕ_{PSII} in turbidostatischen, UVB-behandelten Prozessen verantwortlich sind. Zellen reagieren auf diese Unterdrückung mit einer gesteigerten Synthese von Karotenoiden, Xanthophyllen und α -Tocopherol.
- α -Tocopherol ist durch UVB-Strahlung induzierbar.
- In physiostatischen Prozesses findet eine schnellere Aufregulierung von Karotenoiden, Xanthophyllen und α -Tocopherol als in Kultivierungsprozessen statt, die durch UVB-Intensitäten in turbidostatischem Prozess beeinflusst werden.
- Der Anstieg des antioxidativen Potentials von UVB-bestrahlten Zellen ist in physiostatischen Prozessen ausgeprägter.

Diese Resultate zeigen, dass physiostatischen Prozesse unter Verwendung von UVB-Strahlung als Steuergröße eine viel versprechende Kultivierungsmethode für die gesteigerte Synthese von kommerziell interessanten Substanzen darstellen. In einigen Fällen scheinen diese Prozesse als Ersatz für gentechnisch Veränderungen in Frage zu kommen.

In Tabelle 10.1 werden die Effekte von UVB-Strahlung auf das Cyanobakterium *Synechocystis* sp. PCC 6803 und ihre Interpretation zusammengefasst.

Table 10.1: Überblick über die UVB-induzierten Effekte auf *Synechocystis* ps. PCC 6803 während turbidostatischer Prozesse. Die Zellen wurden entweder einer sprungförmig geänderten UVB-Intensität in turbidostatischen Prozessen oder in rückgekoppelt angesteuerten UVB-Intensitäten zur zusätzlichen physiologischen Regelung ausgesetzt.

Int. abh / unabh. = Effekte sind abhängig / unabhängig von der eingesetzten UVB-Intensität.

SP. abh. = Effekte sind abhängig vom eingesetzten Sollwert

¹ beeinflusst bei hohen UVB-Intensitäten

² beeinflusst bei niedrigen Sollwerten von ϕ_{PSII}

³ exponentieller Anstieg

⁴ linearer Anstieg

⁵ weiterer Anstieg nach 24 h des Prozesses

⁶ verbleiben konstant nach 24 bis 36 h des Prozesses

	Turbidostat mit sprungförmig geänderte UVB-Intensität		Turbidostat mit zusätzlicher physiologischer Regelung	
	Einfluss	Bemerkung	Einfluss	Bemerkung
BDM	Nein	-	Nein	-
μ	Stark	Int. abh	Stark	SP. abh.
F, F _M '	Stark	Int. abh	Stark	SP. abh.
Chl. <i>a</i>	Nein ¹	Int. abh	Nein ²	SP. abh.
Myxoxanthophyll	Schwach	Int. unabh..	Stark ^{3,5}	SP. abh.
Zeaxanthin	Schwach ⁴	Int. unabh.	Stark ^{3,5}	SP. abh.
Echinenon	Schwach	Int. unabh.	Schwach ^{3,6}	SP. abh.
β -Carotin	Schwach	Int. unabh.	Schwach ^{3,6}	SP. abh.
Phycobilisomen	Stark	Int. abh	Stark	SP. abh.
MAA (Shinorin)	Nein	-	Nein	-
α -Tocopherol	Schwach	Int. unabh.	Stark	SP. abh.
AOP	Stark ⁴	Int. unabh.	Stark ^{3,6}	SP. abh.

References

- Allakhverdiev, S. I.; Nishiyama, Y.; Suzuki, I.; Tasaka, Y. & Murata, N. 1999. Genetic engineering of the unsaturation of fatty acids in membrane lipids alters the tolerance of *Synechocystis* to salt stress. *Proc. Natl. Acad. Sci.* 96: 5862 – 5867.
- Anderson, L.E.; Nehrlich, S.C. & Champigny, M.L. 1978. Activation of ribulose biphosphate carboxylase in intact chloroplasts by CO₂ and light. *Archs. Biochem. Biophys.* 185: 39 – 48.
- Anderson, J.A. & Padhye, S.R. 2004. Protein aggregation, radical scavenging capacity, and stability of hydrogen peroxide defense systems in heat-stressed *vinca* and sweet pea leaves. *J. Am. Soc. Hortic Sci.* 129: 54 – 59.
- Antolovic, M.; Prenzler, P.D.; Patsalides, E.; McDonald, S. & Robards, K. 2002. Methods for testing antioxidant activity. *Analyst* 127: 183 – 198.
- Apel, K. & Hirt, H. 2004. Reactive oxygen species: metabolism, oxidative stress and signal transduction. *Annu. Rev. Plant Biol.* 55: 373 – 399.
- Araoz, R. & Häder, D.P. 1997. Ultraviolet radiation induces both degradation and synthesis of phycobilisomes in *Nostoc* sp.: a spectroscopic and biochemical approach. *FEMS Microbiol. Ecol.* 23: 301 – 313.
- Arora, A.; Sairam, R.K. & Srivastave, G.C. 2002. Oxidative stress and antioxidative systems in plants. *Curr. Sci.* 82: 1227 – 1238.
- Baker, N.R. & Webber, N.A. 1987. Interactions between photosystems. *Advances in Botanical Research* 13: 2 – 56.
- Baldry, C.W.; Walker, D.A. & Bucke, C. 1966. Calvin-cycle intermediates in relation to induction phenomenon in photosynthetic carbon fixation by isolated chloroplast. *Biochem. J.* 101: 641 – 646.
- Bandoniene, D.; Murkovic, M.; Pfannhauser, W.; Venskutonis, P.R. & Gruzdiene, D. 2002. Detection and activity evaluation of radical scavenging compounds by using DPPH free radical and on-line HPLC-DPPH methods. *Eur. Food Res. Technol.* 214: 143 – 147.

- Barbato, R.; Friso, G.; Dalla Vecchia, F.; Rigoni, F. & Giacometti, G.M. 1992. Structural changes and lateral redistribution of photosystem II during donor side photoinhibition of thylakoids. *J. Cell. Biol.* 119: 325 – 335.
- Barber, J. & Andersson, B. 1992. Too much of a good thing: light can be bad for photosynthesis. *Trends in Biochem. Sci.* 17: 61 – 66.
- Baroli, I.; Do, A.D.; Yamane, T. & Niyogi, K.K. 2003. Zeaxanthin accumulation in the absence of a functional xanthophyll cycle protects *Chlamydomonas reinhardtii* from photooxidative stress. *Plant Cell* 15: 992 – 1008.
- Belay, A. 2002. The potential application Spirulina (Arthrospira) as a nutritional and therapeutic supplement in health management. *J. Am. Nutraceutical Association*. 5(2): 27 – 48.
- Bendich, A. & Olson, J.A. 1989. Biological actions of carotenoids. *FASEB J.* 3: 1927 – 1932.
- Beretta, E.; Bischi, G.I. & Solimano, F. 1990. Stability in chemostat equations with delayed nutrient recycling. *J. Math. Biol.* 28: 99 – 111.
- Beutler, M.; Wiltshire, K. H.; Reineke, C. & Hansen U.P. 2004. Algorithms and practical fluorescence models of the photosynthetic apparatus of red cyanobacteria and Cryptophyta designed for the fluorescence detection of red cyanobacteria and cryptophytes. *Aquatic microbial ecology*. *Aquat. microb. ecol.* 35: 115 – 129.
- Bhosale, P. & Bernstein, P.S. 2005. Microbial xanthophylls. *Appl. Microbiol. Biotechnol.* 68: 445 – 455.
- Bilger, W., Björkmann, O., 1994. Relationships among violaxanthin deepoxidation, thylakoid membrane conformation, and nonphotochemical chlorophyll fluorescence quenching in leaves of cotton (*Gossypium hirsutum* L.). *Planta* 193: 238 – 246.
- Bilger, W.; Fisahn, J.; Brummet, W.; Kossmann, J. & Willmitzer, L. 1995. Violaxanthin cycle pigment contents in potato and tobacco plants with genetically reduced photosynthetic capacity. *Plant Physiol.* 108: 1479 – 1486.
- Blokhina, O.; Virolainen, E., & Fagerstedt, K.V. 2003. Antioxidants, oxidative damage and oxygen deprivation stress: a review. *Ann. Bot.* 91: 179 – 194.
- Bode, H.W. 1964. *Network Analysis and Feedback Amplifier Design*. Von Nordstrand Comp., New York.

- Bondet, V.; Brand-Williams, W. & Berset, C. 1997. Kinetics and mechanisms of antioxidant activity using the DPPH free radical method. *Lebensm. Wiss. Technol.* 30: 609 – 615.
- Bramley, P.M. & Sandmann, G. 1985. In vitro and in vivo biosynthesis of xanthophylls by the cyanobacterium *Aphanocapsa*. *Phytochem.* 24: 2919 – 2922.
- Bramley, P.M.; Elmadfa, I.; Kafatos, A.; Kelly, F.J.; Manios, Y.; Roxborough, H.E.; Schuch, W.; Sheehy, P.J.A. & Wagner, K.H. 2000. Vitamin E. *J. Sci. Food. Agric.* 80: 913 – 938.
- Britton, G. 1995. Structure and properties of carotenoids in relation of function. *FASEB J.* 9: 1551 – 1558.
- Buchanan, B.B. 1980. Role of light in the regulation of chloroplast enzymes. *Ann. Rev. Plant Physiol.* 31: 341 – 374.
- Buschmann, C. & Grumbach, K. 1985. *Physiologie der Photosynthese*. Springer Verlag Berlin.
- Cahoon, E.B.; Hall, S.E.; Ripp, K.G.; Ganzke, T.S.; Hitz, W.D. & Coughlan, S.J. 2003. Metabolic redesign of vitamin E biosynthesis in plants for tocotrienol production and increased antioxidant content. *Nat. Biotechnol.* 21(9): 1082 – 1087.
- Campbell, D.; Eriksson, M.J.; Öquist, G.; Gustafsson, P. & Clarke, A.K. 1998. The Cyanobacterium *Synechococcus* resists UV-B by exchanging photosystem II reaction-center D1 proteins. *Proc. Natl. Acad. Sci.* 95: 364 – 369.
- Chaturvedi, R. & Shyam, R. 2000. Degradation and de novo synthesis of D1 protein and *psbA* transcript level in *Chlamydomonas reinhardtii* during UV-B inactivation of photosynthesis and its reactivation. *J. Biosci.* 25: 65 – 71.
- Cheng, Z.G.; Sattler, S.; Maeda, H.; Sakuragi, Y.; Bryant, D.A. & DellaPenna, D. 2003. Highly divergent methyltransferases catalyze a conserved reaction in tocopherol and plastoquinone synthesis in cyanobacteria and photosynthetic eukaryotes. *Plant Cell* 15: 1113 – 1124.
- Cifuentes, A.S.; Gonzalez, M.A.; Vargas, S.; Hoeneisen, M. & Gonzalez, N. 2003. Optimization of biomass, total carotenoids and astaxanthin production in *Haematococcus pluvialis* flotox strain Steptoe (Nevada, USA) under laboratory conditions. *Biol. Res.* 36: 343 – 357.
- Clausen, J. & Junge, W. 2004. Detection of an intermediate of photosynthetic water oxidation. *Nature* 430: 480 – 483.

- Cohen, Z. 1999. Chemicals in Microalgae. Taylor & Francis Ltd. 419 pp.
- Collakova, E. & DellaPenna, D. 2001. Isolation and functional analysis of homogenisate phytyltransferase from *Synechocystis* sp. PCC 6803 and Arabidopsis. *Plant Physiol.* 127: 1113 – 1124.
- Dähnhardt, D; Falk, J; Appel, J; van der Kooij, T.A.W.; Schulz-Friedrich, R. & Krupinska, K. 2002 The hydroxyphenylpyruvate dioxygenase from *Synechocystis* sp. PCC 6803 is not required for plastoquinone biosynthesis. *FEBS Letters* 523(1): 177 – 181.
- Dau, H. 1994a. Short-term adaptation of plants to changing light intensities and its relation to photosystem II photochemistry and fluorescence emission. *J. Photochem. Photobiol. B: Biol.* 26: 3 – 28.
- Dau, H. 1994b. Molecular mechanisms and quantitative models of variable photosystem II fluorescence. *Photochemistry and Photobiology* 60: 1 – 23.
- Di Mascio, P.; Murphy, M.E. & Sies, H. 1991. Antioxidant defense systems: the role of carotenoids, tocopherols, and thiols. *Am. J. Clin. Nutr.* 53: 194 – 200.
- Duke, C.S.; Cezeaux, A. & Allen, M.M. 1989. Changes in polypeptide composition of *Synechocystis* sp. Strain 6803 phycobilisomes induced by nitrogen starvation. *J. Bacteriol.* 171(4): 1960 – 1966.
- Dunlap, W.C. & Yamamoto, Y. 1995. Small molecule antioxidants in marine organisms: antioxidant activity of mycosporine-glycine. *Comp. Biochem. Physiol.* 112(1): 105 – 114.
- Edge, R.; McGarvey, D.J. & Truscott, T.G. 1997. The carotenoids as anti-oxidants – a review. *J. Photochem. Photobiol. B* 41: 189 – 200.
- Ehling-Schulz, M. & Scherer, S. 1999. UV protection in cyanobacteria. *Eur. J. Phycol.* 34: 329 – 338.
- Ehling-Schulz, M.; Bilger, W. & Scherer, S. 1997. UV-B-induced synthesis of photoprotective pigments and extracellular polysaccharides in the terrestrial cyanobacterium *Nostoc commune*. *J. Bacteriol.* 179(6): 1940 – 1945.
- Eonseon, J.; Polle, J.E.W.; Lee, H.K.; Hyun, S.M. & Chang, M. 2003. Xanthophylls in microalgae: From Biosynthesis to biotechnological mass production and application. *J. Microbiol. Biotechnol.* 13: 165 – 174.
- Falkowski, P.G. & Raven, J.A. 1997. Aquatic Photosynthesis. Blackwell Science, Oxford.

- Fang, Y.Z.; Yang, S. & Wu, G. 2002. Free radicals, antioxidants, and nutrition. *Nutrition*. 18: 872 – 879.
- Figuerola, F.L.; Escassi, L.; Perez-Rodriguez, E. ; Korbee, N. ; Giles, A.D. & Johnsen, G. 2003. Effects of short-term irradiation on photoinhibition and accumulation of mycosporine-like amino acids in sun and shade species of the red algal genus *Porphyra*. *J. Photochem. Photobiol. B*. 69:21 – 30.
- Garcia-Pichel, F. & Castenholz, R.W. 1993. Occurrence of UV-absorbing, mycosporine-like compounds among cyanobacterial isolates and an estimate of their screening capacity. *Appl. Environ. Microbiol.* 59(1): 163 – 169.
- Gazi, M.R.; Kanda, K.; Yasuda, M. & Kato, F. 2004. Optimisation of cultural conditions and some properties of radical scavenging substances from *sporobolomyces salmonicolor*. *Pak. J. Biol. Sci.* 7: 1365 – 1370.
- Geider, R.J. ; MacIntyre, H. L.; Graziano, L.M. & McKay, R.M.L. 1998. Responses of the photosynthetic apparatus of *Dunaliella tertiolecta* (Chlorophyceae) to nitrogen and phosphorus limitation. *Eur. J. Phycol.* 33: 315 – 332.
- Genty, B.; Briantais, J.M. & Baker, N.R. 1989. The relationship between the quantum yield of photosynthetic electron transport and quenching of chlorophyll fluorescence. *Biochim. Biophys. Acta* 990: 87 – 92.
- Giacometti, G.M.; Barbato, R.; Chiamonte, S.; Friso, G. & Rigoni, F. 1996. Effects of ultraviolet-B radiation on photosystem II of the cyanobacterium *Synechocystis* sp. PCC 6803. *Eur. J. Biochem.* 242: 799 – 806.
- Gomez, P.; Barriga, A.; Cifuentes, A.S. & Gonzalez, M.A. 2003. Effect of salinity on the quantity and quality of carotenoids accumulated by *Dunaliella salina* (strain CONC-007) and *Dunaliella bardawil* (strain ATCC 30861) Chlorophyta. *Biol. Res.* 36: 185 – 192.
- Götz, T.; Windhövel, U.; Böger, P. & Sandmann, G. 1999. Protection of photosynthesis against ultraviolet-B radiation by carotenoids in transformants of the cyanobacterium *Synechococcus* PCC 7942. *Plant Physiol.* 120: 599 – 604.
- Grabolle, M.; Michael Haumann, M.; Müller, C.; Liebisch, P. & Dau, H. 2006. Rapid loss of structural motifs in the manganese complex of oxygenic photosynthesis by X-ray Irradiation at 10–300 K. *J. Biol. Chem.* 281(8): 4580 – 4588.

- Gröniger, A.; Sinha, R.P. & Häder, D.P. 2000. Photoprotective compounds in Cyanobacteria, phytoplankton and macroalgae – a database. *J. Photochem. Photobiol.* 58: 115 – 122.
- Guillard, R.R.L. & Ryther, J.H. 1962. Studies of marine planktonic diatoms I. *Cyclotella nana* Hustedt and *Detonula confervacea* Cleve. *Can. J. Microbiol.* 8: 229 – 239.
- Guo, F.Q.; Okamoto, M. & Crawford, N.M. 2003. Identifikation of a plan nitric oxide synthase gene involved in hormonal signalling. *Science* 302: 100 – 103.
- Häder, D.P. 1999. Photosynthese. Thieme Verlag, Stuttgart.
- Hansen, U.P.; Kolbowski, J. & Dau, H. 1987. Relationship between photosynthesis and plasmalemma transport. *J. Experim. Bot.* 38(197): 1965 – 1981.
- Hansen, U.P.; Dau, H.; Brüning, B.; Fritsch, T. & Moldaenke, C. 1991. Linear analysis applied to the comparative study of the I-D-P phase chlorophyll fluorescence as induced by actinic PS-II light, PS-I light and changes in CO₂-concentration. *Photosynth. Res.* 28: 119 – 130.
- Haumann, M.; Liebisch, P.; Müller C.; Barra, M.; Grabolle, M. & Dau, H. 2005. Photosynthetic O₂ Formation Tracked by Time-Resolved X-ray Experiments, *Science* 310, 1019 – 1021.
- Havaux, M.; Lütz, C. & Grimm, B. 2003. Chloroplast membrane photostability in *chlP* transgenic tobacco plants deficient in tocopherols. *Plant Physiol.* 132:300 – 310.
- Havaux, M.; Eymery, F.; Profirova, S.; Rey, P. & Dörmann, P. 2005. Vitamin E protects against photoinhibition and photooxidative stress in *Arabidopsis thaliana*. *Plant Cell.* 17: 3451 – 3469.
- He, Y.Y. & Häder, D.P. 2002. Reactive oxygen species and UV-B: effect on cyanobacteria. *Photochem. Photobiol. Sci.* 1: 729 – 736.
- He, Y.Y.; Klisch, M. & Häder, D.P. 2002. Adaptation of cyanobacteria to UV-B stress correlated with oxidative stress and oxidative damage. *Photochem. Photobiol.* 76(2): 188 – 196.
- Higed, E. & Vass, I. 1996. UV-B induced free radical production in plant leaves and isolated thylakoid membranes. *Plant Sci.* 115: 251 – 260.
- Hofius, D. & Sonnewald, U. 2003. Vitamin E biosynthesis: biochemistry meets cell biology. *Trends in Plant Sci.* 8(1): 6 – 8.

- Hormann, H.; Neubauer, C.; Asada, K. & Schreiber, U. 1993. Intact chloroplasts display pH 5 optimum of O₂-reduction in the absence of methyl viologen: Indirect evidence for a regulatory role of superoxide protonation. *Photosynth. Res.* 37: 69 – 80.
- Hoshida, H.; Ohira, T.; Minematsu, A.; Akada, R. & Nishizawa, Y. 2005. Accumulation of eicosapentaenoic acid in *Nannochloropsis* sp. in response to elevated CO₂ concentrations. *J. Appl. Phycol.* 17(1): 29 – 34.
- Huang, L.; McCluskey, M.P.; Ni, H. & LaRossa, R.A. 2002. Global Gene Expression Profiles of the Cyanobacterium *Synechocystis* sp. Strain PCC 6803 in Response to Irradiation with UV-B and White Light. *J. Bacteriol.* 184: 6845 – 6858.
- Ihalainen, J.A.; D'Haene, S.; Yeremenko, N.; van Roon, H.; Arteni, A.A.; Boekema, E.J.; van Grondelle, R.; Matthijs, H.C.P. & Dekker, J.P. 2005. Aggregates of the chlorophyll-binding protein IsiA (CP43') dissipate energy in cyanobacteria. *Biochem.* 44:10846 – 10853.
- Iwashima, M.; Mori, J.; Ting, X.; Matsunaga, T.; Hayashi, K.; Shinoda, D.; Saito, H.; Sankawa, U. & Hayashi, T. 2005. Antioxidant and antiviral activities of plastoquinones from the brown alga *Sargassum micracanthum*, and a new chromene derivative converted from the plastoquinones. *Biol. Pharm. Bull.* 28: 374 – 377.
- Jacob, R.A. & Burri, B.J. 1996. Oxidative damage and defense. *Am. J. Clin. Nutr.* 63: 985 – 990.
- Janssen, M.A.K.; Mattoo, A.K. & Edelman, M. 1999. D1-D2 protein degradation in the chloroplast. *Eur. J. Biochem.* 260: 527 – 532.
- Jeffrey, S.W.; MacTavish, H.S.; Dunlap, W.C.; Veski, M. & Groenewoud, K. 1999. Occurrence of UVA- and UVB-absorbing compounds in 152 species (206 strains) of marine microalgae. *Mar. Ecol. Prog. Series.* 189: 35 – 51.
- Jimenez, C & Niell, F. X. 2003. Influence of high salinity and nitrogen limitation on package effect and C/N ratio in *Dunaliella viridis*. *Hydrobiologica.* 492(1 – 3): 201 – 206.
- Junge W.; Lill, H. & Engelbrecht, S. 1997. ATP synthase: an electrochemical transducer with rotatory mechanics. *Trends Biochem. Sci.* 22: 420 – 423.
- Jürgens, U.J. & Mantele, W. 1991. Orientation of carotenoids in the outer membrane of *Synechocystis* PCC 6714 (Cyanobacteria). *Biochim. Biophys. Act.* 1067: 208 – 212.
- Karukstis, K.K. 1992. Chlorophyll fluorescence analyses of photosystem II reaction center heterogeneity. *J. Photochem. Photobiol. B: Biol.* 15: 63 – 74.

- Keren, N.; Berg, A.; Van Kan, P.J.M.; Levanon, H. & Ohad, I. 1997. Mechanism of photosystem II photoinactivation and D1 protein degradation at low light: The role of back electron flow. *Proc. Natl. Acad. Sci.* 94: 1579 – 1584.
- Kobayashi, M.; Kakizono, T.; Nishio, N.; Nagai, S.; Kurimura, Y. & Tsuji, Y. 1997. Antioxidant role of astaxanthin in the green alga *Haematococcus pluvialis*. *Appl. Microbiol. Biotechnol.* 48: 351 – 356.
- Kolber, Z. & Falkowski, P.G. 1993. Use of active fluorescence to estimate phytoplankton photosynthesis in situ. *Limnol. Oceanogr.* 38 (8): 1646 – 1665.
- Koleva, I.I.; van Beek, T.A.; Linssen, J.P.H.; de Groot, A. & Evstatieva, L.N. 2001. Screening of plant extracts for antioxidant activity: a comparative study on three testing methods. *Phytochem. Analysis.* 13: 8 – 17.
- Kosakowska, A.; Lewandowska, J.; Ston, J. & Burkiewicz, K. 2004. Qualitative and quantitative composition of *Phaedactylum tricornutum* (Bacillariophyceae) stressed by iron. *J. Biometals.* 17: 45 – 52.
- Krieger-Liszkay, A. & Trebst, A. 2006. Tocopherol is the scavenger of singlet oxygen produced by the triplet states of chlorophyll in the PSII reaction centre. *J. Exp. Bot.* 57(8): 1677 – 1684.
- Krinsky, N.I. 1994. The biological properties of carotenoids. *Pure & Appl. Chem.* 66: 1003 – 1010.
- Krömer, S. 1995. Respiration during photosynthesis. *Annu. Rev. Plant Physiol. Plant Mol. Biol.* 46: 45 – 70.
- Kruk, J. & Strzałka, K. 2001. Redox changes of cytochrome b559 in the presence of plastoquinones. *J. Biol. Chem.* 276: 86 – 91.
- Kruk, J.; Holländer-Czytko, H.; Oettmeier, W. & Trebst, A. 2005. Tocopherol as singlet oxygen scavenger in photosystem II. *J. Plant Physiol.* 162: 749 – 757.
- Kulisic, T.; Radonic, A.; Katalinic, V. & Milos, M. 2004. Use of different methods for testing antioxidative activity of oregano essential oil. *Food Chem.* 85: 633 – 640.
- Lagarde, D.; Beuf, L. & Vermaas, W. 2000. Increased production of zeaxanthin and other pigments by application of genetic engineering techniques to *Synechocystis* sp. Strain PCC 6803. *Appl. Environ. Microbiol.* 66(1): 64 – 72.
- Lao, K. & Glazer, A.N. 1996. Ultraviolet-B photodestruction of a light-harvesting complex. *Proc. Natl. Acad. Sci.* 93: 5258 – 5263.

- Latimer, P.; Bannister, T.T. & Rabinowitch, E. 1956. Quantum yields of fluorescence of plant pigments. *Science* 124: 585 – 586.
- Lavergne, J. & Leci, E. 1993. Properties of inactive photosystem II centers. *Photosynth. Res.* 35: 323 – 343.
- Lesser, M.P. 2006. Oxidative stress in marine environments. *Ann. Rev. Physiol.* 68: 253 – 278.
- Lippemeier, S.; Frampton, D.; Blackburn, S.; Geier, S. & Negri, A. 2003. Influence of phosphorus limitation on toxicity and photosynthesis of *Alexandrium minutum* (Dinophyceae) monitored by in-line detection of variable chlorophyll fluorescence. *J. Phycol.* 39(2): 320 – 331.
- Lippemeier, S.; Hintze, R.; Vanselow, K.H.; Hartig, P. & Colijn, F. 2001. In-line recording of PAM fluorescence of phytoplankton cultures as a new tool for studying effects of fluctuating nutrient supply on photosynthesis. *Eur. J. Phycol.* 36: 89 – 100.
- Lübke, P.J. 1991. Modelltheoretische Untersuchungen von Methoden zur on-line Identifikation dynamischer Systeme am Beispiel des photosynthetischen Apparates. Dissertation. Univ. Kiel, Kiel.
- MacColl, R. 1998. Cyanobacterial phycobilisomes. *J. Struct. Biol.* 124: 311 – 334.
- MacDonald, T.M.; Dubois, L.; Smith, L.C. & Campbell, D.A. 2003. Sensitivity of cyanobacterial antenna, reaction center and CO₂ assimilation transcripts and proteins to moderate UVB: Light acclimation potentiates resistance to UVB, *Photochem. Photobiol.* 77(4): 405 – 412.
- Maeda, H.; Sakuragi, Y.; Bryant, D.A. & DellaPenna, D. 2005. Tocopherols protect *Synechocystis* sp. PCC 6803 from lipid peroxidation. *Plant Physiol.* 138: 1422 – 1435.
- Margalith, P.Z. 1999. Production of ketocarotenoids by microalgae. *Appl. Microbiol. Biotechnol.* 51: 431 – 438.
- Marshall, J.A.; Ross, T.; Pyecroft, S. & Hallegraeff, G. 2005. Superoxide production in marine microalgae. *Mar. Biol.* 147: 541 – 549.
- Marxen, K.; Vanselow, K.H.; Lippemeier, S.; Hintze, R.; Ruser, A. & Hansen, U.P. 2005. A photobioreactor system for computer controlled cultivation of microalgae. *J. Appl. Phycol.* 17: 535 – 549.

- Masuda, T.; Yonemori, S.; Oyama, Y.; Takeda, Y.; Tanaka, T.; Andoh, T.; Shinohara, A. & Nakata, M. 1999. Evaluation of the antioxidant of environmental plants: activity of the leaf extracts from seashore plants. *J. Agric. Food Chem.* 47: 1749 – 1754.
- Máté, Z.; Sass, L.; Szekeres, M.; Vass, I. & Nagy, F. 1998. UV-B-induced Differential Transcription of *psbA* Genes encoding the D1 Protein of Photosystem II in the Cyanobacterium *Synechocystis* 6803. *J. Biol. Chem.* 273 (28):17439 – 17444.
- McClintock, J.B. & Karentz, D. 1997. Mycosporine-like amino acids in 38 species of subtidal marine organisms from McMurdo Sound, Antarctica. *Antarctic Scien.* 9 (4): 392 – 398.
- Miki, W. 1991. Biological functions and activities of animal carotenoids. *Pure & Appl. Chem.* 63(1): 141 – 146.
- Miller, N.J.; Sampson, J.; Candeias, L.P.; Bramley, P.M. & Rice-Evans, C.A. 1996. Antioxidant activities of carotenes and xanthophylls. *FEBS Letters.* 384: 240 – 242.
- Mitchell, P. 1977. Oxidative phosphorylation and photophosphorylation: vectorial chemiosmotic processes. *Ann. Rev. Biochem.* 46, 996 – 1005.
- Mohamed, H.E.; van de Meene, A.M.L.; Roberson, R.W. & Vermaas, W.F.J. 2005. Myxoxanthophyll is required for normal cell wall structure and thylakoid organization in the cyanobacterium *Synechocystis* sp. PCC 6803. *J. Bacteriol.* 187(20): 6883 – 6892.
- Molyneux, P. 2004. The use of the stable free radical diphenylpicryl-hydrazyl (DPPH) for estimating antioxidant activity. *Songklanakarin J. Sci. Technol.* 26: 211 – 219.
- Mundt, S.; Kreitlow, S. & Jansen, R. 2003. Fatty acids with antibacterial activity from the cyanobacterium *Oscillatoria redekei* HUB 051. *J. Appl. Phycol.* 15: 263 – 267.
- Naguib, Y.M.A. 2000. Antioxidant activities of astaxanthin and related carotenoids. *J. Agri. Food Chem.* 48: 1150 – 1154.
- Niyogi, K.K.; Björkman, O. & Grossman, A.R. 1997. The roles of specific xanthophylls in photoprotection. *Proc. Natl. Acad. Sci.* 94: 14162 – 14167.
- Nishiyama, Y.; Allakhverdiev, S.I. & Murata, N. 2005. Inhibition of the repair of photosystem II by oxidative stress in cyanobacteria. *Photosynth. Res.* 84: 1 – 7.
- Noctor G. and C. H. Foyer 1998. Ascobate and glutathione: Keeping active oxygen under control. *Annu. Rev. Plant Physiol. Plant Mol. Biol.* 49: 249 – 279.

- Oren, A. 1997. Mycosporine-like amino acids as osmotic solutes in a community of halophilic Cyanobacteria. *Geomicrobiol. J.* 14:231 – 240.
- Ort, D.R. & Withmarsh, J. 1996. Specific features of excitation migration in photosynthesis. Light as an energy source and information carrier in plant physiology (ed. Jennings Rea). Plenum Press, New York.
- Paiva, S.A.R. & Russell, R.M. 1999. β -carotene and other carotenoids as antioxidants. *J. Am. Coll. Nutr.* 18: 426 – 433.
- Pandey, R.; Chauhan, S. & Singhal, G.S. 1997. UVB-induced photodamage to phycobilisomes of *Synechococcus* sp. PCC 7942. *J. Photochem. Photobiol. B.* 40: 228 – 232.
- Papageorgiou, G.C. 1996. The photosynthesis of cyanobacteria (blue bacteria) from the perspective of signal analysis of chlorophyll *a* fluorescence. *J. Sci. Ind. Res.* 596 – 617.
- Pavlov, A.; Kovatcheva, P.; Georgiev, V.; Koleva, I. & Ilieva, M. 2002. Biosynthesis and radical scavenging activity of betalains during the cultivation of red beet (*Beta vulgaris*) hairy root cultures. *Z. Naturforsch.* 57c: 640 – 644.
- Peterman, E.J.G.; Dukker, F.M.; van Grondelle, R. & van Amerongen, H. 1995. Chlorophyll *a* and carotenoid triplet states in light-harvesting complex II of higher plants. *Biophys. J.* 69: 2670 – 2678.
- Pfündel, E. & Bilger, W. 1994. Regulation and possible function of the violaxanthin cycle. *Photosynth. Res.* 43(2): 89 – 109.
- Pinchuk, I. & Lichtenberg, D. 2002. The mechanism of action of antioxidants against lipoprotein peroxidation, evaluation based on kinetic experiments. *Prog. Lipid Res.* 41: 279 – 314.
- Portwich, A. & Garcia-Pichel, F. 1999. Ultraviolet and osmotic stresses induce and regulate the synthesis of mycosporines in the cyanobacterium *Chlorogleopsis* PCC 6912. *Arch. Microbiol.* 172:187 – 192.
- Prior, R.L.; Wu, X. & Schaich, K. 2005. Standardized methods for the determination of antioxidant capacity and phenolics in foods and dietary supplements. *J. Agric. Food Chem.* 53: 4290 – 4303.
- Pulz, O. & Gross, W. 2004. Valuable products from biotechnology of microalgae. *Appl. Microbiol. Biotechnol.* 65: 635 – 648.

- Rabinowitch, E. 1959. Primary Photochemical and Photophysical Processes in Photosynthesis. *Plant Physiol.* 34: 213 – 218.
- Rakhimberdieva, M.G.; Stadnichuk, I.N.; Elanskaya, I.V. & Karapetyan, N.V. 2004. Carotenoid-induced quenching of the phycobilisome fluorescence in photosystem II-deficient mutant of *Synechocystis* sp. *FEBS Letters.* 574: 85 – 88.
- Rhee, K.-H. 2001. Photosystem II: The Solid Structural. *Era. Annu. Rev. Biophys. Biomol. Struct.* 30: 307 – 328.
- Reising, H. & Schreiber, U. 1992. Pulse-modulated photoacoustic measurements reveal strong gas-uptake component at high CO₂ concentrations. *Photosynth. Res.* 31: 227 – 238.
- Reuter, M. 1994. *Regelungstechnik für Ingenieure.* Vieweg. 153 pp.
- Richaud, C.; Zabulon, G.; Joder, A. & Thomas, J.C. 2001. Nitrogen or sulfur starvation differentially affects phycobilisome degradation and expression of the *nblA* gene in *Synechocystis* strain PCC 6803. *J. Bacteriol.* 183(10): 2989 – 2994.
- Richmond, A. 2004. *Microalgal Culture.* Blackwell Science Ltd. 566 pp.
- Riethmann, H.; Bullerjahn, G.; Reddy, K.J. & Sherman, L.A. 1988. Regulation of cyanobacterial pigment-protein composition and organization by environmental factors. *Photosyn. Res.* 18: 133 – 161.
- Rijstenbil, J.W. 2002. Assessment of oxidative stress in the planktonic diatom *Thalassiosira pseudonana* in response to UVA and UVB radiation. *J. Plankton Res.* 24: 1277 – 1288.
- Rmiki, N.E.; Brunet, C.; Cabioch, J. & Lemoinel, Y. 1996. Xanthophyll-cycle and photosynthetic adaptation to environment in macro- and microalga. *Hydrobiol.* 326/327: 407 – 413.
- Rippert, P.; Scimeni, C.; Dubald, M. & Matringe, M. 2004. Engineering plant shikimate pathway for production of tocotrienol and improving herbicide resistance. *Plant Physiol.* 134: 92 – 100.
- Rippka, R.; Deruelles, J.; Waterbury, J.; Herdman, M. & Stanier, R. 1979. Generic assignments, strain histories and properties of pure cultures of cyanobacteria. *J. Gen. Microbiol.* 111: 1 – 61.
- Romay, C.; Armesto, J.; Ramirez, D.; González, R.; Ledon, N. & García, I. 1998. Antioxidant and anti-inflammatory properties of C-phycocyanin from blue-green algae. *Inflamm. Res.* 47: 36 – 41.

- Sass, L.; Spetea, C.; Mate, Z.; Nagy, F. & Vass, I. 1997. Repair of UV-B induced damage of photosystem II via de novo synthesis of the D1 and D2 reaction centre subunits in *Synechocystis* sp. PCC 6803. *Photosynt. Res.* 54: 55 – 62.
- Sattler, S.E.; Cahoon, E.B.; Coughlan, S.J. & DellaPenna, D. 2003. Characterization of tocopherol cyclases from higher plants and cyanobacteria: evolutionary implications for tocopherol synthesis and function. *Plant Physiol.* 132: 2184 – 2195.
- Schäfer, L.; Sandmann, M.; Woitsch, S. & Sandmann, G. 2006. Coordinate up-regulation of carotenoid biosynthesis as a response to light stress in *Synechococcus* PCC 7942. *Plant, Cell and Environm.* 29: 1349 – 1356.
- Schreiber, U.; Bilger, W. & Neubauer, C. 1995b. Chlorophyll Fluorescence as a Noninvasive Indicator for Rapid Assessment of In Vivo Photosynthesis. In: Schulze ED and Caldwell MM (eds.) *Ecophysiology of Photosynthesis*, Springer-Verlag, Berlin, pp. 49 – 70.
- Schreiber, U.; Hormann, H.; Neubauer, C. & Klughammer, C. 1995a. Assessment of Photosystem II Photochemical Quantum Yield by Chlorophyll Fluorescence Quenching Analysis. *Aust. J. Plant Physiol.* 22: 209 – 220.
- Schubert, H.; Andersson, M. & Snoeijs, P. 2006. Relationship between photosynthesis and non-photochemical quenching of chlorophyll fluorescence in two red algae with different carotenoid compositions. *Mar. Biol.* 149: 1003 – 1013.
- Shick, J.M.; Romaine-Lioud, S.; Ferrier-Pages, C. & Gattuso J.P. 1999. Ultraviolet-B radiation stimulates shikimate pathway-dependent accumulation of mycosporine-like amino acids in the coral *Stylophora pistillata* despite decreases in its population of symbiotic dinoflagellates. *Limnol Oceanogr.* 44(7): 1667 – 1682.
- Shintani, D.K.; Chang, Z. & DellaPenna, D. 2001. The role of 2-methyl-6-phytylbenzoquinone methyltransferase in determining tocopherol composition in *Synechocystis* sp. PCC 6803. *FEBS Letters* 511: 1 – 5.
- Shipton, C.A. & Barber, J. 1991. Photoinduced degradation of the D1 polypeptide in isolated reaction centers of photosystem II: evidence for an autoproteolytic process triggered by the oxidizing side of the photosystem. *Proc. Natl. Acad. Sci.* 88: 6691 – 6695.
- Sies, H. & Stahl, W. 1995. Vitamins E and C, β -carotene, and other carotenoids as antioxidants. *Am. J. Clin. Nutr.* 62 (suppl): 1315 – 1321.

- Sinha, R. P.; Klisch, M. & Häder, D.P. 1999. Induction of mycosporine-like amino acids (MAA) in the rice-field cyanobacterium *Anabaena* sp. By UV irradiation. J. Photochem. Photobiol. B 52: 59 – 64.
- Sinha, R.P. & Häder, D.P. 2002. UV-induced DNA damage and repair: a review. Photochem. Photobiol. Sci. 1: 225 – 236.
- Sinha, R.P.; Ambasht, N.K.; Sinha, J.P. & Häder, D.P. 2003. Wavelength-dependent induction of a mycosporine-like amino acid in a rice-field cyanobacterium, *Nostoc commune*: role of inhibitors and salt stress. Photochem. Photobiol. Sci. 2: 171 – 176.
- Sinha, R.P.; Kumar, H.; Kumar, A. & Häder, D.P. 1995. Effects of UV-B Irradiation on Growth, Survival, Pigmentation and Nitrogen Metabolism Enzymes in Cyanobacteria. Acta Protozool. 34: 187 – 192.
- Smirnoff, N. 2000. Ascobate biosynthesis and function in photoprotection. Phil. Trans. R. Soc. Lond. B. 355: 1455 – 1464.
- Spolaore, P.; Joannis-Cassan, C.; Duran, E. & Isambert, A. 2006. Commercial application of microalgae. J. Biosci. Bioeng. 101: 87 – 96.
- Steiger, S.; Schäfer, L. & Sandmann, G. 1999. High-light-dependent upregulation of carotenoids and their antioxidative properties in the cyanobacterium *Synechocystis* PCC 6803. J. Photochem. Photobiol. 52: 14 – 18.
- Suh, H.J.; Lee, H.W. & Jung, J. 2003. Mycosporine glycine protects biological systems against photodynamic damage by quenching singlet oxygen with a high efficiency. Photochem. Photobiol. 78 (2): 109 – 113.
- Telfer, A.; Bishop, S.M.; Phillips, D. & Barber, J. 1994. Isolated photosynthetic reaction centre of photosystem II as a sensitizer for the formation of singlet oxygen. J. Biol. Chem. 269(18).13244 – 13253.
- Tichy, M. & Vermaas, W. 1999. In vivo role of catalase-peroxidase in *Synechocystis* sp. PCC 6803. J Bacteriol. 181(6): 1875 – 1882.
- Torzillo, G.; Accolla, P; Pinzani, E. & Masojidek, J. 1996. *In situ* monitoring of chlorophyll fluorescence to assess the synergistic effect of low temperature and high irradiance stresses in *Spirulina* cultures grown outdoors in photobioreactors J. Appl. Phycol. 8(4 – 5): 283 – 291.
- Traber, M.G. & Sies, H. 1996. Vitamin E and humans: demand and delivery. Annu. Rev. Nutr. 16: 321 – 347.

- Trebst, A. 2003. Function of β -carotene and tocopherol in photosystem II. *Zeitschr. Naturforsch.* 58c: 609 – 620.
- Trebst, A.; Depka, B. & Holländer-Czytko, H. 2002. A specific role for tocopherol and of chemical singlet oxygen quenchers in the maintenance of photosystem II structure and function in *Chlamydomonas reinhardtii*. *FEBS Letters*. 516: 156 – 160.
- Ughy, B. & Ajlani, G. 2004. Phycobilisome rod mutants in *Synechocystis* sp. strain PCC6803. *Microbiol.* 150: 4147 – 4156.
- v. Kooten, O. & Snel, J.F.H. 1990. The use of chlorophyll fluorescence nomenclature in plant stress physiology. *Photosynth. Res.* 25: 147 – 150.
- Valentin, H.E. & Qi, Q. 2005. Biotechnological production and application of vitamin E: current state and prospects. *Appl. Microbiol. Biotechnol.* 68: 436 – 444.
- Vanselow, K.H. 1993. The effect of N-nutrients on the acceptor pool of PS I and thylakoid energization as measured by chlorophyll fluorescence of *Dunaliella salina*. *J. Experiment. Biol.* 44(8): 1331 – 1340.
- Vanselow, K.H.; Kolbowski, J. & Hansen, U.P. 1988. Analysis of Chlorophyll Fluorescence By Means of Noisy Light. *J. Exp. Bot.* 40: 247 – 256.
- Vanselow, K. H.; Kolbowski, J. & Hansen, U.P. 1989. Further evidence for the relationship between light-induced changes of the plasmalemma transport and thransthylakoid proton uptake. *J. Experim. Bot.* 40(211): 239 – 245.
- Vass, I.; Sass, L.; Spetea, C.; Bakou, A.; Ghanotakis, D.F. & Petrouleas, V. 1996. UV-B-induced inhibition of photosystem II electron transport studied by EPR and chlorophyll fluorescence. Impairment of donor and acceptor side components. *Biochem.* 35(27): 8964 – 8973.
- Vass, I.; Styring, S.; Hundal, T.; Koivunniemi, A.; Aro, E.M. & Andersson, B. 1992. Reversible and irreversible intermediates during photoinhibition of photosystem II: stable reduced Q_A species promote chlorophyll triplet formation. *Proc. Natl. Acad. Sci.* 89: 1408 – 1412.
- Vaya, J. & Aviram, M. 2001. Nutritional antioxidants: mechanism of action, analyses of activities and medical applications. *Curr. Med. Chem.–Imm., Endoc. & Metab. Agents.* 1: 99 – 117.
- Wada, H. & Murata, N. 1990. Temperature-induced changes in the fatty acid composition of the cyanobacterium, *Synechocystis* PCC 6803. *Plant Physiol.* 92: 1062–1069.

- Wada, H. & Murate, N. 1989. *Synechocystis* PCC 6803 mutants defective in desaturation of fatty acids. *Plant Cell Physiol.* 30(7): 971 – 978.
- Walker, D.A. 1981. Secondary fluorescence kinetics of spinach leaves in relation to the onset of photosynthetic carbon assimilation. *Planta* 153: 273 – 278.
- Wang, B.; Zarka, A.; Trebst, A. & Boussiba, S. 2003. Astaxanthin accumulation in *Haematococcus pluvialis* (Chlorophyceae) as an active photoprotective process under high irradiance. *J. Phycol.* 39: 1116 – 1124.
- Wilson, A.; Ailani, G.; Verbavatz, J.M.; Vass, I.; Kerfeld, C.A. & Kirilovsky, D. 2006. A soluble carotenoid protein involved in phycobilisome-related energy dissipation in cyanobacteria. *Plant Cell* 18: 992 – 1007.
- Witt, H.T. 1979. Energy conversion in the functional membrane of photosynthesis. Analysis by light pulse and electric pulse methods. *Biochim. Biophys. Acta* 505, 355 – 427.
- Wu, Y.P. & Krogmann, D.W. 1997. The orange carotenoid protein of *Synechocystis* PCC 6803. *Biochim. Biophys. Acta* 1322: 1 – 7.
- Xiong, F.; Kopecky, J. & Nedbal, L. 1999. The occurrence of UV-B absorbing mycosporine-like amino acids in freshwater and terrestrial microalgae (Chlorophyta). *Aquat. Bot.* 63: 37 – 49.
- Yen, G.C. & Duh, P.D. 1994. Scavenging effect of methanolic extracts of peanut hulls on free-radical and active-oxygen species. *J. Agric. Food Chem.* 42: 629 – 632.
- Yongmanitchai, W. & Ward, O.P. 1991. Growth of and omega-3 fatty acid production by *Phaeodactylum tricornerutum* under different culture conditions. *J. Appl. Environm. Microb.* 57: 419 – 425.
- Yordabov, N.D. & Christova, A.G. 1997. Quantitative spectrophotometric and EPR-determination of 1,1-diphenyl-2-picryl-hydrazyl (DPPH). *Fresen. J. Anal. Chem.* 358: 610 – 613.
- Young, A.J.; Phillip, D., Ruban, A.V.; Horton, P. & Frank, H.A. 1997. The xanthophyll cycle and carotenoid-mediated of excess excitation energy in dissipation photosynthesis. *Pure & Appl. Chem.*, 69(10): 2125 – 2130.
- Zolla, L. & Bianchetti, M. 2001. High-performance liquid chromatography coupled on-line with electrospray ionization mass spectrometry for the simultaneous separation and identification of the *Synechocystis* PCC 6803 phycobilisome proteins. *J. Chromat.* 912: 269 – 279.

Zolla, L.; Bianchetti, M. & Rinalducci, S. 2002. Functional studies of the *Synechocystis* phycobilisomes organization by high performance liquid chromatography on line with a mass spectrometer. Eur. J. Biochem. 269:1534 – 1542.

Danksagung

An dieser Stelle möchte ich allen meinen Dank aussprechen, die zum Gelingen dieser Arbeit maßgeblich beigetragen haben.

An erster Stelle sei meinem Doktorvater Herrn Prof. U. P. Hansen gedankt. Seine ruhige und besonnene Art in Kombination mit seiner fachlichen Kompetenz hat in mir immer einen Motivationsschub hervorgebracht und mir Zuversicht gegeben.

Herr Prof. F. Colijn sei gedankt für die Bereitstellung des Arbeitsplatzes. Durch diesen war es möglich, am FTZ die Erfahrung einer interdisziplinären Zusammenarbeit unterschiedlicher Wissenschaftszweige zu machen.

Für seine stetige Bereitschaft zur Diskussion, lektorale Überarbeitungen und seiner Hilfe in allen administrativen Fragen sei an dieser Stelle Dr. K. H. Vanselow gedankt.

Dr. R. Hintze, Dr. S. Lippemeier und Dr. P. Hartig dürfen hier nicht unerwähnt bleiben. Die Bereitstellung des für diese Arbeit erforderlichen Freiraums, ihre fachliche Kompetenz und Diskussionsbereitschaft haben im erhöhtem Maße an dieser Arbeit einen positiven Einfluss gehabt.

Dr. A. Ruser sei nicht nur für seinen fachlichen Beitrag, sondern auch für die vielen kleinen Nebentätigkeiten gedankt.

G. Bojens, B. Meyer, W. Voigt, B. Egge, M. Hoffmann und natürlich allen anderen FTZ-Mitarbeitern muss gedankt werden für ihre stetige Bereitschaft zur Mitarbeit und das Interesse an dieser Arbeit.

Hiermit erkläre ich an Eides statt, daß ich die vorliegende Dissertation selbständig angefertigt habe und dabei als Hilfsmittel nur die genannten Quellen benutzt habe.

Des Weiteren versichere ich, dass die vorliegende Dissertation weder ganz, noch zum Teil bei einer anderen Stelle im Rahmen eines Prüfungsverfahrens vorgelegt wurde.

Kiel, Dezember 2006